PL-TR-92-2029

Prediction of Thunderstorm Initiation Through 4-Dimensional Data Assimilation of Doppler Radar Data

Thomas M. Hamill

Atmospheric and Environmental Research, Inc.
840 Memorial Drive
Cambridge, MA 02139

2 January 1992

Scientific Report No. 1

PHILLIPS LABORATORY
AIR FORCE SYSTEMS COMMAND
HANSCOM AFB, MASSACHUSETTS 01731-5000

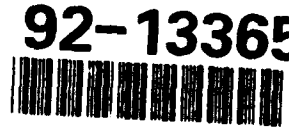

This technical report has been reviewed and is approved for publication.

ALLAN J. BUSSEY
Contract Manager

ROBERT A. McCLATCHEY
Division Director

This report has been reviewed by the ESD Public Affairs Office (PA) and is releasable to the National Technical Information Service (NTIS).

Qualified requestors may obtain additional copies from the Defense Technical Information Center. All others should apply to the National Technical Information Service.

If your address has changed, or if you wish to be removed from the mailing list, or if the addressee is no longer employed by your organization, please notify PL/TSI, Hanscom AFB, MA 01731-5000. This will assist us in maintaining a current mailing list.

Do not return copies of this report unless contractual obligations or notices on a specific document requires that it be returned.

REPORT DOCUMENTATION PAGE

Form Approved
OMB No 0704-0188

1. AGENCY USE ONLY (Leave blank)	2. REPORT DATE	3. REPORT TYPE AND DATES COVERED
	2 January 1992	Scientific No. 1

4. TITLE AND SUBTITLE

Prediction of Thunderstorm Initiation Through
4-Dimensional Data Assimilation of Doppler Radar Data

5. FUNDING NUMBERS

PE 62101F
PR 6670 TA 17 WU CA
Contract F19628-91-C-0011

6. AUTHOR(S)

Thomas M. Hamill

7. PERFORMING ORGANIZATION NAME(S) AND ADDRESS(ES)

Atmospheric & Environmental Research Inc.
840 Memorial Drive
Cambridge, MA 02139

8. PERFORMING ORGANIZATION REPORT NUMBER

9. SPONSORING/MONITORING AGENCY NAME(S) AND ADDRESS(ES)

Phillips Laboratory
Hanscom AFB, MA 01731-5000

Contract Manager: Allan Bussey/GPA

10. SPONSORING/MONITORING AGENCY REPORT NUMBER

PL-TR-92-2029

11. SUPPLEMENTARY NOTES

12a. DISTRIBUTION/AVAILABILITY STATEMENT

Approved for public release;
Distribution unlimited

12b. DISTRIBUTION CODE

13. ABSTRACT *(Maximum 200 words)*

Results from the first year of a three-year contract to prototype a local thunderstorm forecast model are presented. This model seeks to use single Doppler radar data to continuously update a mesoscale forecast model which will predict crucial thunderstorm forecast parameters.

Previous research has shown that assimilating Doppler wind information alone will not produce accurate model forecasts; a compatible temperature analysis must also be generated and assimilated alongside. We present results from an Observing System Simulation Experiment confirming these results and outlining a new assimilation and forecast system. This system will generate a quality 3-dimension wind analysis from the single Doppler radar data, and will generate a compatible temperature analysis consistent with the wind analysis. It will then use the wind and temperature analyses to continuously nudge a mesoscale model toward the evolving boundary layer wind and temperature field.

14. SUBJECT TERMS

Numerical weather prediction
Doppler radar data analysis
Mesoscale meteorology
Thunderstorm forecasting

15. NUMBER OF PAGES
92

16. PRICE CODE

17. SECURITY CLASSIFICATION OF REPORT	18. SECURITY CLASSIFICATION OF THIS PAGE	19. SECURITY CLASSIFICATION OF ABSTRACT	20. LIMITATION OF ABSTRACT
Unclassified	Unclassified	Unclassified	SAR

TABLE OF CONTENTS

LIST OF FIGURES

LIST OF FIGURES

(continued)

LIST OF FIGURES
(continued)

LIST OF TABLES

1. Introduction

Over the next few years the Air Force will modernize its base weather prediction facilities. It will install meteorological workstations to analyze and process DMSP and GOES satellites, NEXRAD Doppler radar data, and wind profiler information. The technical challenge at hand is to use this new data to improve weather forecast accuracy. To address this, the Atmospheric Prediction Branch of the U. S. Air Force Phillips Laboratory, Geophysics Directorate (PL/GPAP, or simply "PL") is developing techniques for predicting airfield weather (Chisholm et al., 1989). The goal is to develop, test, and evaluate both numerically-based and expert system procedures for the assessment, analysis, and short-range prediction of weather events critical to safe and efficient aviation activities on and around individual air bases.

One of the areas of emphasis under this program is to develop numerically-based prediction models suitable for real-time execution on a microcomputer. This technical report documents background research for a possible prototype. The intent of the current research is to demonstrate the ability to more accurately predict thunderstorm initiation by assimilating Doppler radar data into a simple mesoscale forecast model.

NEXRAD Doppler radars were primarily designed to improve the forecasting of severe weather events such as tornados or downbursts through the observation of wind shear in and around convective storms. However, Doppler radar data may still be useful in the preconvective environment. During the warm season, boundary layer radial velocities (from 3-5 cm wavelength radars) can be determined from the movement of suspended particulates such as seeds or insects (Kropfli, 1986). Since thunderstorm initiation is usually preceded by low-level convergence (Wilson and Schreiber, 1986), Doppler signatures of this convergence may also be detected in advance.

Thus, a reasonable local forecast model for the Air Force might be one that would assimilate Doppler radar data and more accurately predict the movement of the low-level convergence zones associated with

convection. Due to computational restraints, this model must be very simple. Modelling the movement of convective cells after their formation is probably beyond the computational capacity of the planned host system; this would require sophisticated physical and microphysical parameterizations. However, even a simple forecast model might reasonably predict some of the important parameters for thunderstorm formation, such as the magnitude and position of the low-level convergence zones, or the magnitude of the associated upward vertical velocity. It may be possible to get even more sophisticated. Using the model output and parcel theory, the timing and location of convective initiation may be forecast.

A previous research project funded by PL was to assimilate Doppler radar winds into a numerical model (Cotton et al., 1989). In Cotton's research, a hydrostatic version of the Colorado State University (CSU) Regional Atmospheric Modeling System (RAMS) was coded with a Newtonian nudging scheme (Stauffer and Seaman, 1990) to assimilate Doppler wind information. In this scheme the model winds were nudged to the observed Doppler radial winds. Early tests indicated no skill at forecasting convergence patterns and vertical velocities (and thus convective initiation). In a stable atmosphere, assimilation of Doppler-derived winds could force low-level convergence and upward vertical velocities. However, as soon as the assimilation stopped, the upwardly displaced parcels, now negatively buoyant, would reverse course, descending and diverging at the ground. Liou (1989) obtained similar results. Such a collapse in the convergence field does not mimic reality; Doppler observations indicate areas of convergence and upward motion generally remain so over periods of tens of minutes or hours.

The hypothesis driving Cotton et al.'s research was that convergence drives upward motion and convection. For a numerical model, this would imply that assimilating winds will improve forecasts of convective initiation. Their results indicated the hypothesized cause (convergence) and effect (buoyancy) are not so clearly delineated. Though indeed convergence may cause upward motion, frequently it is the upward motion of heated air that causes convergence in its wake. For the upward motion to persist, parcel theory asserts that the ascending air must be buoyant.

Thus, to numerically predict the initiation of convection, temperature information would need to be assimilated in addition to Doppler wind information. If a convergence zone persists, the associated temperature field should exhibit negative or neutral stability; restated, the atmosphere should be buoyant in convergence zones.

Doppler radars are unable to detect temperature. However, Gal-Chen (1978) demonstrated how the temperature structure can be inferred using the wind field and a technique involving the calculus of variations (Courant and Hilbert, 1937). If the state variables U, V, W, and their spatial and local time derivatives are known, then by using the U, V, and W equations of motion one can formulate a Poisson equation which can be solved to yield an associated temperature field. When assimilated alongside wind information, this derived temperature field, it is postulated, should thus allow more successful prediction of the convective initiation.

There is an added complication: single Doppler radars are also unable to determine three-dimensional wind velocities. Doppler radars measure radial velocity (toward / away from the radar), so a given point may need to be scanned by two or three Doppler radars to unambiguously determine wind velocity. Even then, atmospheric particles must be present as scatterers for the Doppler radar to have an acceptable signal-to-noise ratio. Since the NEXRAD network will have very little areal coverage by multiple radars, the 3-dimensional wind field must be mathematically inferred from the available 1-dimensional data. Numerous algorithms have been tried. Cotton et al. (1989) simply combined the model-generated wind field with the Doppler-observed winds, converting the model winds from U- and V-components to radial and tangential components, replacing the model radial component with the Doppler observed, and converting back. Tuttle and Foote (1990) show how boundary layer winds can be inferred from correlations of reflectivity patterns between successive radar scans. Koscielny et al. (1982) discusses the applicability of a regression technique called Velocity Volume Processing (VVP). One of these, or a combination may be used to determine a wind field suitable for Gal-Chen's thermodynamic retrieval technique and for use in a data assimilation scheme.

The current research effort, now one third complete, seeks to demonstrate the utility of Doppler radar data in forecasting convective initiation. Building on the previous work, we plan to develop a new front-end assimilation system for a mesoscale model which will allow insertion of Doppler wind information and temperature fields inferred through the Gal-Chen technique. We also plan to test this using real Doppler data. This technical report summarizes the work completed to date: first, Section 2 will give a brief summary of our documentation and integration testing of the model and its current assimilation scheme; next, Section 3 will describe some relatively simple model simulations of assimilation with and without thermodynamic observations, demonstrating the utility of a full assimilation technique. Section 4 summarizes our planned technical approach to developing a new front-end assimilation system for the mesoscale model. Section 5 provides conclusions to date.

2. Documentation and Integration Testing of the PL-3D Model

The current research effort is largely a direct follow-on to Cotton et al.'s (1989) previous work with the CSU/RAMS model. PL was given a technical report and code, but new code needs to be developed before the model will be useful for the planned Doppler assimilation study. These changes can only be made easily if the existing code is well-understood. Hence, the first steps taken were to understand and better document the model and to tailor it to run on AIMS (Air Force Interactive Meteorological System). Below, we describe the effort to document the model and then the coding and preliminary testing on AIMS.

2.1 Model Documentation

The CSU/RAMS model, as delivered, consisted of a series of loosely grouped modules containing code for initialization, advection, radiation, soil heat transfer, etc. The code was written in a version of Fortran which had a number of nonstandard extensions (activation/deactivation of lines, "include"-statement like constructs, etc.). Before compilation, a separate preprocessor (written by CSU) had to be used. Documentation was limited to a few journal articles and infrequent comments embedded in the code. We have since analyzed the basic components of the model line-by-line, documenting the algorithms used and compiling a data dictionary and calling tree. The CSU/RAMS model has been renamed "PL-3D" (Phillips Lab, 3-Dimensional) because of the extensive changes made to tailor the model to the AIMS, to add documentation to the code, and the planned addition of a new assimilation system as a front-end for the model. Henceforth it will be referred to as such. The model version used in this project is described in Cotton et al. (1989) and Gustafson et al. (1991).

2.2 Coding and Preliminary Testing on the AIMS

As received, the PL-3D model was not only in nonstandard Fortran and poorly documented, but was not ready use as an *interactive* research model. For example, the original generated plotted output as part of the execution of the model; if the users wanted to look at different cross-sections

from the output, they could only do so by re-running the model. Thus, in addition to tailoring the model to run on the AIMS and creating a scheme to convert to standard Fortran, the model was also changed to store gridded fields to hard disk, and new programs were developed to read these, generate the metacode to plot the data, and then to generate the plots, either through a user-friendly windows interface or on laser printer.

The next step was to run the model enough to establish user confidence and to duplicate previous model results at CSU. To this end, we performed a number of tests, running the model for a case of upslope convection and for a sea-breeze experiment. With the sea-breeze experiment, we were able to closely duplicate the results obtained at CSU; we are confident that the minor differences between model simulations are due only to incomplete knowledge of the initial conditions, such as soil moisture content. Figure 1 (a) shows a cross-section of potential temperature for the fourth hour of a sea-breeze simulation, generated at CSU using the RAMS model (see Cotton et al., 1989 for information on the model initial conditions and configuration). Figure 1 (b) shows the same cross-section generated from the PL-3D model on the AIMS system.

Another preliminary test was prompted by recently published research indicating that most numerical prediction models have insufficient vertical resolution when compared to their horizontal resolution (Lindzen and Fox-Rabinovitz, 1989; Persson and Warner, 1991). These studies, the first a theoretical study and the second a model test, both indicate that inadequate vertical resolution can cause excessive noise in model forecasts. Lindzen and Fox-Rabinovitz conclude that typically the strong diffusion used in numerical models suppresses the evidence of this. We tried a simple test to determine whether the accuracy of our hypothetical sea-breeze simulations would be affected by poor vertical resolution. We performed a test of the model with 10 layers in the vertical and with 25 layers. Figure 2 (a) and 2 (b) show 4-hour forecasts of the potential temperature and U/W wind vectors for a cross section through the domains of the low-resolution and high resolution runs, respectively. There are notable differences; presumably due to the higher resolution near the surface, there is much stronger cooling over the water in the high-resolu-

tion run (the water temperature is 283 K, and the surface air temperature is initialized at 297.2 K); presumably, energy transfer is more efficient. Associated with this cooling over the ocean is a stronger horizontal potential temperature gradient along the coast in the high-resolution run. However, this test showed no evidence of model degradation of the low-resolution run due to spurious noise generation.

Admittedly, this test does not offer proof that all numerical simulations can be carried out with resolutions as low as 10 vertical levels. The sea-breeze test is initialized with horizontally homogeneous temperature and wind fields, and a circulation develops simply due to the evolution of surface temperature gradients from differential heating. Problems that will occur with real models, such as gravity wave generation due to shock from ongoing data insertion are not present in this simple test. The only reasonable conclusion that should be drawn is that our sea-breeze simulations can continue with relatively low vertical resolution. This is still an important result, as the simulations described in the next chapter are again done on a hypothetical sea-breeze case.

3. Simulating the Effect of Assimilating Doppler Winds and Derived Temperature Observations

Before coding a new Doppler processing and assimilation system we demonstrate its expected benefit. Future research with real Doppler data will focus on its utility for forecasting convective initiation along a sea-breeze front. We expect to use data from the CaPE (Convection and Precipitation Experiment) conducted during the summer of 1991 in central Florida. Thus, the tests described here sought to determine the effects of different data configurations on the formation of an idealized sea-breeze front.

3.1 Previous Research

Liou (1989) has already studied the impact of derived temperature and Doppler wind assimilations on forecast accuracy, though not for a case of sea-breeze initiated convection. The non-hydrostatic CSU/RAMS model was used to test wind and temperature assimilation in the modeling of a buoyant thermal bubble. Liou assumed the Doppler data would uniquely supply the U-component winds for a model, and then the V- and W-components were derived through a variational analysis. Next, the Gal-Chen thermodynamic retrieval technique was used to create a compatible temperature field. Liou's results showed that having no knowledge of the temperature structure was indeed detrimental to forecast accuracy; when assimilating wind only, the model forecasts showed a rapid decrease of kinetic energy shortly after assimilation stopped. However, when the retrieved temperatures were also assimilated, forecast accuracy was much higher. This was so even when the wind and temperature observations were highly inaccurate.

Another interesting conclusion Liou reached was that assimilation runs with frequent updating produced more accurate forecasts than ones with infrequent updates. This contradicts previous work by other researchers (Williamson and Dickinson, 1972; Talagrand, 1972), who have found that updating too frequently can decrease accuracy because the continually shocked model can never adjust to the gravity waves created by

the data insertion. None of these studies, however, were done with a Newtonian nudging scheme. Liou simply replaces some of the model fields with observational data, and some with fields that were variationally adjusted to the observational data. Williamson and Dickinson and Talagrand similarly replace the ongoing forecast with new analyses in their studies. This replacement technique is not recommended for use in real forecast models, as the data assimilation scheme must properly use irregularly spaced observations. Thus, another question studied during our assimilation testing was the effect of noise generated by the inevitable errors in the analysis data and whether frequent or infrequent data insertion was preferable with a Newtonian nudging scheme.

3.2 Sea-Breeze Assimilation Tests Using the PL-3D Model

We have extended Liou's tests with an identical-twin Observing System Simulation Experiment for a sea-breeze case. Here we tested the utility of assimilating boundary layer wind data with and without simultaneous derived temperature observations. A 2-dimensional, dry, hydrostatic version of the PL-3D model was used for the assimilation tests. There were 25 horizontal gridpoints spaced 5 km apart, and 16 levels in the vertical between the surface and approximately 500 mb, with 250 m resolution in the boundary layer and 400 m resolution above. The date of the hypothetical experiment was July 17 at 10 AM, and the latitude 25 degrees N. The surface was half land ($X \geq 0$, 10 cm roughness length) which warms with time and half cool water ($X < 0$). The atmosphere was initialized to be horizontally homogeneous, though quickly with the integration of the model the lower layers over the water cooled, and the lower layers over the land heated rapidly due to solar insolation. This building temperature contrast drove the formation of the sea-breeze front. For the nudging experiments, the processed output from this "nature run" was used in the subsequent nudging. For example, gridpoint (2,2) at time (t) from model run (a) was used to nudge gridpoint (2,2) at time (t) for model run (b). In these experiments, we either used perfect observations, or observations with added random errors, since the main emphasis was on the nudging technique itself, and not on the characteristics of a particular data source.

Table 1 identifies a matrix of assimilation experiments that were performed. As shown in the table, the first experiment was to run the model with the true initial conditions. This ground truth nature run was initialized with cool, 283 K water, and a relatively dry soil (top layer 40 percent saturated), allowing strong heating over land. Figures 3(a) - (e) show cross-sections of potential temperature and scaled U/W wind vectors at 0, 1, 2, 3, and 4 hours, respectively. As can be seen, there is a rapid cooling of the air over the water, rapid heating over land, and the resulting start of a sea-breeze circulation which deepens and pushes 20 km onshore by the fourth hour.

Assume now that a forecast model for the sea-breeze is poorly initialized, with water temperatures specified to a warm 293 K and overly moist soil (60 percent saturated). The resulting forecast (experiment 2 in table 1) will naturally have a less intense circulation due to weaker land/sea temperature contrasts. The resulting 0, 1, 2, 3, and 4 hour forecasts are shown in Figures 4 (a) - (e). This model simulation was used as the baseline; the next four nudging experiments will be updating a model run from these initial and boundary conditions. The subsequent model forecasts will be compared to this model run to determine if their data insertion schemes provided improvement.

We now performed a set of assimilation experiments where the model was nudged using wind and temperature fields extracted from the nature run data set. The first two tests, experiments 3 and 4, compared nudging with perfect (no observation/analysis error added) wind data alone versus perfect wind and temperature data. For all nudging experiments, new nudging data was supplied from the nature run every 5 minutes through the first 2 1/3 hours of the integration. After that, forecasts proceeded without nudging to 4 hours. The difference between the nudging data and the model forecast was used to adjust the local tendencies according to the equation:

Table 1 A matrix of sea-breeze assimilation experiments.

Experiment Number	Fields Nudged	Nudging Coefficients (by level)	Comments
1	none	none	nature run
2	none	none	baseline run with warmer sea-surface temp and moister soil, yielding less sea-breeze circulation; used as initial conditions for next four experiments.
3	U	.000556 for bottom 12 levels	nudge away from exp. 2 initial conditions; wind insertion only; new data from nature run assimilated every 5 minutes; insertion stops at T=8400 sec.
4	U,T	.000556 for bottom 12 levels	nudge away from exp. 2 initial conditions; wind and temperature insertion; new data from nature run assimilated every 5 minutes.
5	U	.00556 for bottom 12 levels	nudge away from exp. 2 initial conditions; wind insertion only; same as experiment 3. only higher nudging coefficient.
6	U,T	.00556 for bottom 12 levels	nudge away from exp. 2 initial conditions; wind and temperature insertion; new data from nature run assimilated every 5 minutes.
7	none	none	new baseline run with -4°K error in low-level temperatures and 2.5 ms^{-1} offshore flow.
8	U	.000556 for bottom 12 levels	nudge away from exp. 7 initial conditions; wind insertion only; new data from nature run assimilated every 5 minutes; insertion stops at T=8400 sec.
9	U,T	.000556 for bottom 12 levels	nudge away from exp. 7 initial conditions; wind and temperature insertion; new data from nature run assimilated every 5 minutes.
10	U,T	.000556 for levels 2 and 3	same as exp. 9, except 2 levels of nudging only.
11	U,T	.000556 for bottom 12 levels	5 percent wind error and +/- 2 degree K temperature error
12	U,T	.000556 for bottom 12 levels	12 percent wind error and +/- 5 degree K temperature error
13	U,T	.000556 for bottom 12 levels	nature run data inserted every 20 minutes; 12 percent wind error and +/- 5 degree K temperature error

$$F_{tot} = F_{mod} + (X_{obs} - X_{mod}) * R * W_t * Q \qquad (3.1)$$

where

F_{tot} = $\partial X/\partial t$ = total local tendency for the gridpoint at a given timestep

F_{mod} = normal model terms of the local tendency (e.g., advection, coriolis)

X_{obs} = observed field's value for a gridpoint at time (t)

X_{mod} = model forecast value for a gridpoint at time (t)

R = nudging coefficient

W_t = weight applied to this timestep

Q = analysis quality factor

For experiments 3 and 4, the nudging coefficient was set to $5.56 * 10^{-4}$ (1/1800 sec, the same timescale as used in Cotton et al.'s (1989) tests). This coefficient was applied to the lowest 12 model levels, which contained most of the simulated circulation. W_t is 1.0 at beginning time of each new data insertion, but decreases to 0.0 at the time of the next data insertion (when it is again reset to 1.0). For all tests, the analysis quality factor is set to 1.0. For the future real Doppler data assimilation experiments, this factor will be dependent on local data quality and observational data density.

The wind-only assimilation forecasts (experiment 3) for 2, 3, and 4 hours are shown in Figures 5 (a) - (c), and the wind and temperature assimilation forecasts (experiment 4) are shown in Figures 6 (a) - (c). Visually inspecting these and comparing them against the nature run (see Figure 3) and the baseline run (see Figure 4), it is apparent that neither simulation accurately reproduces the strength of the circulation associated with the sea-breeze front, though the simulation with temperature and wind assimilation is clearly an improvement over the wind-only assimilation.

Since both model simulations produced weaker circulations than in the nature run, the next two experiments repeated experiments 2 and 3, but with a ten times higher nudging coefficient used. This should force the

model solution more toward the nature run solution during the assimilation period. The results from experiment 5 (wind only) and experiment 6 (wind and temperature) are shown in Figures 7 (a) - (c) and 8 (a) - (c), respectively. Whereas the wind-only assimilation shows little change in character with the use of a higher nudging coefficient, the wind and temperature assimilation shows a markedly different circulation pattern. In experiment 6, the resulting circulation is much stronger than in experiment 4, and the sea-breeze circulation has moved much further onshore, more so than even in the nature run.

These results illustrate the limitations of the nudging technique for cases where forecast errors are due to errors in the boundary conditions (the sea and land surface characteristics remain essentially constant throughout the simulations), rather than initial conditions in atmospheric temperatures and winds. Though the wind and temperatures can be nudged away from the conditions in the baseline run, there is a restoring force attempting to counteract the nudging. For example, even though the atmosphere is cooled over the ocean by nudging, the warm ocean water reheats the boundary layer air after the nudging has stopped. It should also be noted that the size of the error in water temperature (10 K) was rather large, representing an extreme case. In this case, a stronger nudging coefficient does not necessarily yield a better forecast, even when noise and model shock are nonexistent, as they were for these tests. The stronger nudging coefficient in experiment 6 produced a stronger circulation than in its weaker twin, experiment 4, but the position of the sea-breeze front was much worse in experiment 6.

To test the effect of temperature data in a more realistic scenario, we conducted a set of experiments where the model was initialized with incorrect *atmospheric* conditions. For these experiments, the boundary layer is set too cold (293.2 K surface temp, 4 K lower than in the nature run). Similarly, there is a wind error, with a 2.5 ms^{-1} offshore flow in the low layers, as compared to no wind in the nature run. Experiment 1 is still the nature run and ground truth. Experiment 7 is the new baseline case, integrating the model with the faulty initial conditions and no data assimilation. The 0-4 hour output is shown in Figures 9 (a) - (e). Compared

with the nature run in Figure 3, the baseline run has a weaker circulation, and the sea-breeze front is displaced toward the coast.

Uncorrupted nature run data from experiment 1 were now used to nudge the model away from the initial conditions of experiment 7. For experiment 8, only winds were nudged. For experiment 9, both winds and temperatures were nudged. In both experiments, the nudging coefficients were set to $5.56 * 10^{-4}$ for the bottom 12 layers. The 2, 3, and 4-hour forecasts from these two assimilation experiments are shown in Figures 10 (a) - (c) and Figures 11 (a) - (c), respectively. Whereas the wind-only experiment looks very similar to the baseline experiment, the wind and temperature assimilation is much closer to the nature run; the circulation center is nearly as far inland, and the strength of the circulation is quite similar to that of the nature run. Presumably the poorer results from the wind-only assimilation experiment are due to less frontogenetical forcing due to cooler temperatures over land. This test more conclusively demonstrates the potential benefit of temperature in addition to wind data assimilation.

Since our planned Doppler data assimilation system is likely to determine winds for only one level (in the boundary layer), the above temperature/wind experiment certainly overstates the potential benefit of additional temperature data, where all of the lowest 12 layers were nudged. The next test, experiment 10 in Table 1, thus nudged only layers 2 and 3 in the model, simulating this limited effect of Doppler data insertion. The model output for hours 2, 3, and 4 of this integration is shown in Figures 12 (a) - (c). As shown, the results appear to compare favorably with the full wind/temperature assimilation experiment. With the low-level temperature forcing captured, the circulation was quite similar to that from experiment 3, the wind and temperature nudging for the full boundary layer. Experiment 10 did show a slight displacement of the circulation toward the coast and an anomalously strong return flow aloft.

Still, these results may again overstate the beneficial effect of temperature assimilation. So far, only *uncorrupted* nature run data has been used for nudging. During real assimilation, the analyses we nudge to may be noisy and have errors. If these errors are large, then they could

potentially overwhelm the benefit of nudging by inducing spurious gravity waves. In experiments 11 and 12, we generated random noise to add to the nudging data in a similar way Liou did in his thesis. For each point in the domain and for each time slice, a random error is created and added to the nudging data generated by the nature run. In experiment 11, the U-component error is a random number +/- 5 percent of the original windspeed, and the temperature error is +/- 2°K. In experiment 12, the windspeed error is +/- 12 percent, and the temperature error is +/- 5 K. A standard 5-point horizontal smoothing filter is applied to the fields to roughly approximate the effect of doing an analysis of these simulated observations. For comparison with the ideal nudging simulation shown in Figures 11, the full 12 levels are nudged for 2 1/3 hours every 5 minutes with the same $5.56 * 10^{-4}$ nudging coefficient.

Figures 13 (a) - (c) show the model output for experiment 11 at the 2, 3, and 4-hour points. Though the field appears to be dominated by noise at the two-hour point, by the third hour the original sea-breeze signal is apparent, and even at 4 hours the final forecast still closely resembles the best-case scenario shown in Figure 11. For experiment 12, the noise is still greater, but the important dynamics are still preserved for the forecast period, as shown in Figures 14 (a) - (c). For this sea-breeze simulation, what appears to be important is to capture the differential surface heating; even with noise, as long as this heating is captured, the circulation pattern is better defined.

An associated question that arises when noisy data are used is whether forecasts will be more accurate if winds are assimilated less often, presumably to allow more time to adjust to the shock of each data insertion. The next experiment was designed to yield some answers to this question. Rather than nudging to new data every five minutes, in experiment 13 new nudging data is supplied every twenty minutes. The same nudging coefficient, $5.56 * 10^{-4}$, is used. The results from this assimilation test are shown in Figures 15 (a) - (c). As compared with the 5-minute experiments, the temperature field appears to be less well forecast, but the wind field appears quite similar.

A quantitative assessment was now sought to determine the relative forecast accuracies for experiments 12 and 13. Temperature and U and W-component wind biases and root mean square error statistics were generated for the 3- and 4-hour forecasts for each of the assimilation experiments. In order to emphasize the differences in circulation around the sea breeze, calculations were only done on part of the domain. The sample area was from X= -5 km to X = 40 km, and from levels 1 to 12 in the Z-direction (approximately 0 to 3300 m). This is well-centered around the circulation in the nature run. Table 2 gives statistics for the 3-hour forecasts, and Table 3 for the 4-hour forecasts.

As can be seen by comparing the results from experiments 12 and 13, the U and W wind forecasts are less accurate for the 20-minute data assimilation. For example the 3-hour W-component RMS is 2.14 cm s^{-1} for experiment 12 and 3.11 cm s^{-1} for experiment 13. One should be conservative in drawing conclusions from such a limited test. Another test we performed, but did not show, nudged the model very heavily for one timestep and then did not nudge again for 5 or 20 minutes. In this test, the 20-minute nudging outperformed the 5-minute nudging. However, one possible explanation for the better performance of experiment 12 (5 minute) over experiment 13 (20 minute) is the lack of adjustment with shorter assimilation period. Adjustment to meteorological features is desirable, but adjustment to noisy patterns is not. Perhaps the less frequent nudging allows more time for the model solution to readjust mass and wind fields to be compatible with the error-filled nudging data. Conversely, with more frequent updates and assuming no correlation between the error from one nudging timestep to the next, the model is less likely to readjust mass and wind to the erroneous nudging data. Clearly, however, there is not yet enough definitive evidence to recommend either frequent or infrequent nudging. Since Doppler data observations are generally available every 5 minutes, we will continue to plan to nudge this often.

Let us use the Tables 2 and 3 for a last quantitative assessment of the full suite of experiments. We will consider two groups, the first group with experiments 2-6, initialized with errors in the boundary conditions,

Table 2: 3-hour sea-breeze forecast statistics. Temperature errors are in Kelvins, and wind errors in meters per second.

Experiment	Bias Temp.	Bias U-comp.	Bias W-comp.	RMS Temp.	RMS U-comp.	RMS W-comp.
1 (ground truth)	0.0	0.0	0.0	0.0	0.0	0.0
2 (baseline)	0.737	0.354	0.00755	1.170	1.370	0.049
3 (U only)	0.753	0.312	0.00813	1.20	1.20	0.0473
4 (U and T)	0.517	0.177	0.00526	0.794	0.693	0.0344
5 (U heavy)	0.776	0.283	0.0098	1.23	1.06	0.0483
6 (U, T heavy)	0.0344	0.0613	0.00249	0.562	0.424	0.0265
7 (new baseline)	1.56	1.46	0.00224	2.01	1.57	0.0347
8 (U only)	1.26	0.634	0.00608	2.08	0.836	0.0311
9 (U and T)	-.0253	0.505	0.00186	0.256	0.545	0.0139
10 (low-level)	0.606	1.05	-.00346	0.828	1.25	0.0370
11 (5 % err)	-.0252	0.497	0.00469	0.256	0.542	0.0164
12 (12 % err)	-.0199	0.485	0.00931	0.270	0.546	0.0214
13 (20 min)	0.154	0.512	0.0107	0.384	0.645	0.0311

Table 3: 4-hour sea-breeze forecast statistics. Temperature errors are in degrees Kelvin, and wind errors in meters per second.

Experiment	Bias Temp.	Bias U-comp.	Bias W-comp.	RMS Temp.	RMS U-comp.	RMS W-comp.
1 (ground truth)	0.0	0.0	0.0	0.0	0.0	0.0
2 (baseline)	0.871	0.620	0.00781	1.31	2.21	0.0790
3 (U only)	0.883	0.598	0.00866	1.33	2.16	0.0791
4 (U and T)	0.728	0.395	0.00748	1.07	1.48	0.0678
5 (U heavy)	0.900	0.588	0.00972	1.36	2.13	0.0803
6 (U, T heavy)	0.626	0.223	0.00666	0.98	1.21	0.0771
7 (new baseline)	1.49	1.56	0.00214	1.88	1.84	0.0612
8 (U only)	1.20	0.842	0.00502	1.98	1.27	0.0532
9 (U and T)	-.0676	0.632	-.00069	0.254	0.751	0.0331
10 (low-level)	0.582	1.11	-.00437	0.808	1.40	0.0524
11 (5 % err)	-.0747	0.636	0.00158	0.251	0.762	0.0318
12 (12 % err)	0.0811	0.640	0.00538	0.260	0.793	0.0307
13 (20 min)	0.105	0.700	0.00300	0.364	0.892	0.0358

and the second group, experiments 7-13, initialized with errors in the atmospheric conditions. For the first group, there was only a small fractional improvement in the forecast of vertical velocities when assimilating temperature data (experiment 4). Here we see the vertical velocity error is 6.78 cm s^{-1}, whereas it was only fractionally larger, 7.90 cm s^{-1}, for the baseline case. Similarly undramatic improvements were noted for the temperature and U-component errors. However, it is worth noting that experiment 3, with wind nudging only, produced consistently worse forecasts than experiment 4, with wind and temperature assimilation. As mentioned earlier, the generally small improvement in forecast skill for experiments 3-6 are likely due to building errors into the fixed boundary conditions, the water temperature and soil moisture. A certain weak sea-breeze circulation is all that could be dynamically expected from the resulting small land-sea temperature contrast. Though nudging could force the model away from this weak circulation, the preferred model state dynamically reasserted itself after nudging stopped. It is realistic to expect some of these errors to occur in real models; however, as a test, it did not fully illuminate the question of the benefit of temperature assimilation.

Experiments 7-13 were tests of the effect of assimilation on correcting errors in atmospheric conditions. With no errors in the fixed boundary conditions, the issue of wind only versus wind/temperature assimilation could be more properly explored. Comparing the wind-only assimilation statistics of experiment 8 to the wind and temperature of experiment 9, the potentially dramatic improvement afforded by temperature assimilation is apparent; wind errors are roughly half the magnitude of the baseline experiment's errors. Interestingly, however, for experiment 10, where only low-level information was assimilated, the errors indicate considerably less forecast skill than are achieved with full data assimilation. This is somewhat of a surprise because the visual pattern of the sea-breeze circulation seems to be well-reproduced, as shown in Figure 12. The last three experiments, illustrating the effects of assimilating error-filled data, show that the model has resiliency and can quickly adjust to eliminate gravity wave noise, though possibly less so with infrequent data insertion.

Figure 16 illustrates one last way of viewing the model errors. In this scatterplot, the error in the maximum vertical velocity and the error in position of the maximum vertical velocity are plotted for the four-hour forecasts. To emphasize vertical positioning errors, the vertical error is scaled by a factor of 25 (i.e., a 500 m vertical error would be equivalent to a 12.5 km horizontal error). This scatterplot is directly generated from gridded data, and thus some of the subtlety that can be seen in the model output is lost here. However, some important points can be made. First, experiments 9 and 10 both showed very favorable accuracy in the position and strength of the vertical motion field, and the experiments with the induced errors were all slightly less accurate. We do not believe much should be read into the lower vertical velocity error for experiment 13 as compared with experiment 12; when viewing the overall circulations (see Figures 14 and 15) it is clear that experiment 12's circulation is slightly better forecast. Another obvious conclusion: all of the wind/temperature assimilations (experiments 9-13) from the second baseline were more accurate than the wind assimilation alone (experiment 8).

4. Technical Approach to the Development of a New Doppler Data Assimilation System for the PL-3D Model

Results from the sea-breeze forecast experiments in Section 3 reinforced Cotton et al.'s (1989) and Liou's (1989) conclusion that to be successful in forecasting thunderstorm formation, temperature as well as wind information must be assimilated. We now specify some other desired qualities of a data assimilation system and propose a design which will produce these qualities.

First, the data assimilation system must produce highly accurate, three-dimensional, gridded wind analyses derived from the Doppler radar data. Not only are the quality wind fields needed for nudging, but these quality winds are also needed to derive the temperature fields using the Gal-Chen technique. Of course this is problematic, since Doppler data measures instantaneous radial velocities along an altitiude-varying scan, not the desired smooth (time-averaged) three-dimensional gridded wind velocities. Further, Doppler velocities usually can only be measured with an acceptable signal-to-noise ratio when there are scatterers in the boundary layer. Thus, the proposed assimilation system must thus be able to filter, process, coordinate-convert, and grid the raw Doppler data.

Second, as discussed in Chapter 3, noisy fields are not desired. Noisy fields will shock the model, generating spurious gravity waves and degrading forecast skill. Liou's theoretical experiments demonstrated that it is preferable to insert new Doppler observations as frequently as possible. However, previous studies (Williamson and Dickinson, 1972) using direct insertions and synoptic-scale models conclude that the model needs time to adjust to the newly inserted data; updating too frequently may degrade forecast quality through the excessive generation of noise with little time for adjustment. Hence, if the noise can be controlled, more frequent data insertions should be possible. Our own tests using Newtonian nudging showed that even in a noisy environment, more frequent updates are indeed preferable.

Our proposed design, shown in Figure 17, incorporates these desired qualities. In this diagram, the boxes represent processes, or algorithms that need to be coded or adapted from existing programs. The parallel lines indicate "data stores," the input, intermediate, and output data flowing into and between the processes.

Consider first the need for quality wind analyses. The code in the top half of Figure 17 is devoted to producing this. The processes are described individually in the following sections.

4.1 The TREC Processor

TREC is the Tracking of Radar Echoes by Correlation, a method described in Tuttle and Foote (1990). This procedure separates a volume slice of the Doppler reflectivities into small blocks, and then attempts to find the best correlation between patterns from one time slice to the next. In a preconvective environment, tracers should advect with the wind, and general patterns of these tracers preserved. Knowing this, the most highly correlated pattern for a box in time slice (2) should mark the wind displacement from the starting box in time slice (1). This concept is illustrated in Figures 18 and 19, taken from Tuttle and Foote's article. Figure18 illustrates the computed TREC vector identified with a maximum correlation. Figure 19 illustrates a typical 2-D plot of correlation coefficients between the original box and surrounding boxes. The displacement vector (i.e., the horizontal wind vector) is from the original box to the coordinates with the highest correlation coefficient.

The main advantage of the TREC scheme is the ability to determine both U and V components of the wind, not just a radial component. However, the scheme is computationally expensive. Another disadvantage is its large sensitivity to noisy data and ground clutter. At long ranges, the Doppler radar is looking at the top of or above the boundary layer, even when scanning at low elevation angles. With fewer aerosols aloft, the signal-to-noise ratio decreases, and the returned velocities are more suspect. To account for this, derived wind observations with low correlation (< 0.25) and high local standard deviations ($> 10\text{-}15\ m^2s^{-2}$) are removed.

Similarly, close to the radar ground clutter is a problem; areas with ground clutter should have small displacement vectors and high correlations (e.g., a hill looks the same from scan to scan). Some of these erroneous points are thus removed by imposing a maximum allowable correlation coefficient. The authors selected a correlation coefficient of 0.7 as their upper threshold. This eliminated many bad observations, but there were still several observations with zero displacement that were surrounded by areas with strong radial velocities. One last constraint was imposed: the absolute difference between the TREC-derived velocity and the radial velocity was given an upper bound of 3 ms^{-1}. After imposing these constraints, the resulting wind field is generally now high-quality.

The TREC code was received from the authors and studied, but it has not yet been tailored to work on AIMS. The previous code was designed to be used on an Alliant minisuper or a Cray, and some redesign may be necessary. After conversations with its primary author, Mr. Tuttle, however, we believe that transporting his code to the AIMS VAX computers should not be too burdensome; there are command scripts to define the input data and set up the TREC code for execution that are now in UNIX and will need to be converted to VAX/VMS. Also, there are calls to GKS and NCAR Graphics utilities, but these software libraries should be standard from one computer to the next. Doppler velocity unfolding will likely not be necessary since the fields of interest are the comparatively slow boundary layer winds.

We do hope this method can be used as one of the wind sources for the assimilation since it will generate both U and V components of the wind, something the next processing algorithm will not.

4.2 Adjustment of Model Radial Velocities to Doppler Measurements

A simple way of deriving a new wind field is to directly modify the model winds to match the newly observed Doppler velocities (Figure 20). Of course, only radial velocities are observed, so the information will not be complete. We expect to preprocess the Doppler data using NCAR-supplied CEDRIC software (Mohr et al., 1986) to convert the radial components to a

Cartesian grid. Since Doppler observations are non-simultaneous, during this step the observations will also be interpolated to be valid at the same time. We may also filter or smooth the data in space and/or time to yield a less noisy field.

With the radial wind components gridded, the model-supplied winds can also be converted to radial and tangential components, and the model radial component replaced. This will then provide another set of wind observations for the next step, the objective analysis.

4.3 Objective Analysis

An appropriate next step is to combine all wind observations into one analysis that can later be used for the thermodynamic retrieval and nudging. There are likely to be two sources of winds: (1) the TREC-derived winds (see Section 4.1), and (2) the Doppler-modified model winds (see Section 4.2). The former provides useful information on both radial and tangential wind components, and the latter should accurately depict the radial wind component. A successive corrections objective analysis scheme will be used for this purpose. This may be based on the Cressman scheme (Cressman, 1959; Benjamin and Seaman, 1985) or the Barnes scheme (Barnes, 1964; Barnes, 1973).

The desired outputs are: (1) a relatively noise-free analysis and, (2) a an analysis quality factor for each point. The former will be used in the thermodynamic retrieval and nudging scheme. The latter will be used only in the nudging scheme; the weight given to the nudged analysis will be a function of this analysis quality; where the wind observations were frequent and reliable, the quality factor will be high, and the model will be strongly nudged toward the wind analysis; conversely, where the wind observations were sparse, the model will be nudged lightly.

4.4 Noise Suppression / Computation of W

In this step the objective analysis of the horizontal wind velocities may be smoothed. Also, the vertical velocity W will be calculated from the

result by upwardly integrating the continuity equation, analogous to how it is calculated in the PL-3D model. The smoothing step may not be necessary, or may be more properly placed after the dynamic retrieval step. However, if the objective analysis is still noisy, the resulting vertical velocity may have unrealistic magnitudes and spatial distribution. If this turns out to be the case, we may either apply a simple smoother to the analysis, or impose constraints of smoothness and physical reasonableness on the vertical velocity field and adjust the horizontal velocities accordingly. A variational method might be used in the latter case.

It is possible that smoothing could do as much damage as good. As will be discussed later, the Gal-Chen retrieval may lose accuracy with a priori smoothing. Also, if thunderstorms are likely to be initiated only with a strong vertical velocity, such as would be necessary to break a capping inversion, then the smoothing may well dampen these features excessively. On the other hand, a Newtonian nudging scheme which nudges toward a noisy analysis may generate spurious vertical velocities and thus inaccurately forecast thunderstorm formation. Ideally, we would like to design a scheme which will control noise but leave important meteorological features intact.

4.5 Get Time Rates of Change

The Gal-Chen dynamic temperature retrieval technique, discussed in 4.7 below, will require not only the U, V, and W fields, but their local time derivatives as well. To derive this field, U, V, and W will be needed at time (t) and time (t-1). Using the latest and the previous iteration's U, V, and W fields (see 4.6), the time rates of change will be calculated. It is noted here that the calculation of the time derivative will not be centered in time, but will be backwards in time; i.e., the fields are available at time (t) and time (t-1), and the derivative will be estimated for time (t). It would be more proper to estimate the time derivative using times (t+1) and (t-1), but the design will not permit this, since the adjustment of model radial velocities to Doppler measurements (see 4.2) is performed on the latest available data, which is time (t) data. We hope the error of this approximation will be minimal.

4.6 Store Winds for Next Timestep's Rate of Change Calculation

This step stores the data so at the next time step this data will be available to step 4.5 (see above) as the (t-1) field.

4.7 Gal-Chen Dynamic Temperature Retrieval

With the latest U, V, and W fields and their time derivatives computed, a compatible temperature field can now be retrieved. We expect the Gal-Chen (1978) technique will be used. Rather than explaining the technique in detail here, the reader is referred to Gal-Chen's article, or a succinct summary by Hane et al. (1988). Basically, the U- and V- equations of motion are used to formulate a Poisson equation, which can be solved to yield pressure perturbations. With the pressure perturbation calculated, the third equation of motion is used to calculate a horizontal buoyancy deviation, from which the potential temperature deviation can be calculated. Adding the potential temperature deviation to the horizontal mean thus creates a temperature field suitable for use in nudging.

Gal-Chen's technique has now been widely tested and used (Hane et al., 1981; Gal-Chen and Hane, 1981; Mohr et al., 1986; Hane et al., 1988; Liou, 1989) with generally positive results. However, we believe our application will be one of the first to try to use single Doppler radar data to determine the input wind field to the retrieval. This may pose some difficult problems. As Gal-Chen (1978) mentions, there are many nonlinear terms to calculate for the retrieval (e.g., dU/dX*dU/dy) which are more accurate when calculated directly from the wind data and then interpolated to a grid rather than calculated on a grid; the interpolation to a grid is in effect a priori smoothing, which can decrease accuracy. Our proposed technique may seem inconsistent; we plan to determine wind observations, grid them through an objective analysis, and calculate the nonlinear terms on the cartesian grid. We believe that this is nonetheless necessary. Calculation in "observation space" is much more easily done with multiple Doppler radar data than with single Doppler. To make up for the information loss of the second radar, we plan to use multiple techniques

to generate wind observations (see Sections 4.1 and 4.2 above). Calculating nonlinear interactions in observation space could be done on either set of observations, but not both simultaneously; there would doubtlessly be inconsistencies between the nonlinear terms calculated from each data set. Performing an objective analysis first yields one unique wind field from the two sets of observations, one we presume will be more accurate than either alone. We hope the added accuracy of the wind field will offset any errors due to the a priori smoothing.

4.8 Newtonian Nudging of U, V, and T

Equation 3.1 gives the standard equation used for Newtonian nudging schemes. As shown, the accumulated forcing function is incremented by a value proportional to the difference between the observed value and the model forecast value. With U, V, and T analyses now calculated, this difference can also be calculated.

It is likely that the differences will also be weighted by an analysis quality factor, calculated during the objective analysis. This factor will indicate how many observations were used in the Doppler analysis for each gridpoint and their quality. For example, the more observations, the higher quality the analysis, and thus the greater weight that should be given to the analysis at this point. Conversely, in data-sparse areas, even if the analysis indicates notably different winds than from the model forecast, the model should not be nudged heavily because of a presumed lower analysis quality. An analysis quality factor permits the Newtonian nudging scheme to properly weight the data according to quality.

Finally, with the differences calculated, they are now used in the Newtonian nudging scheme to nudge both the horizontal winds and temperature field. As explained in Chapter 3, this simultaneous nudging of temperature and wind fields should improve the chances of successfully forecasting convective initiation.

5. Conclusions

The first year of work on a local thunderstorm forecast model which assimilates Doppler radar data is now complete. The project is on schedule, with some notable accomplishments.

(a) The CSU/RAMS model has now been successfully converted to run on the AIMS computer system. Whereas the version given to us required plots to be generated as part of the model execution, the model has now been recoded to store data to disk. We also have a suite of new interactive display routines available for interpreting this stored output.

(b) A series of assimilation experiments were performed which verified the need for temperature as well as wind assimilation to forecast convective initiation, as had been suggested in previous research.

(c) Development of a sophisticated front-end data assimilation system is underway. After a careful literature search, we have designed a new system which should produce high-quality wind and temperature analyses, suitable for use in a Newtonian nudging scheme. The proposed design largely uses off-the-shelf technology.

During the next year we will be piecing together and testing this assimilation system, and time permitting, testing the model with real Doppler data from the CaPE experiment.

6. References

Barnes, S.L., 1964: A technique for maximizing details in numerical weather map analysis. *Journ. Appl. Met.*, **3**, 396-409.

Barnes, S.L., 1973: Mesoscale objective map analysis using weighted time-series observations. *NOAA Technical Memorandum NSSL-62.* National Severe Storms Laboratory, Norman, OK, 60 pp.

Benjamin, S.G., and N.L. Seaman, 1985: A simple scheme for objective analysis in curved flow. *Mon. Wea. Rev.*, 113, 1184-1198.

Chisholm, D., Bohne, A.R., and Dyer, R., 1989: The development of numerically-based and expert system approaches for airfield nowcasting/very short range forecasting. *Preprints, 3rd Conf. Aviation Weather Systems.* Amer. Meteor. Soc., Boston, MA.

Cotton, W.R., R. McAnelly, C. Tremback, and R. Walko, 1989: A dynamic model for forecasting new cloud development. *AFGL Tech Report 89-0011*, Phillips Laboratory, Hanscom AFB, MA 01731, 81 pp. ADA213939

Courant, R., and D. Hilbert, 1937: *Methods of Mathematical Physics, Vol. I.* Reprinted in 1989 by John Wiley and Sons, NY, 559 pp.

Cressman, G P., 1959: An operational objective analysis system. *Mon. Wea. Rev.*, **87**, 367-374.

Gal-Chen, T., 1978: A method for the initialization of the anelastic equations: implications for matching models with observations. *Mon. Wea. Rev.*, **106**, 587-606.

Gal-Chen, T., and Hane, C.E., 1981: Retrieving buoyancy and pressure fluctuations from Doppler radar observations: a status report. *Atmospheric Technology, volume 13: Recent Progress in Radar Meteorology*. NCAR, Boulder, CO. 98-104.

Gustafson, G.B., Moncet, J.-L., Ivaldi, C.F., Huang, H.-C., and Sparrow, J. M., 1991: Mesoscale prediction and satellite cloud analysis for advanced meteorological processing systems. *PL-TR-91-2008*, Phillips Laboratory, Geophysics Directorate, Hanscom AFB, MA 01731. 112 pp. ADA240510

Hane, C.E., Wilhelmson, R.B., and Gal-Chen, T., 1981: Retrieval of thermodynamic variables within deep convective clouds: experiments in three dimensions. *Mon. Wea. Rev.*, **109**, 564-576.

Hane, C.E., Ziegler, C.L., and Ray, P.S., 1988: Use of velocity fields from Doppler radars to retrieve other variables in thunderstorms. *Chapter 13, Instruments and Techniques for Thunderstorm Observation and Analysis*. Ed. by Edwin Kessler, University of Oklahoma Press, Norman, OK, 1988. 268 pp.

Huang, H.-C., and Preston, M., 1991: *Internal Report of Project P393: Module's Description of the PL-3D Model*. Atmospheric and Environmental Research, Inc., Cambridge, MA 02139.

Kropfli, R.A., 1986: Single Doppler radar measurements of turbulence profiles in the convective boundary layer. *Journ. Atmos. Ocean. Tech.*, **3**, 305-314.

Liou, Y.-C., 1989: Retrieval of three-dimensional wind and temperature fields from one-component wind data using the four-dimensional data assimilation technique. M.S. Thesis, University of Oklahoma, 112 pp.

Lindzen, R.S., and Fox-Rabinovitz, M., 1989: Consistent vertical and horizontal resolution. *Mon. Wea. Rev.*, **117**, 2575-2583.

Mohr, C.G., L.J. Miller, R L. Vaughan, and H.W. Frank, 1986: The merger of mesoscale data sets into a common cartesian format for efficient systematic analyses. *J. Atmos. Ocean. Tech.*, **3**, 143-161.

Persson, O., and T.T. Warner, 1991: Model generation of spurious gravity waves due to inconsistency of vertical and horizontal resolution. *Mon Wea. Rev.*, **119**, 917-935.

Stauffer, D.R., and N.L. Seaman, 1990: Use of four-dimensional data assimilation in a limited-area mesoscale model. Part I: experiments with synoptic-scale data. *Mon Wea. Rev.*, **118**, 1250-1277.

Talagrand, O., 1972: On the damping of high-frequency motions in four-dimensional data assimilation of meteorological data. *J. Atmos. Sci.*, **29**, 1571-1574.

Tuttle, J.D., and G B. Foote, 1990: Determination of the boundary layer airflow from a single Doppler radar. *Journ. Atmos. Ocean. Tech.*, **7**, 218-232.

Williamson, D.L., and R.E. Dickinson, 1972: Periodical updating of meteorological variables. *J. Atmos. Sci.*, **29**, 190-193

Wilson, J.W., and W.E. Schreiber, 1986: Initiation of convective storms at radar-observed convergence lines. *Mon Wea. Rev.*, **114**, 2516-2536.

(a)

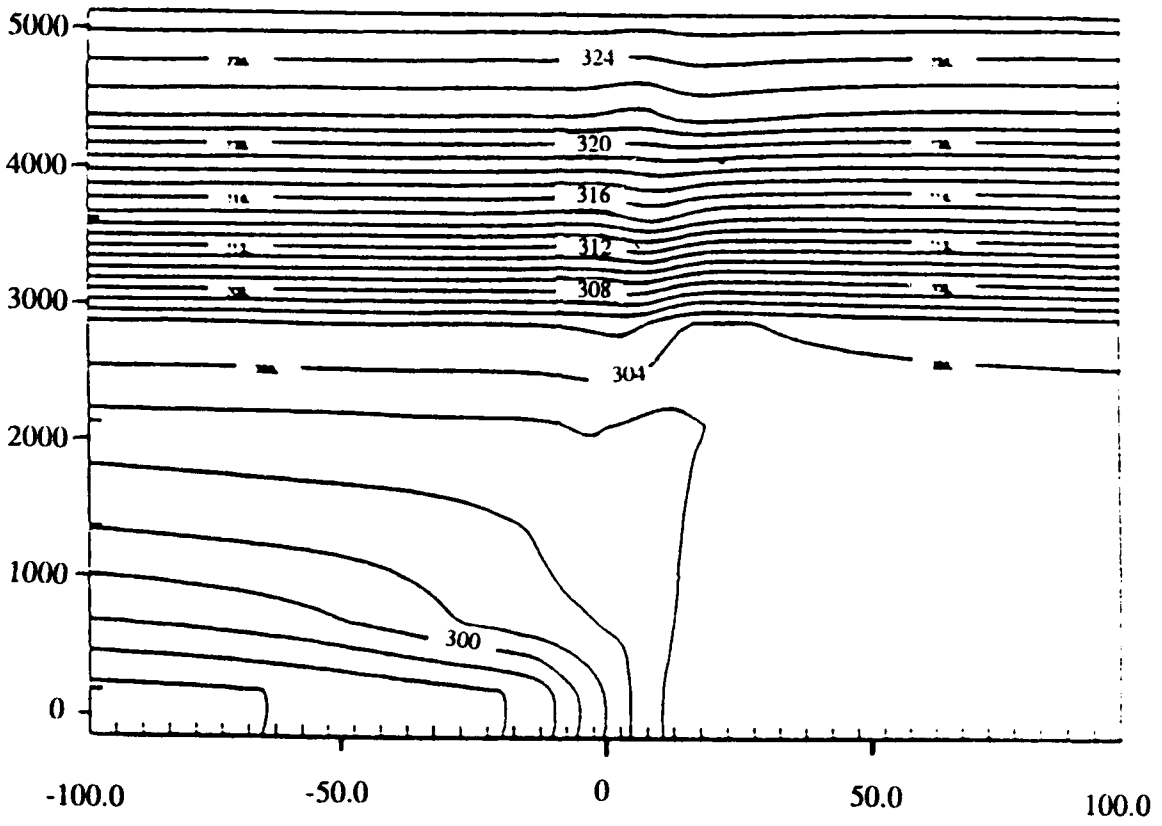

Figure 1: Intercomparison of sea-breeze potential temperature forecasts generated (a) by CSU/RAMS (from AFGL-TR-89-0011), and (b) by the PL-3D model with similar initial conditions.

(b)

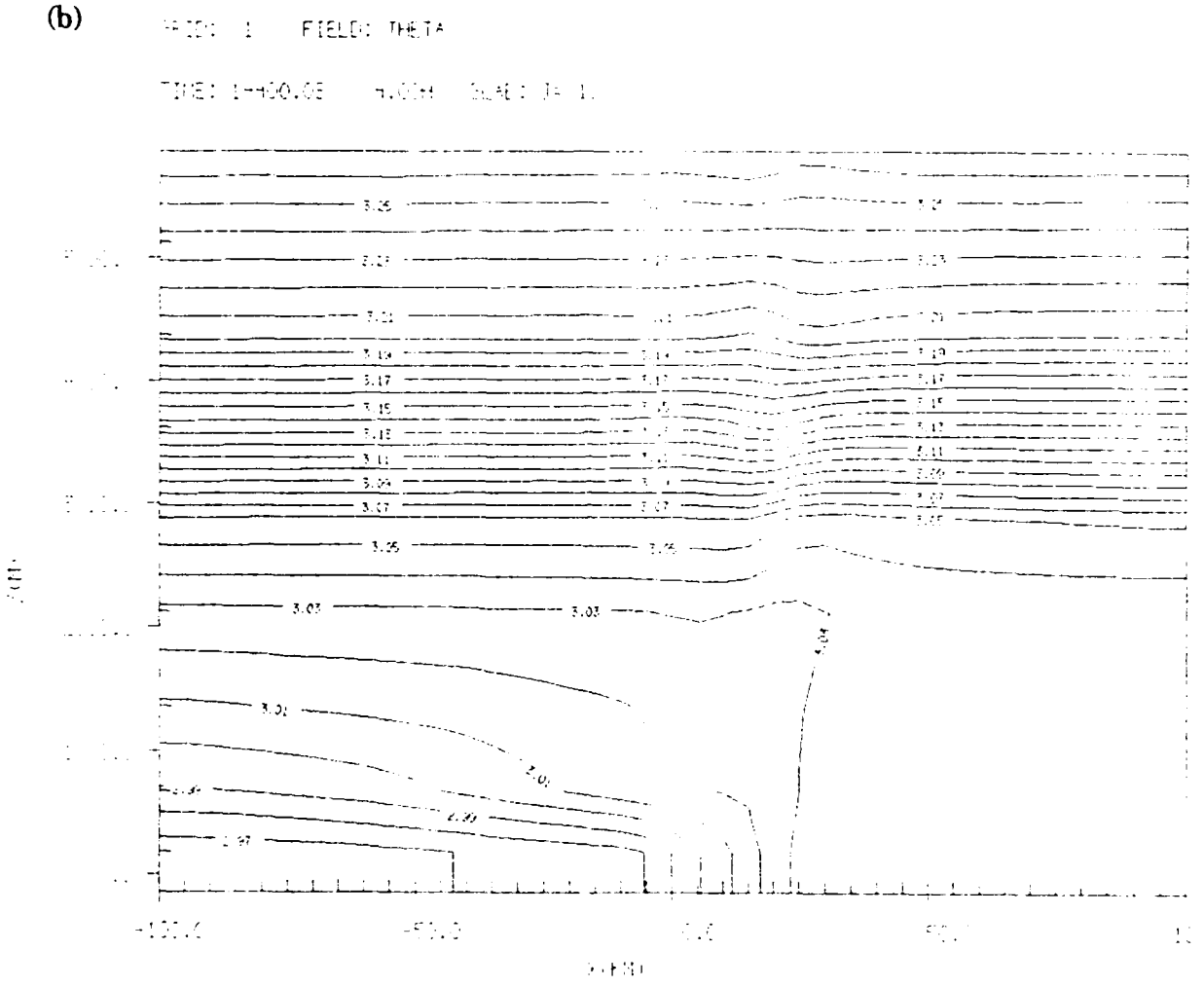

Figure 1(b)

(a)

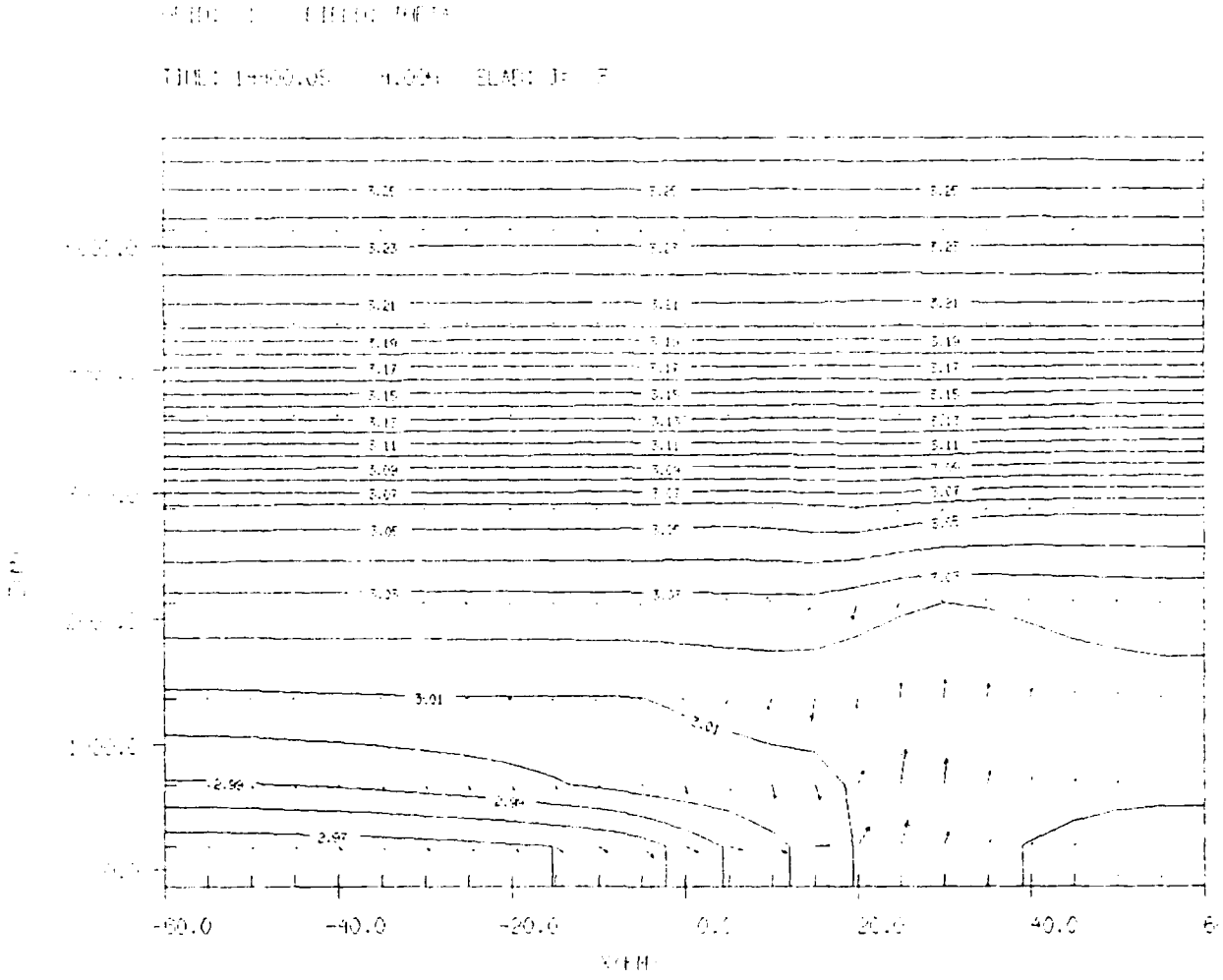

FROM 2.94 TO 3.26 BY .01 LABELS * 100

Figure 2: Intercomparison of 4-hour potential temperature and wind forecasts for low- and high-vertical resolution runs of a hypothetical sea-breeze case: (a) 10 layer model output, and (b) 25-layer model output.

(b)

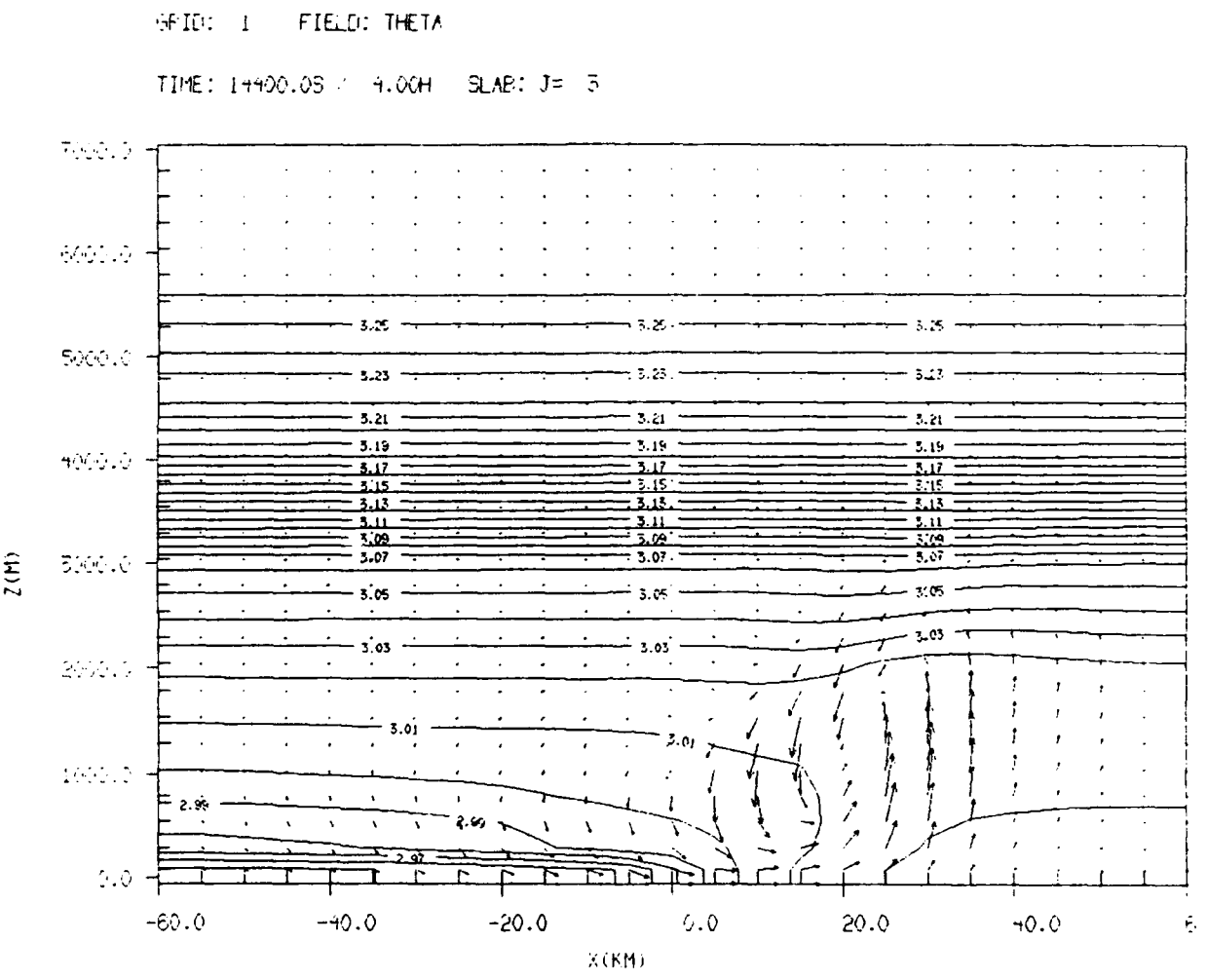

FROM 2.94 TO 3.26 BY .01 LABELS * 100

Figure 2(b)

(a)

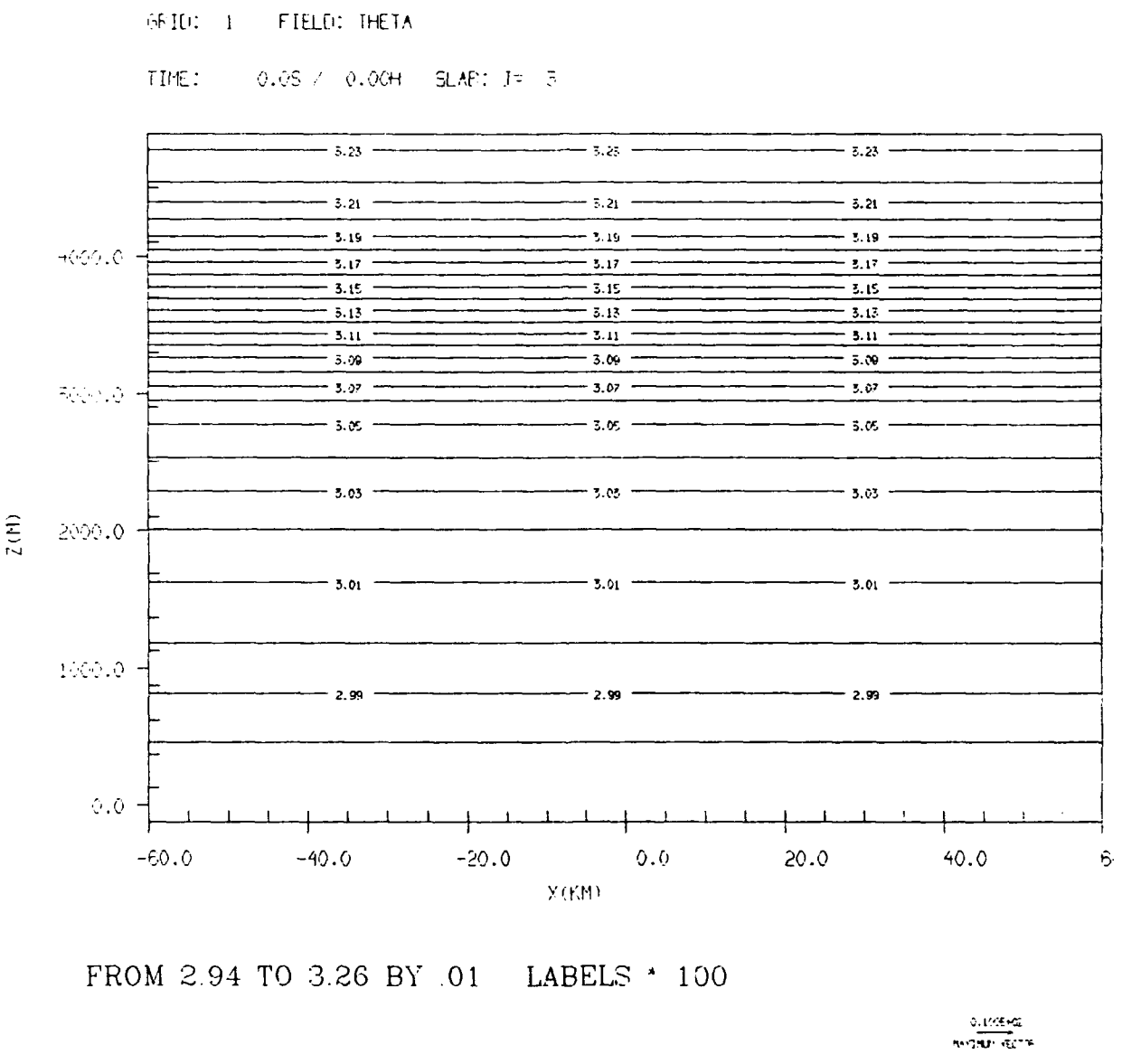

Figure 3: Output from Experiment 1. Nature run model simulation of the evolution of potential temperature and winds for a hypothetical sea-breeze case. (a) 0-hour forecast, (b) 1-hour, (c) 2-hour, (d) 3-hour, (e) 4-hour.

(b)

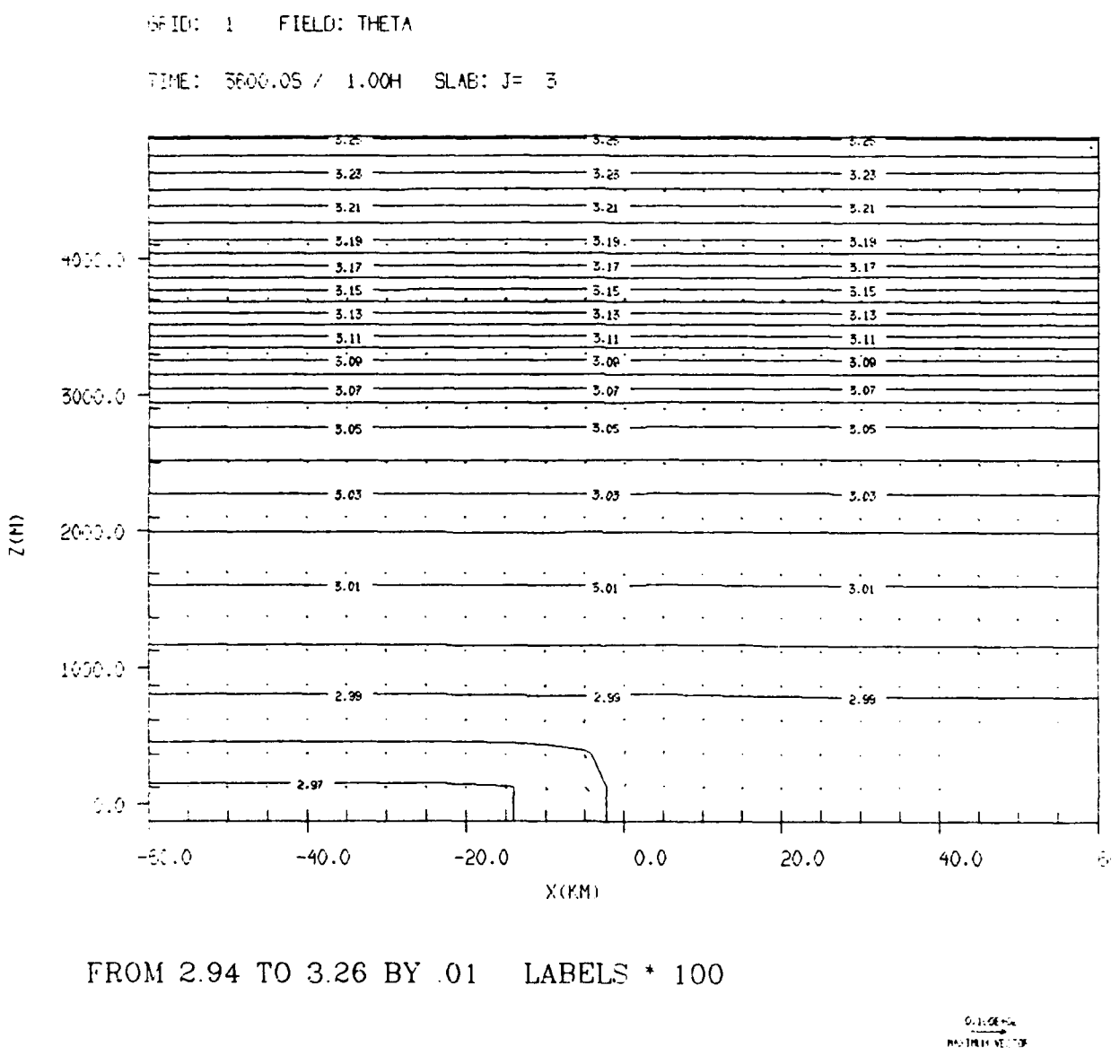
GRID: 1 FIELD: THETA
TIME: 3600.0S / 1.00H SLAB: J= 3
3.23
3.21
3.19
3.17
3.15
3.13
3.11
3.09
3.07
3.05
3.03
3.01
2.99
2.97
4000.0
3000.0
2000.0
1000.0
0.0
Z(M)
-60.0
-40.0
-20.0
0.0
20.0
40.0
X(KM)
FROM 2.94 TO 3.26 BY .01 LABELS * 100

Figure 3(b)

(c)

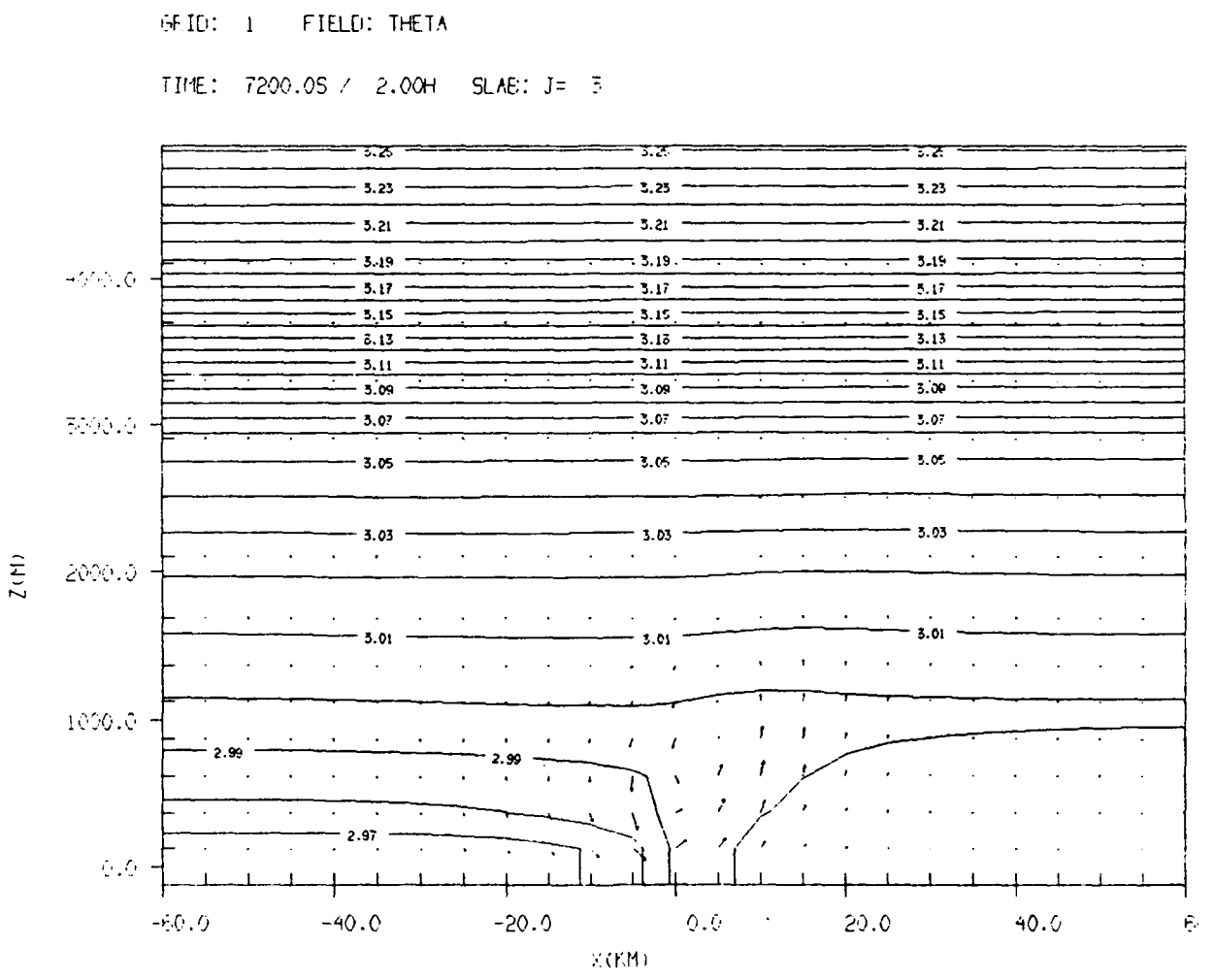
GRID: 1 FIELD: THETA
TIME: 7200.0S / 2.00H SLAB: J= 3
3.25
3.23
3.21
3.19
3.17
3.15
3.13
3.11
3.09
3.07
3.05
3.03
3.01
2.99
2.97
5000.0
2000.0
1000.0
0.0
Z(M)
-60.0
-40.0
-20.0
0.0
20.0
40.0
X(KM)
FROM 2.94 TO 3.26 BY .01 LABELS * 100

Figure 3(c)

(d)

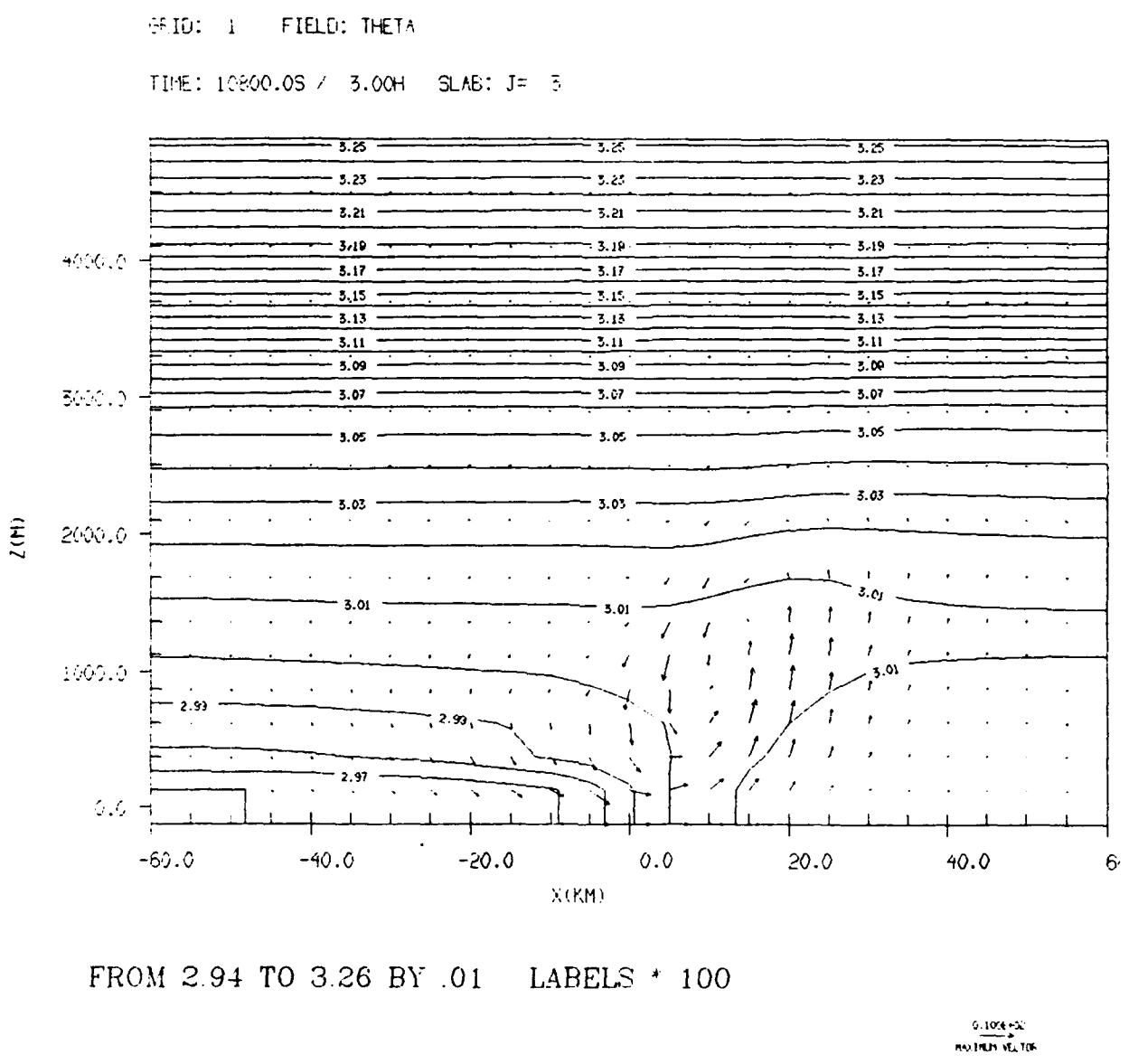

FROM 2.94 TO 3.26 BY .01 LABELS * 100

Figure 3(d)

(e)

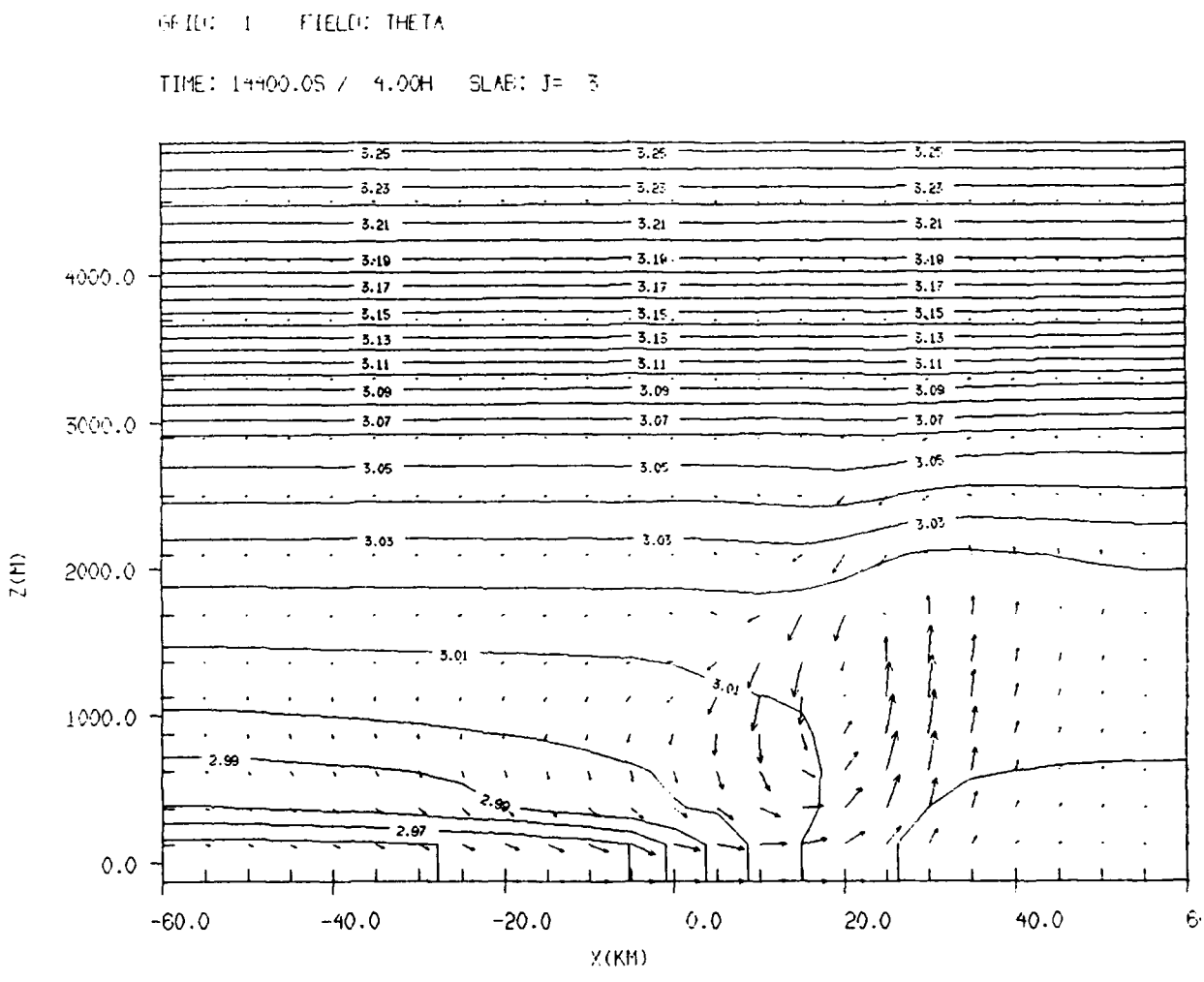

FROM 2.94 TO 3.26 BY .01 LABELS * 100

Figure 3(e)

(a)

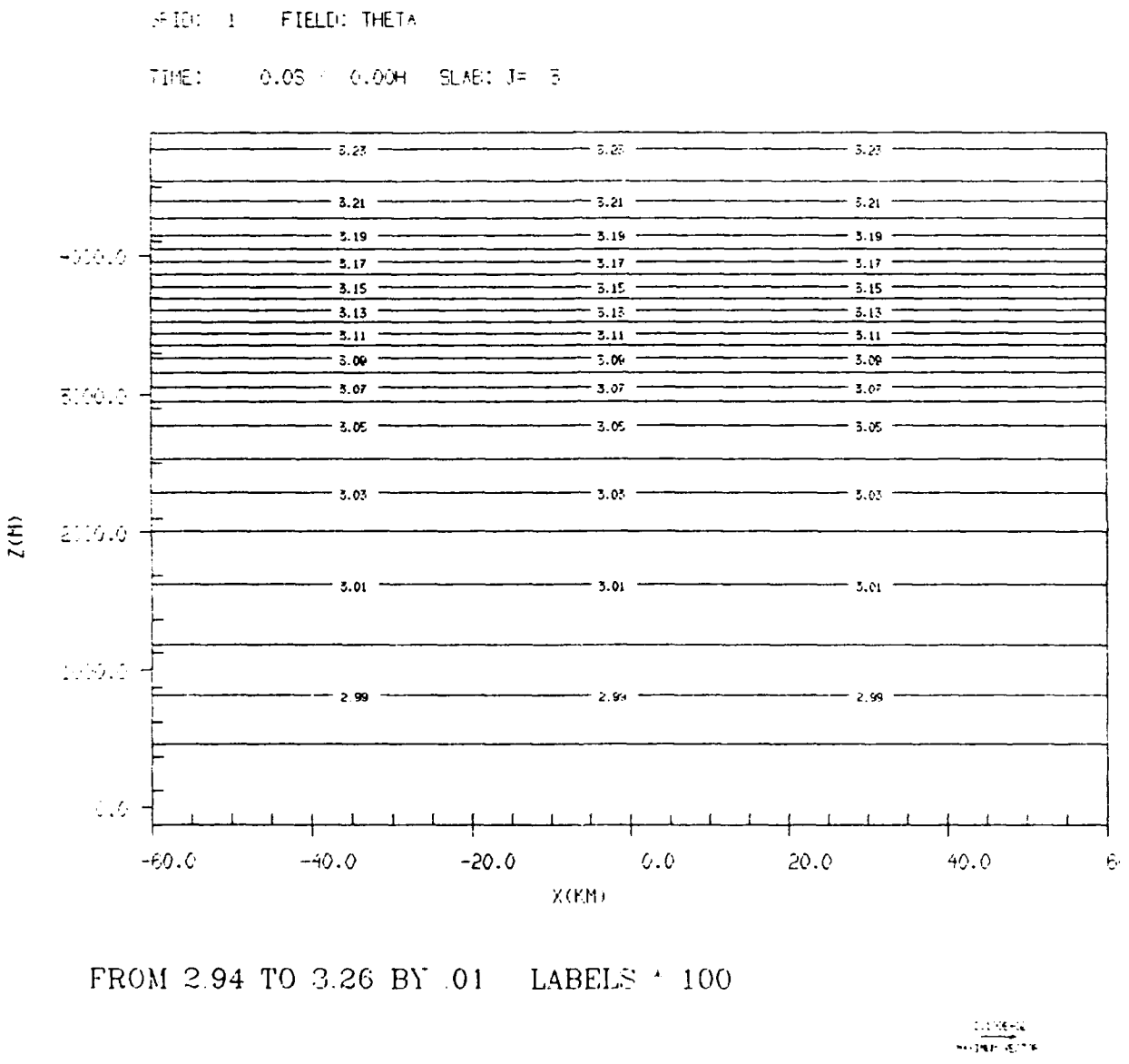

Figure 4: Output from Experiment 2. Baseline model potential temperature and wind forecasts initialized with faulty boundary conditions (warmer sea surface temperature, moister soil). (a) 0-hour forecast, (b) 1-hour, (c) 2-hour, (d) 3-hour, (e) 4-hour.

(b)

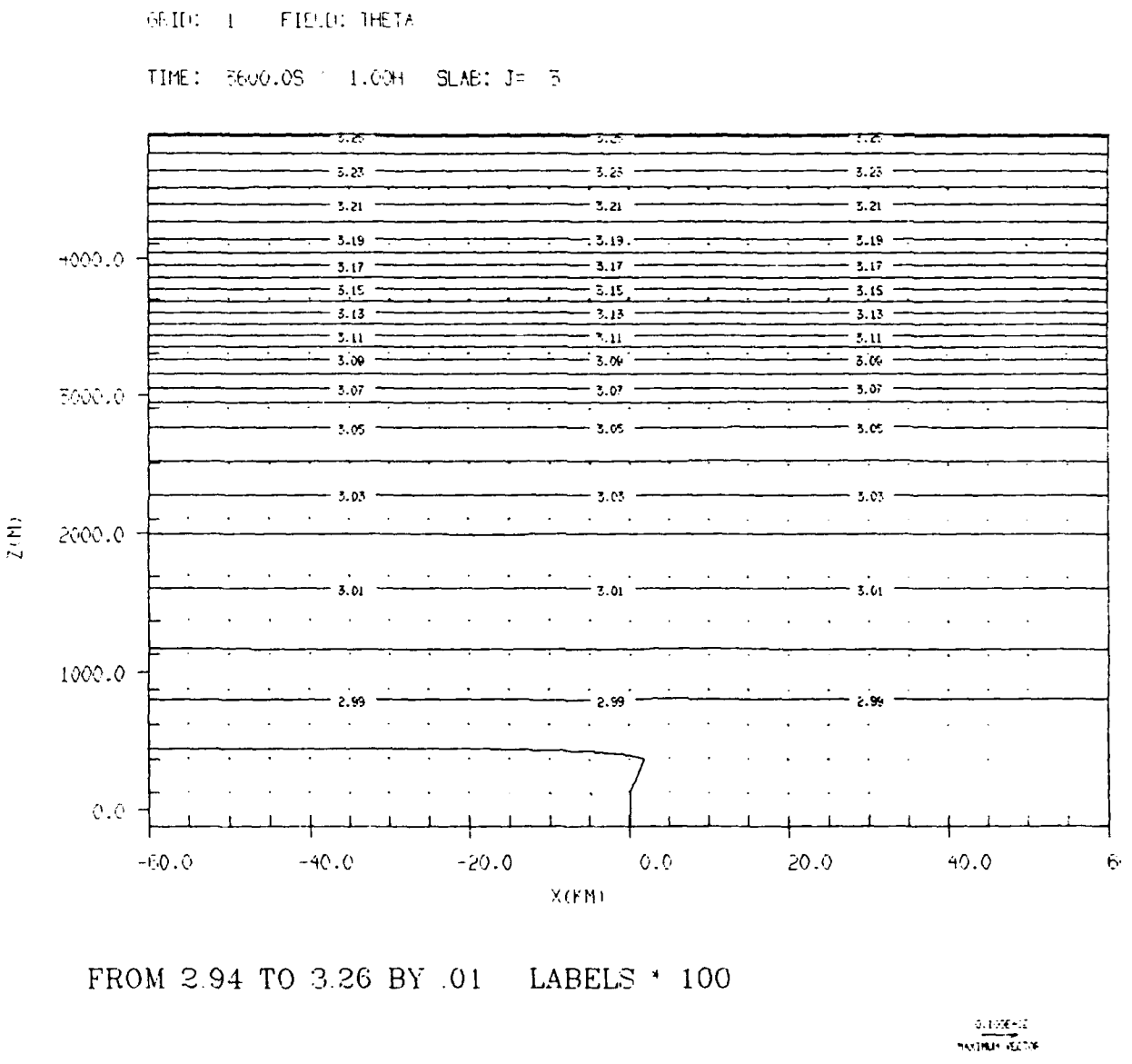
TIME: 3600.0S 1.00H SLAB: J= 5
3.25
3.23
3.21
3.19
3.17
3.15
3.13
3.11
3.09
3.07
3.05
3.03
3.01
2.99
4000.0
3000.0
2000.0
1000.0
0.0
Z(M)
-60.0
-40.0
-20.0
0.0
20.0
40.0
X(KM)
FROM 2.94 TO 3.26 BY .01 LABELS * 100

Figure 4(b)

(c)

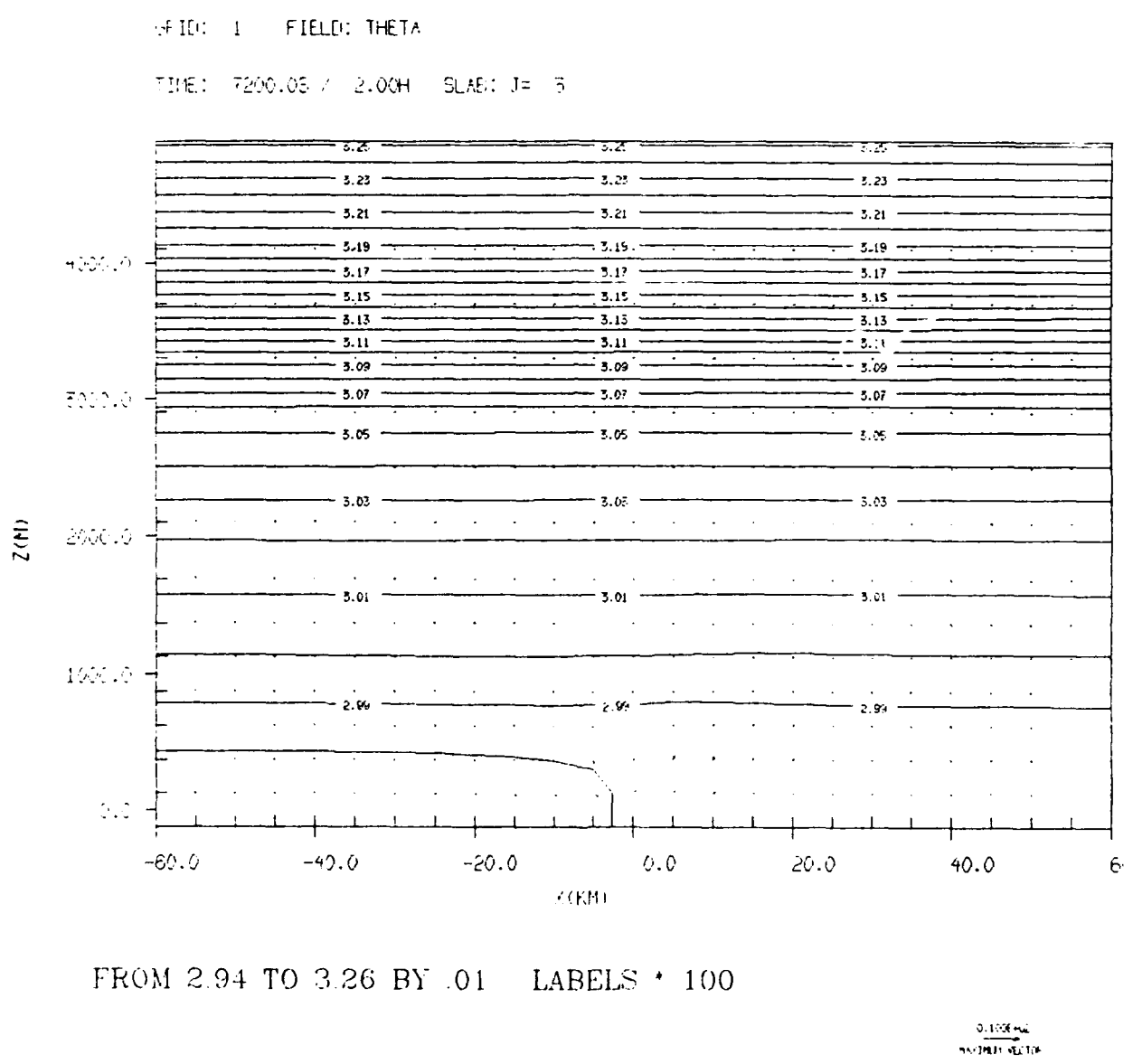

FROM 2.94 TO 3.26 BY .01 LABELS * 100

Figure 4(c)

(d)

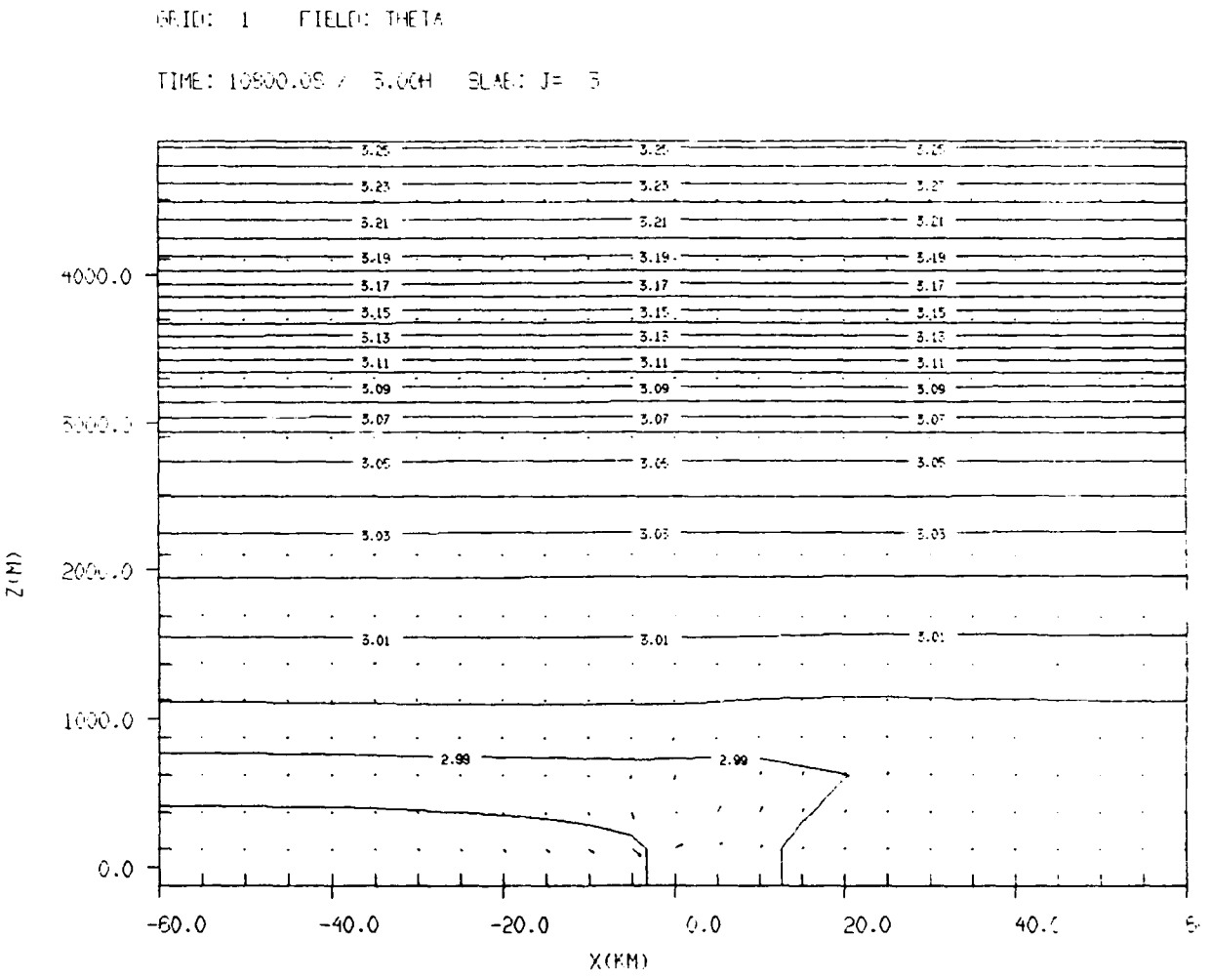

FROM 2.94 TO 3.26 BY .01 LABELS * 100

Figure 4(d)

(e)

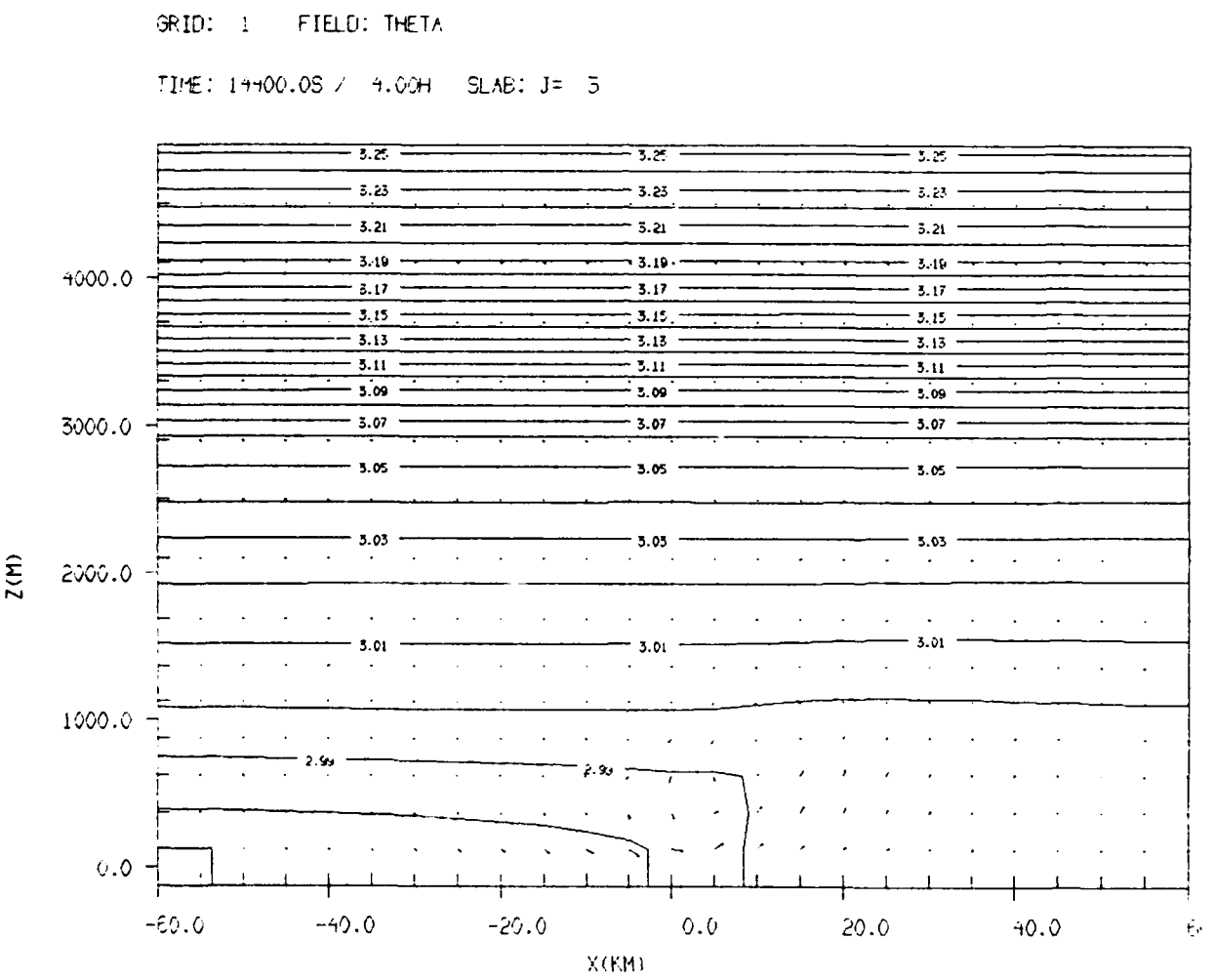
GRID: 1 FIELD: THETA
TIME: 14400.0S / 4.00H SLAB: J= 5
4000.0
3000.0
2000.0
1000.0
0.0
Z(M)
-60.0
-40.0
-20.0
0.0
20.0
40.0
X(KM)
FROM 2.94 TO 3.26 BY .01 LABELS * 100
MAXIMUM VECTOR

Figure 4(e)

(a)

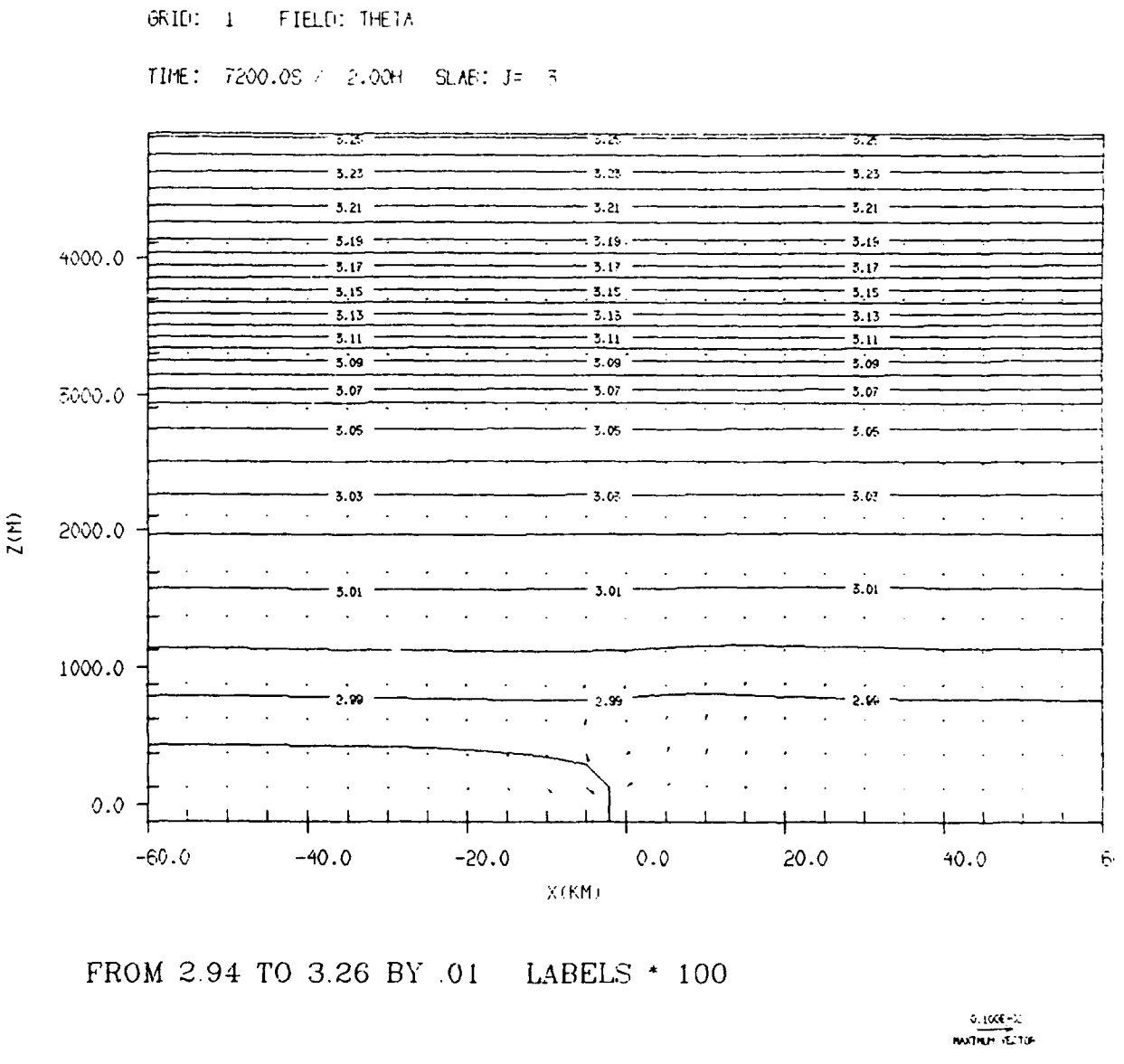

Figure 5: Output from Experiment 3. Potential temperature and wind forecasts for model run with faulty boundary conditions and nudged by nature run's winds (using 5.56 *10^{-4} nudging coefficient and 5-minute updates). (a) 2-hour forecast, (b) 3-hour, (c) 4-hour.

(b)

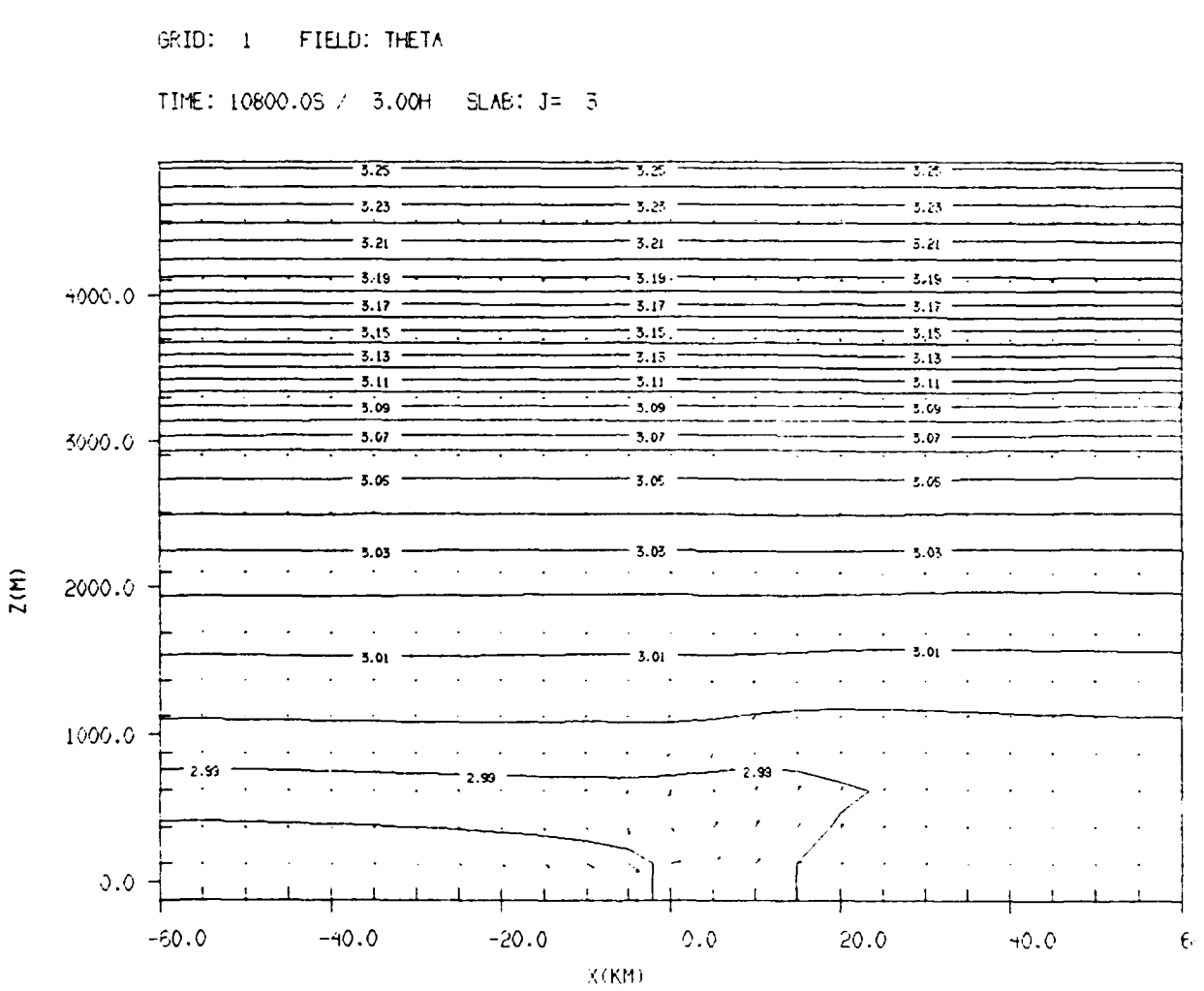

FROM 2.94 TO 3.26 BY .01 LABELS * 100

Figure 5(b)

(c)

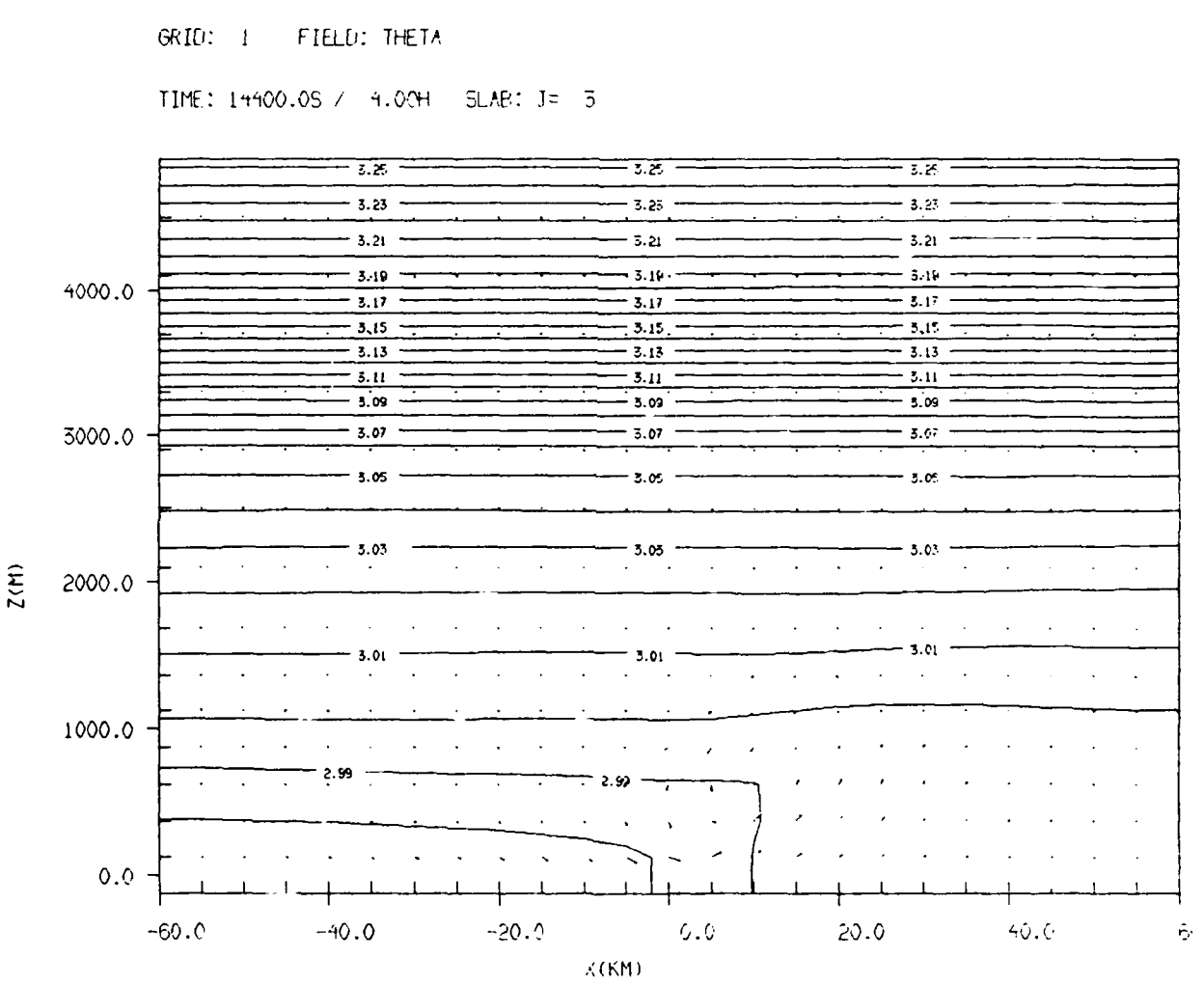

FROM 2.94 TO 3.26 BY .01 LABELS * 100

Figure 5(c)

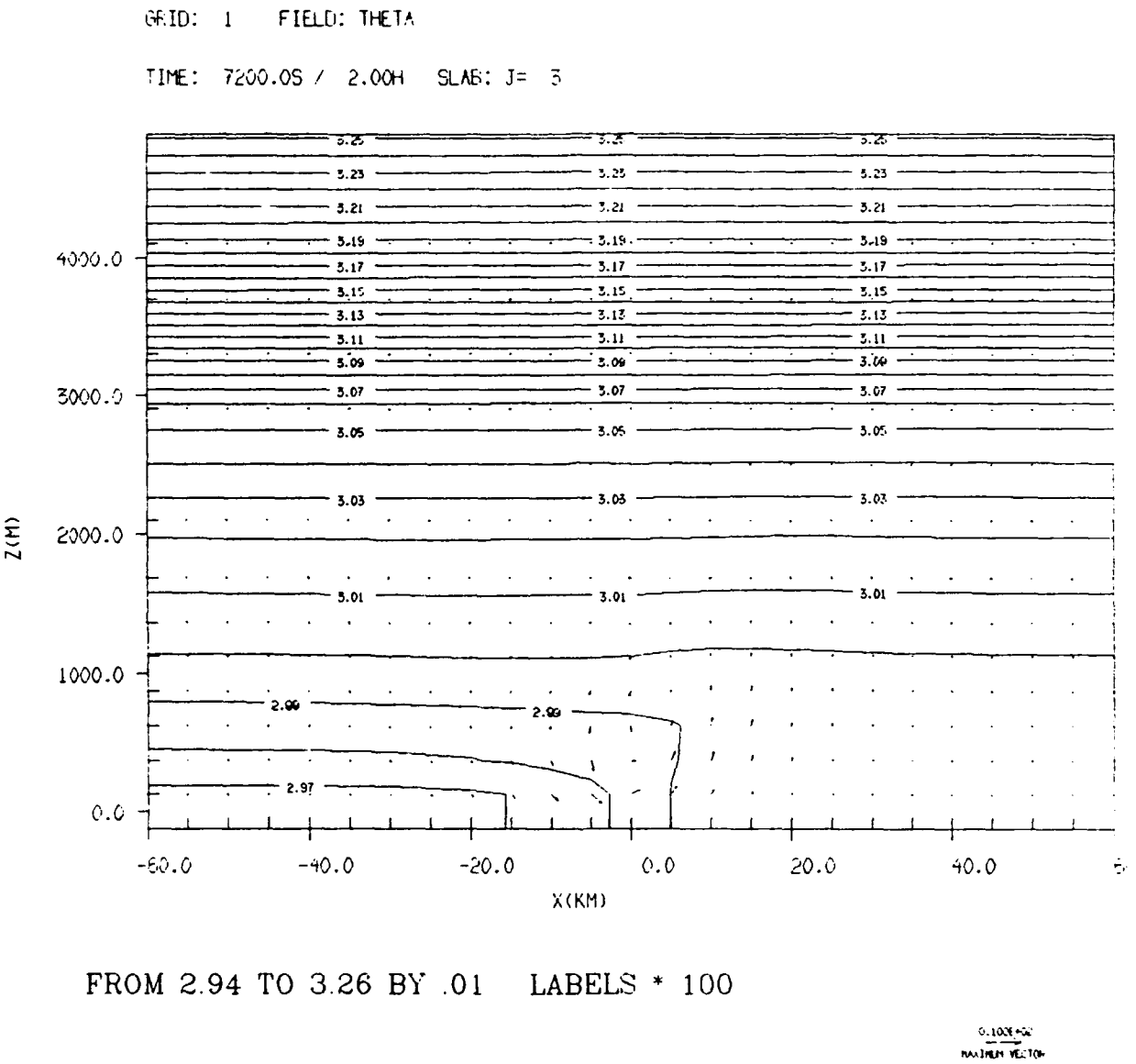

Figure 6: Output from Experiment 4. Potential temperature and wind forecasts for model run with faulty boundary conditions and nudged by nature run's winds and temperatures (using 5.56 $*10^{-4}$ nudging coefficient and 5-minute updates). (a) 2-hour forecast, (b) 3-hour, (c) 4-hour.

(b)

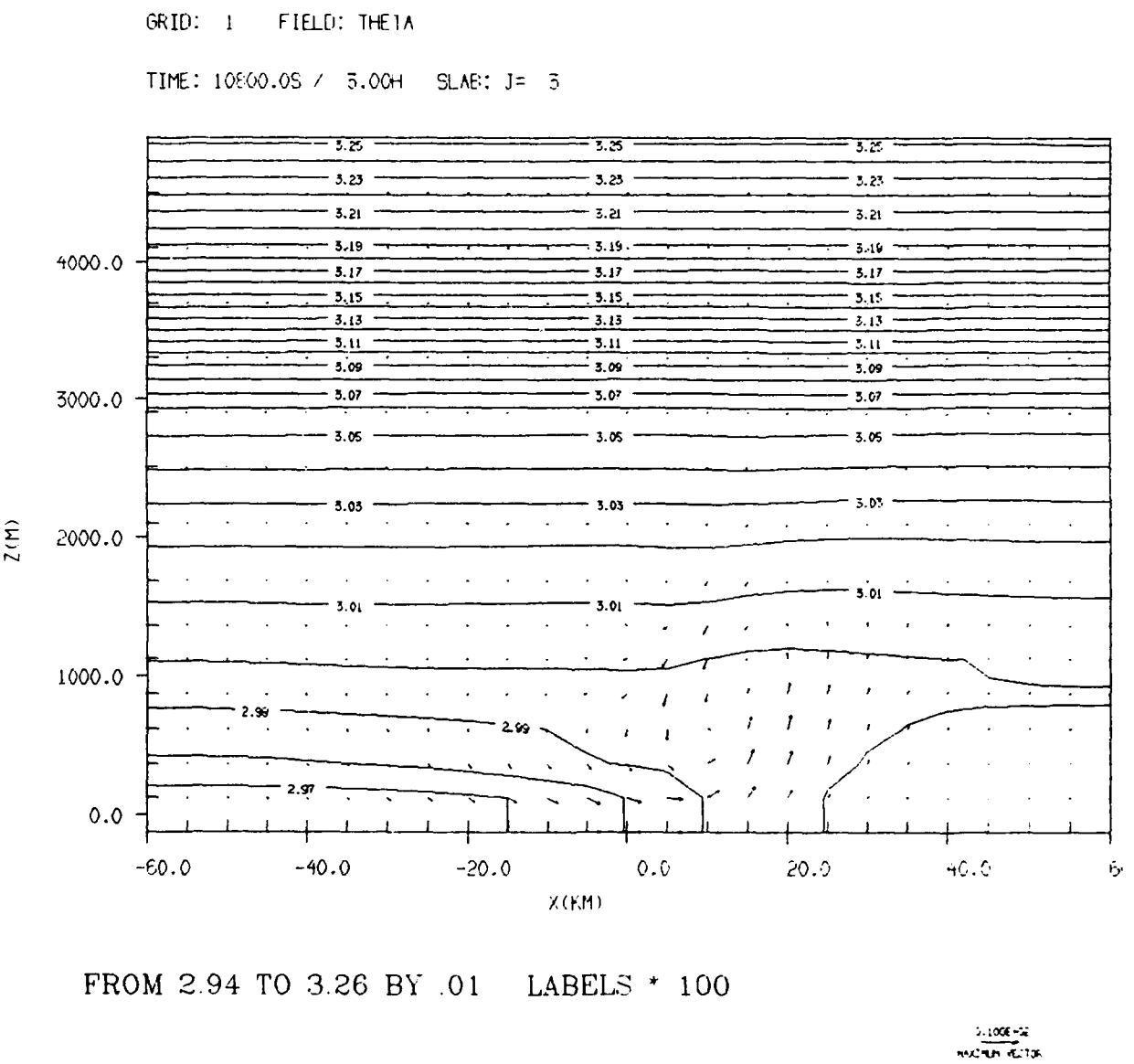

FROM 2.94 TO 3.26 BY .01 LABELS * 100

Figure 6(b)

(c)

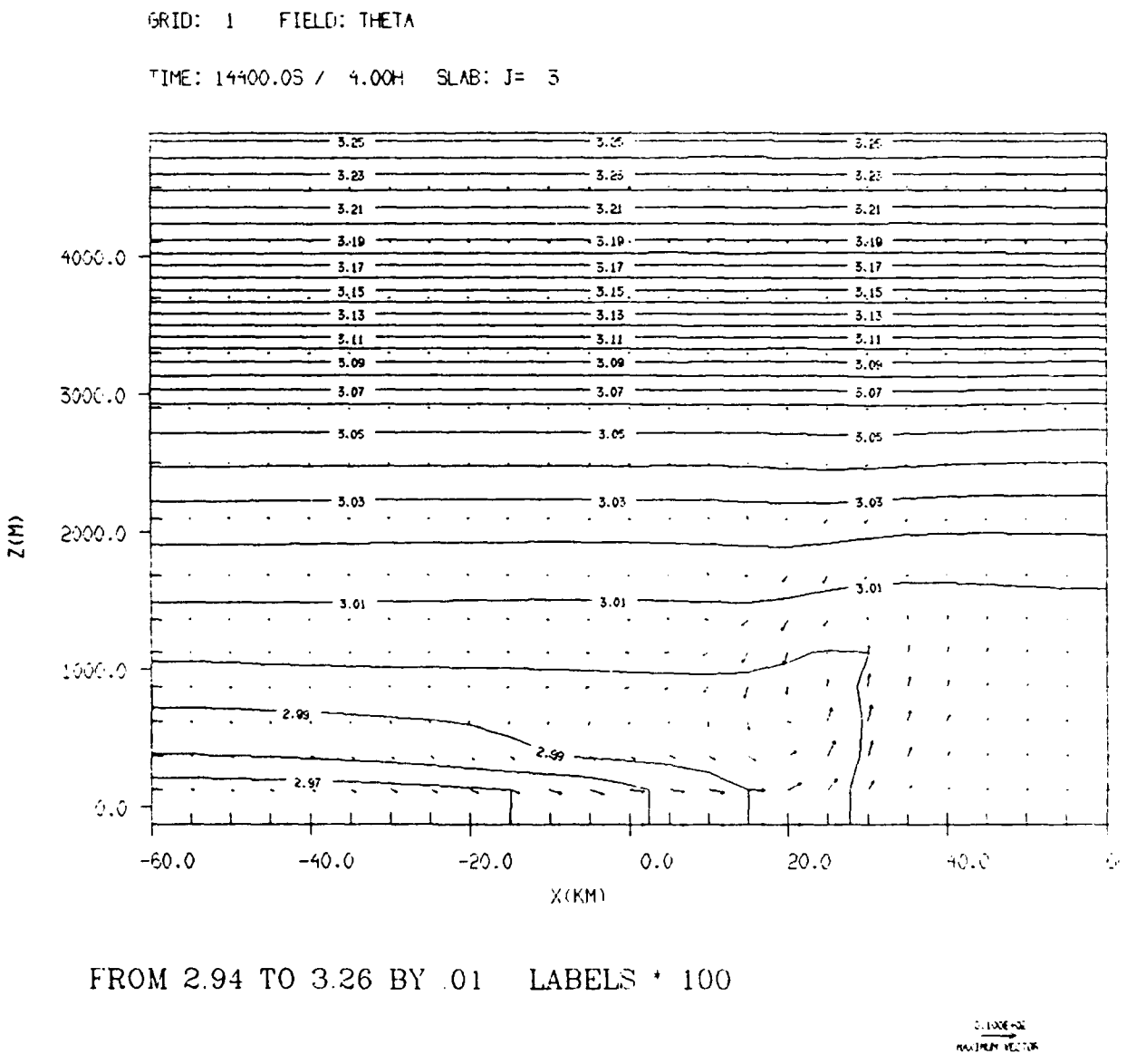
GRID: 1 FIELD: THETA
TIME: 14400.0S / 4.00H SLAB: J= 3
3.25
3.23
3.21
3.19
3.17
3.15
3.13
3.11
3.09
3.07
3.05
3.03
3.01
2.99
2.97
4000.0
3000.0
2000.0
1000.0
0.0
Z(M)
-60.0
-40.0
-20.0
0.0
20.0
40.0
X(KM)
FROM 2.94 TO 3.26 BY .01 LABELS * 100

Figure 6(c)

(a)

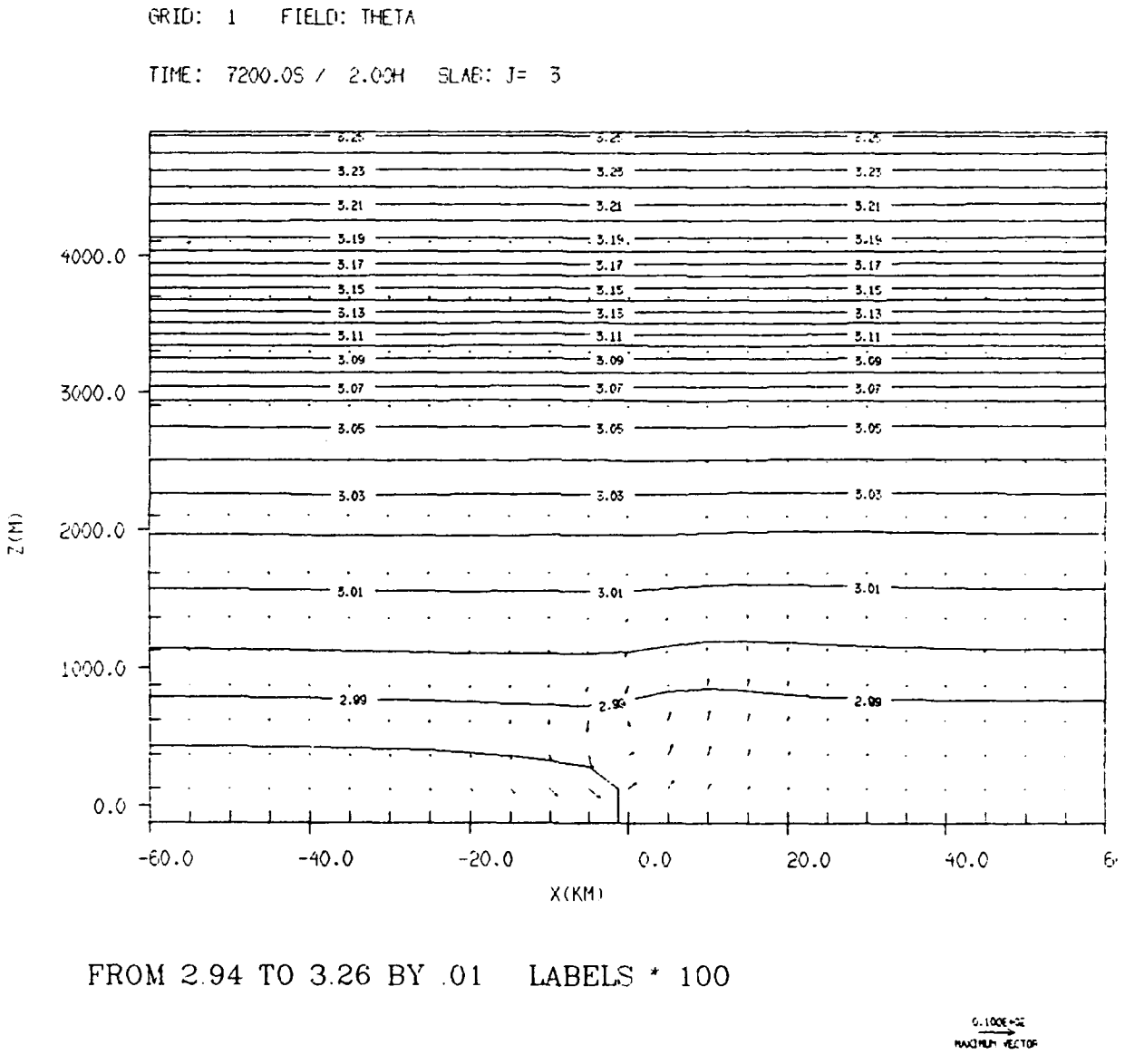

Figure 7: Output from Experiment 5. Potential temperature and wind forecasts for model run with faulty boundary conditions and nudged by nature run's winds (using 5.56 $*10^{-3}$ nudging coefficient and 5-minute updates). (a) 2-hour forecast, (b) 3-hour, (c) 4-hour.

(b)

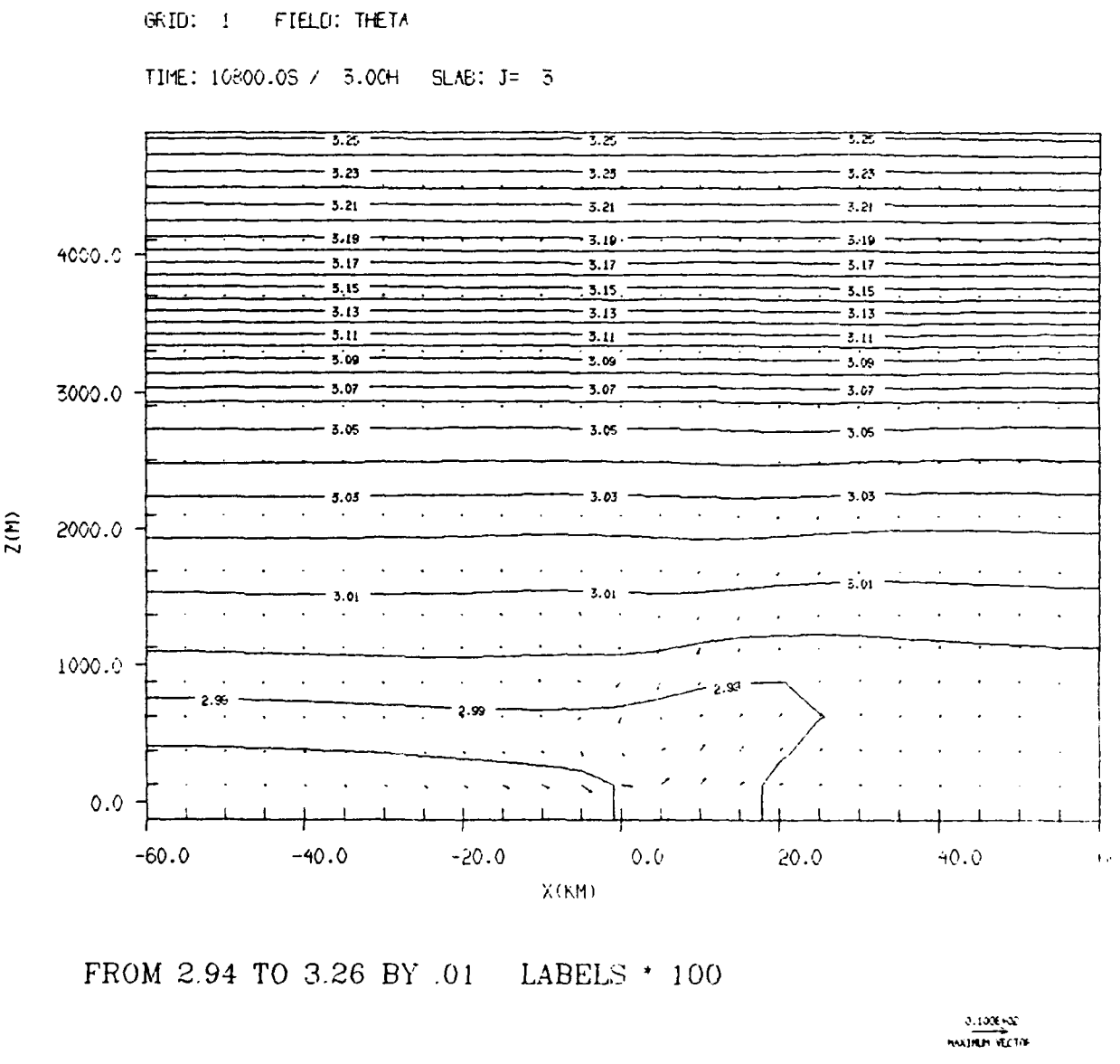
GRID: 1 FIELD: THETA
TIME: 10800.0S / 3.0CH SLAB: J= 3
3.25
3.23
3.21
3.19
3.17
3.15
3.13
3.11
3.09
3.07
3.05
3.03
3.01
2.99
2.97
4000.0
3000.0
2000.0
1000.0
0.0
Z(M)
-60.0
-40.0
-20.0
0.0
20.0
40.0
X(KM)
FROM 2.94 TO 3.26 BY .01 LABELS * 100

Figure 7(b)

(c)

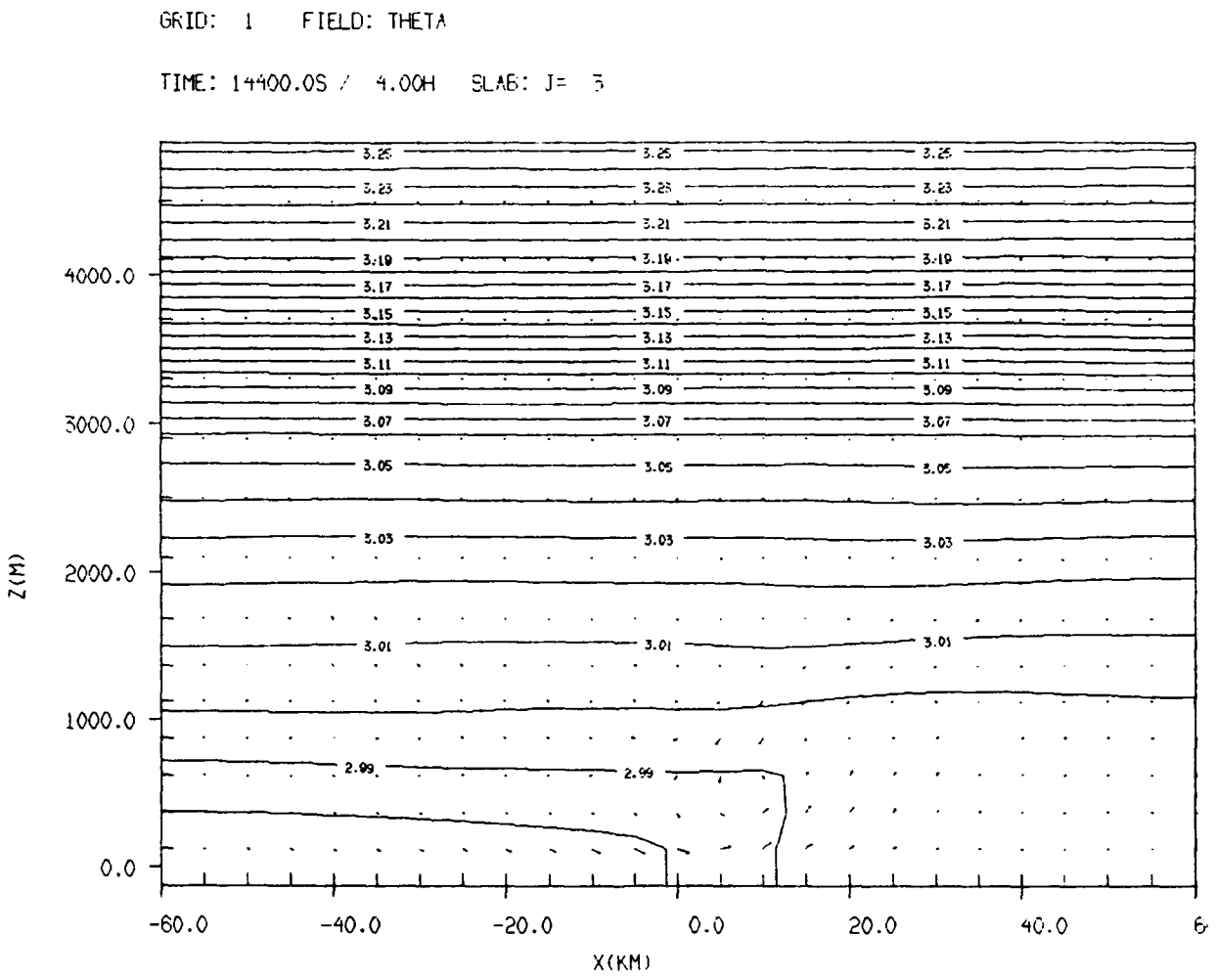

FROM 2.94 TO 3.26 BY .01 LABELS * 100

Figure 7(c)

(a)

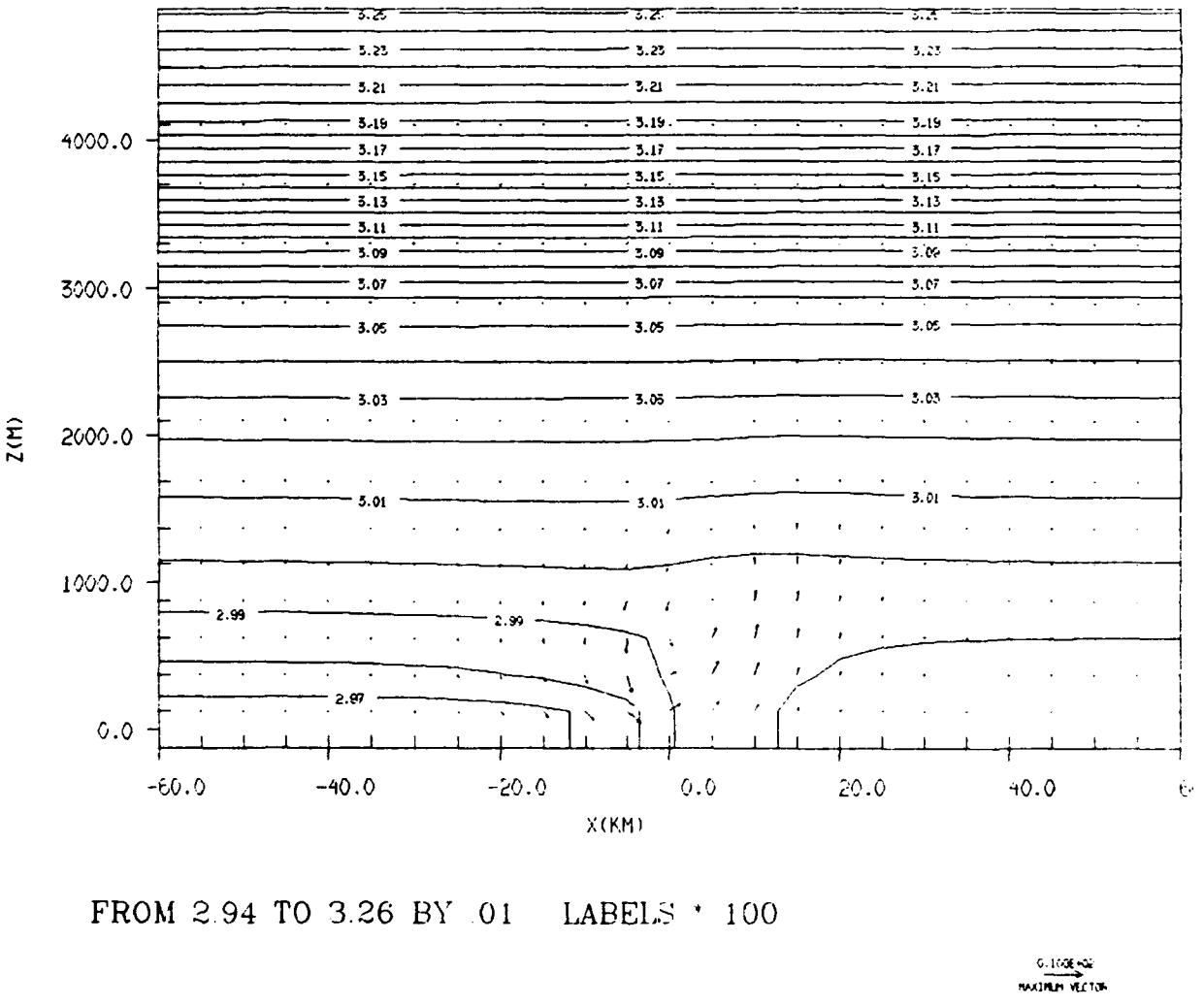

FROM 2.94 TO 3.26 BY .01 LABELS * 100

Figure 8: Output from Experiment 6. Potential temperature and wind forecasts for model run with faulty boundary conditions and nudged by nature run's winds and temperatures (using 5.56 $*10^{-3}$ nudging coefficient and 5-minute updates). (a) 2-hour forecast, (b) 3-hour, (c) 4-hour.

(b)

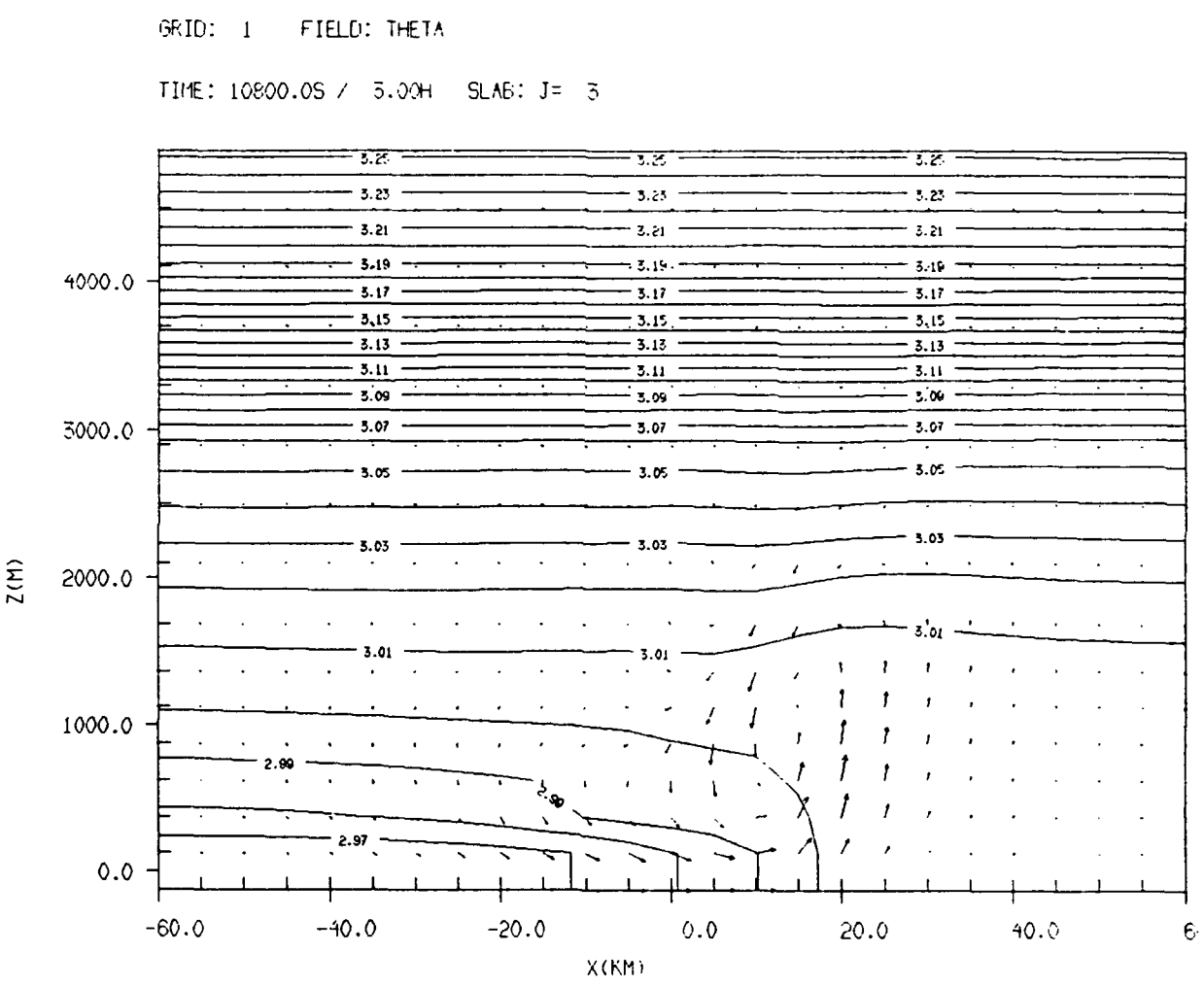
GRID: 1 FIELD: THETA
TIME: 10800.0S / 3.00H SLAB: J= 3
4000.0
3000.0
2000.0
1000.0
0.0
Z(M)
-60.0
-40.0
-20.0
0.0
20.0
40.0
X(KM)
FROM 2.94 TO 3.26 BY .01 LABELS * 100
MAXIMUM VECTOR

Figure 8(b)

(c)

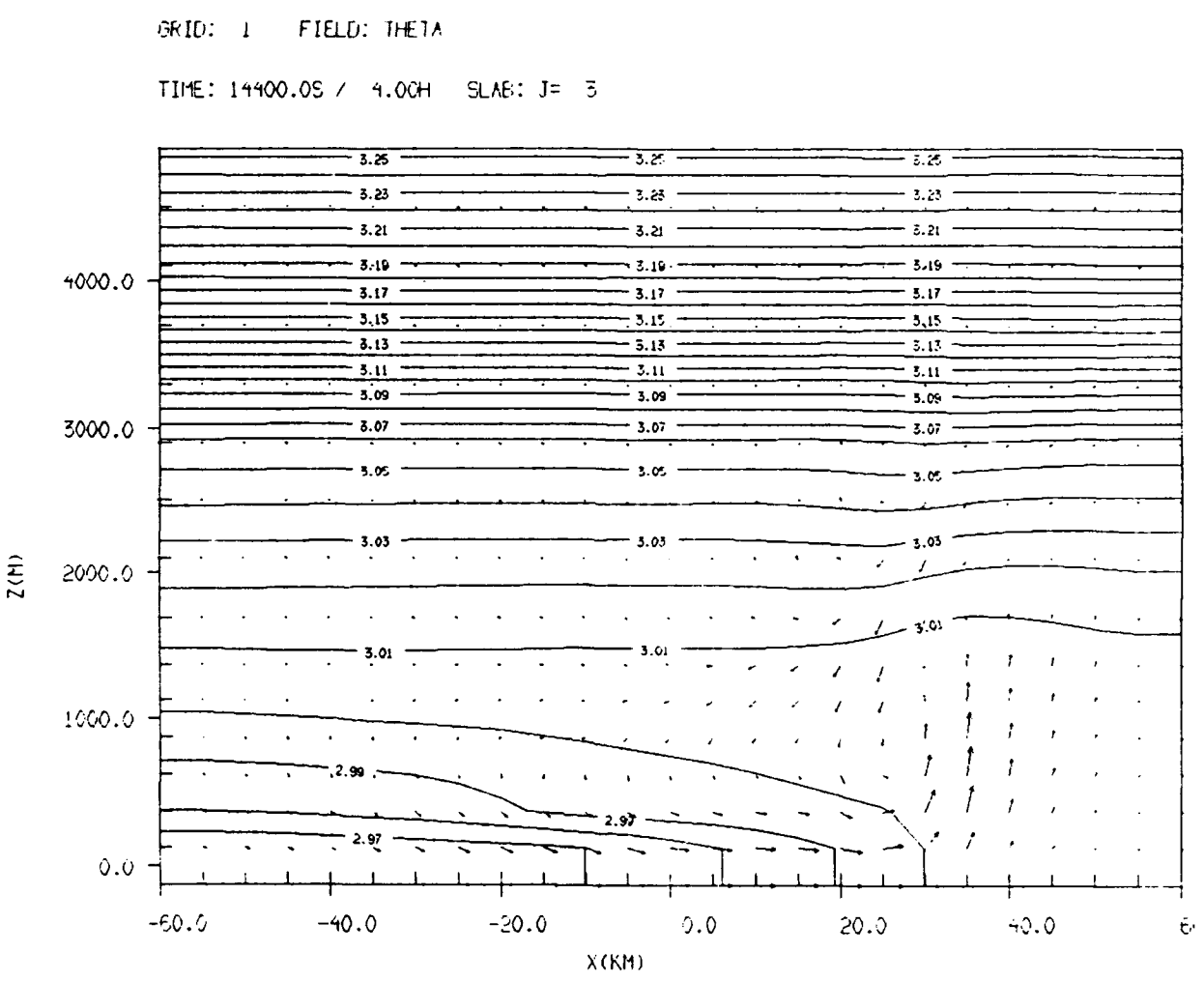

FROM 2.94 TO 3.26 BY .01 LABELS * 100

Figure 8(c)

(a)

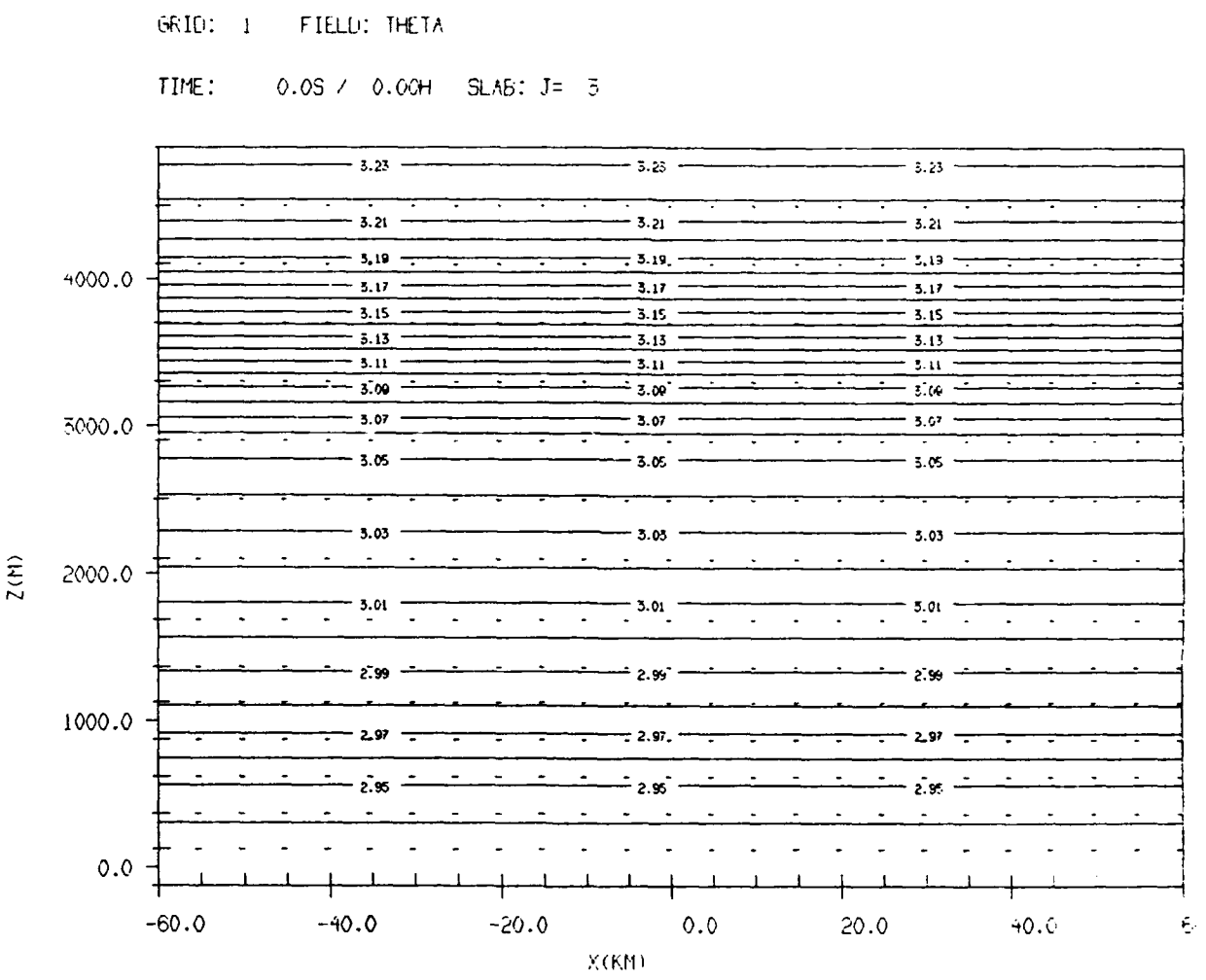

FROM 2.94 TO 3.26 BY .01 LABELS * 100

Figure 9: Output from Experiment 7. New baseline model potential temperature and wind forecasts initialized with faulty atmospheric conditions (-4 K low-level temperature error, 2.5 ms-1 low-level offshore flow). (a) 0-hour forecast, (b) 1-hour, (c) 2-hour, (d) 3-hour, (e) 4-hour.

(b)

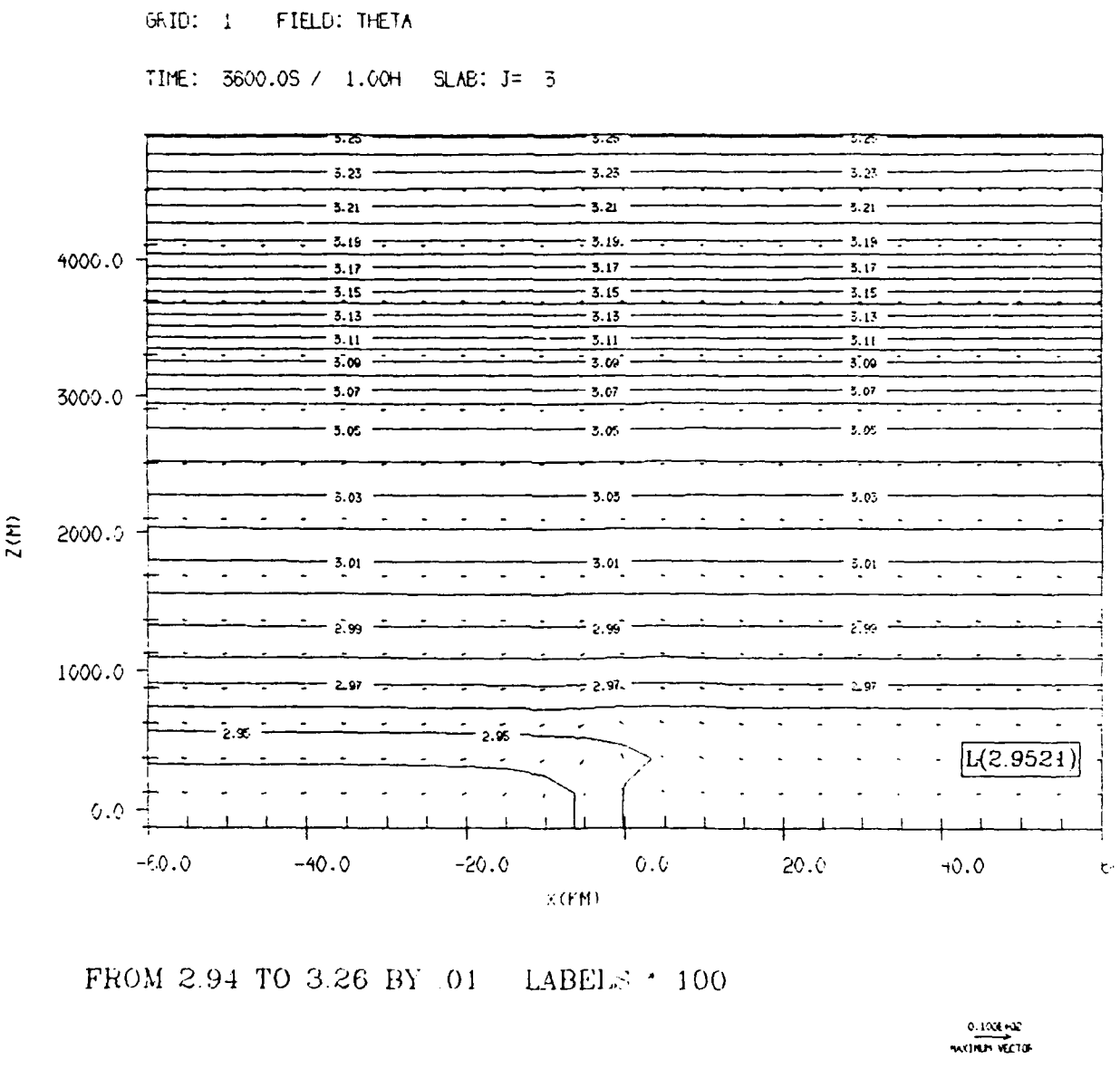

FROM 2.94 TO 3.26 BY .01 LABELS * 100

Figure 9(b)

(c)

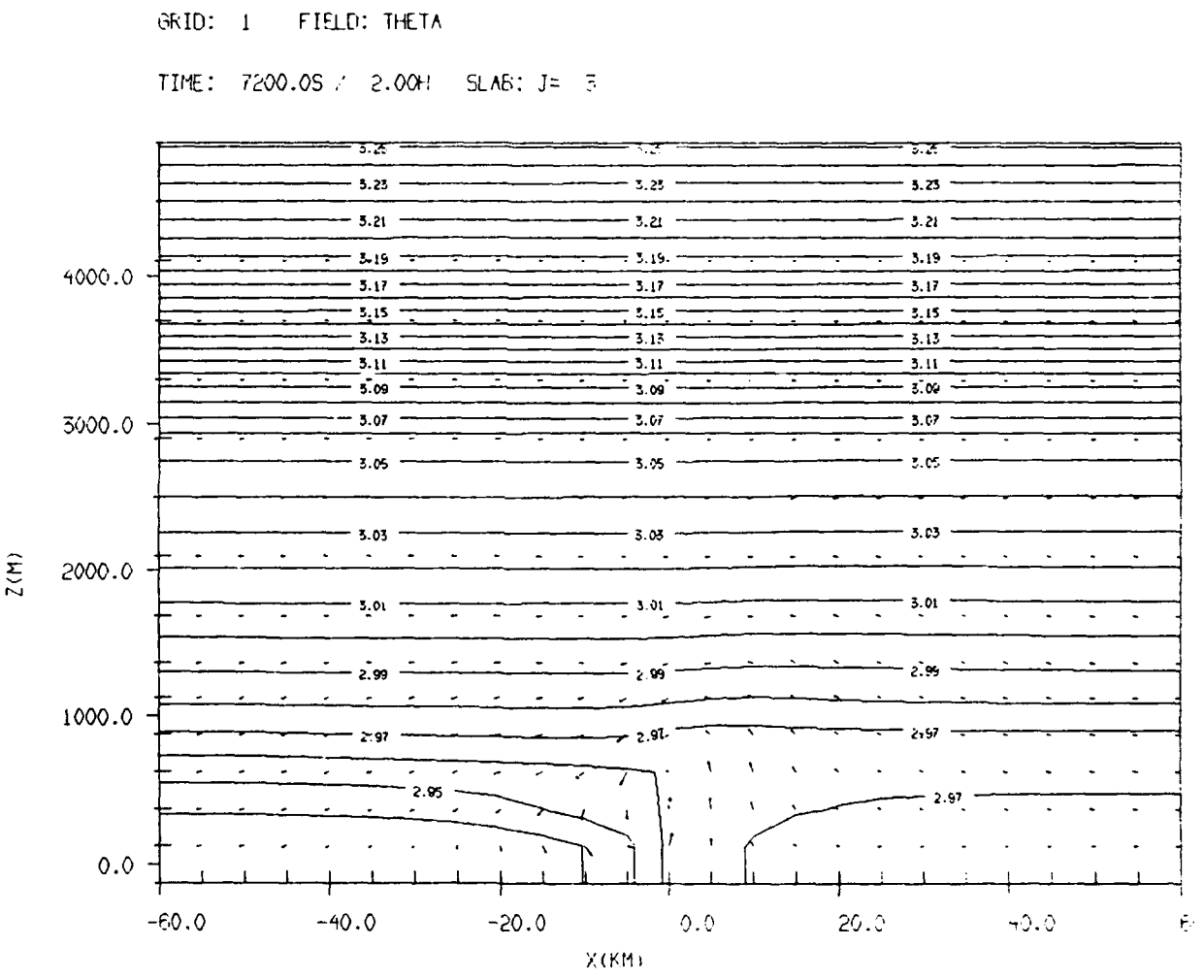
GRID: 1 FIELD: THETA
TIME: 7200.0S / 2.00H SLAB: J= 3
4000.0
3000.0
2000.0
1000.0
0.0
Z(M)
-60.0
-40.0
-20.0
0.0
20.0
40.0
X(KM)
3.25
3.23
3.21
3.19
3.17
3.15
3.13
3.11
3.09
3.07
3.05
3.03
3.01
2.99
2.97
2.95
FROM 2.94 TO 3.26 BY .01 LABELS * 100
MAXIMUM VECTOR

Figure 9(c)

(d)

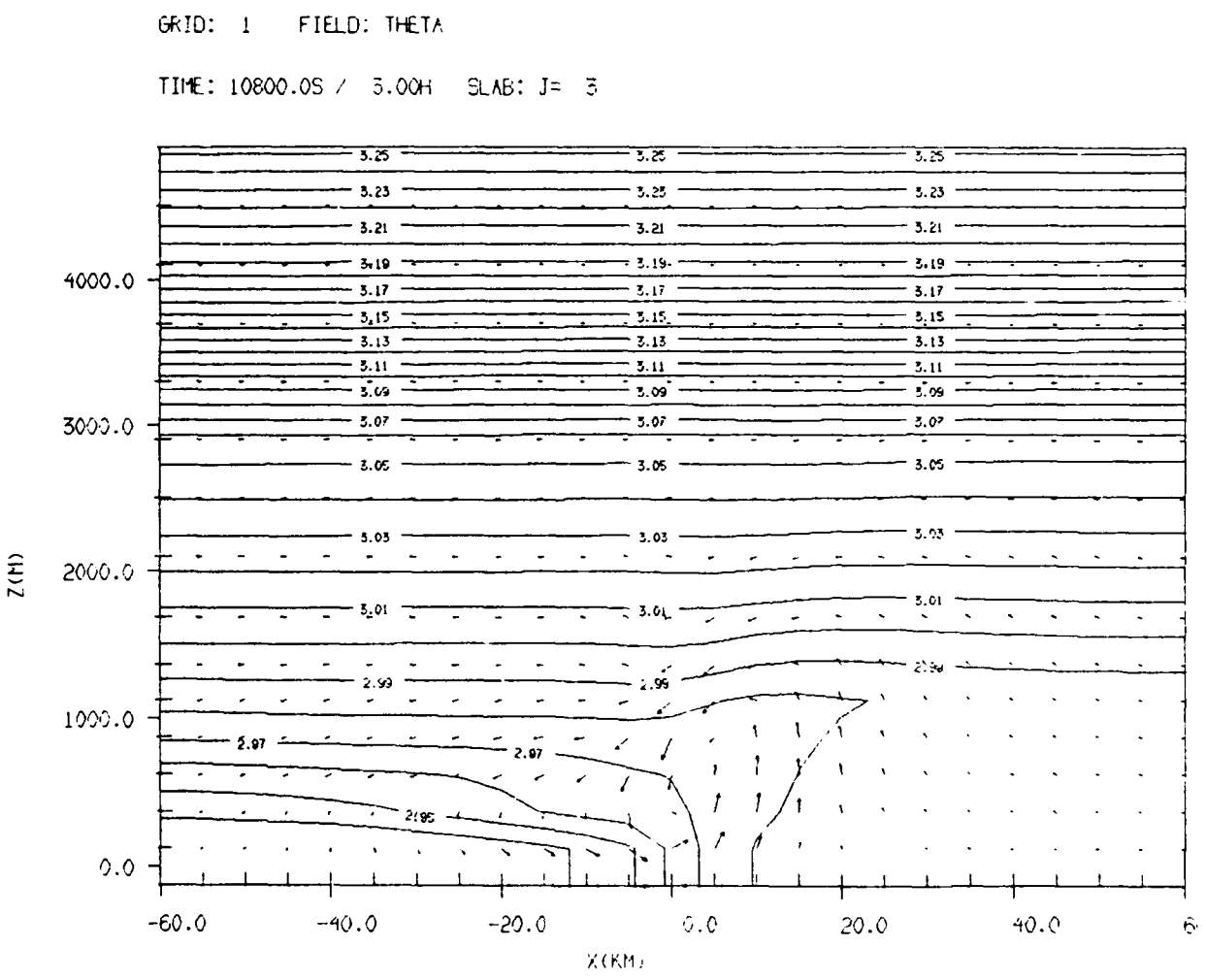
GRID: 1 FIELD: THETA
TIME: 10800.0S / 3.00H SLAB: J= 3
4000.0
3000.0
2000.0
1000.0
0.0
Z(M)
-60.0
-40.0
-20.0
0.0
20.0
40.0
X(KM)
FROM 2.94 TO 3.26 BY .01 LABELS * 100

Figure 9(d)

(c)

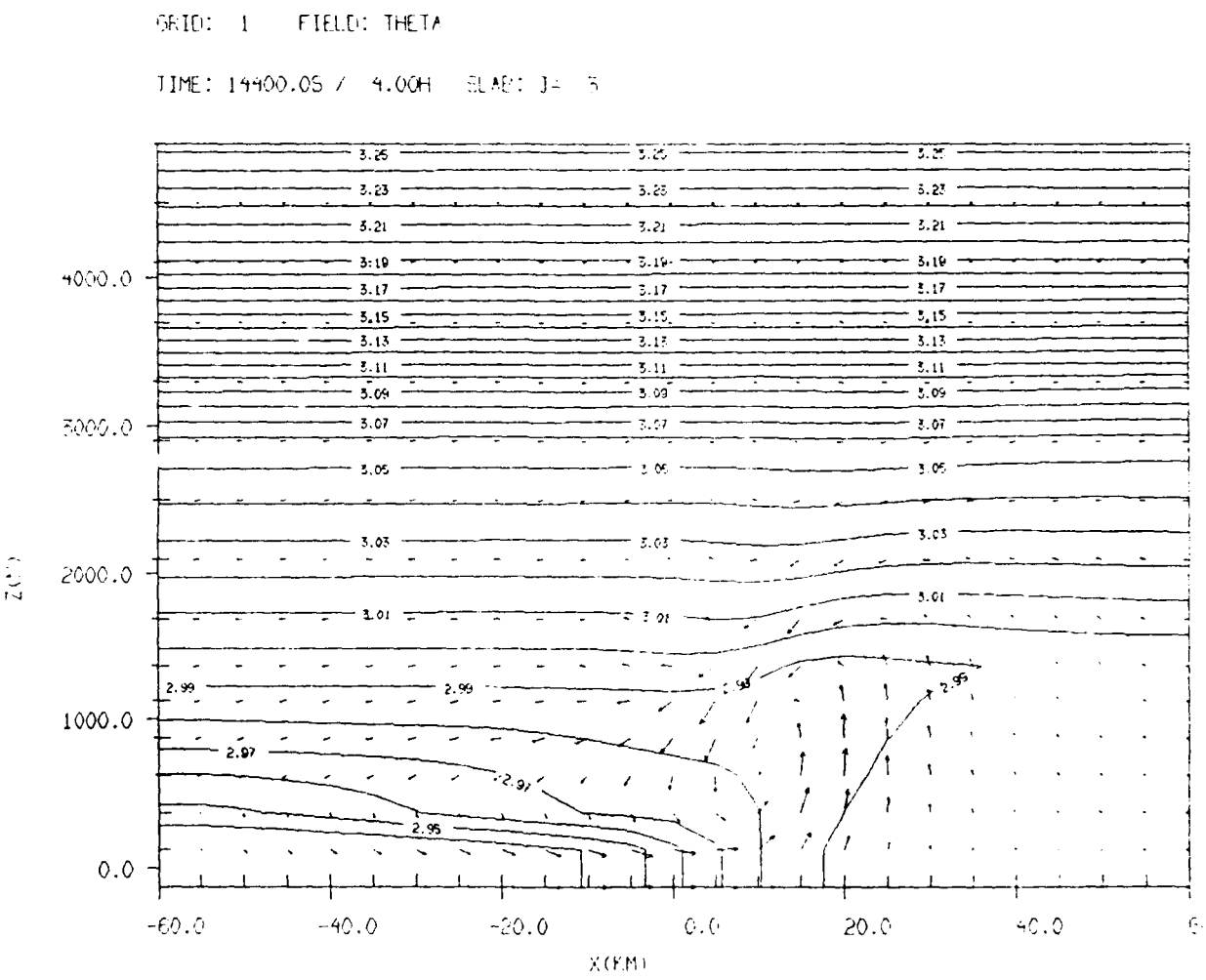

FROM 2.94 TO 3.26 BY 01 LABELS * 100

Figure 9(e)

(a)

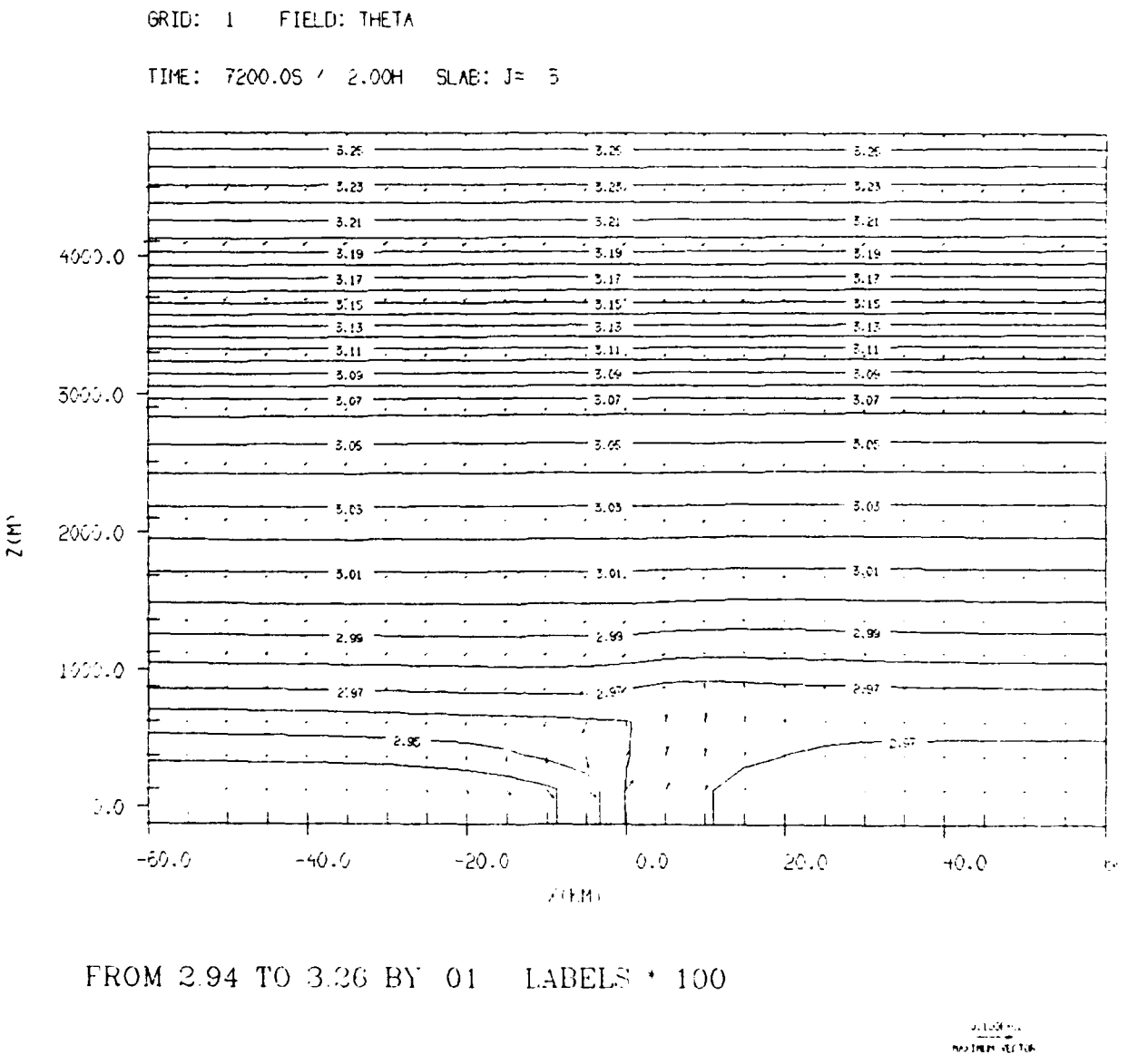

Figure 10: Output from Experiment 8. Potential temperature and wind forecasts for model initialized with faulty atmospheric conditions, and nudged by nature run's winds (using 5.56 *10^{-4} nudging coefficient and 5-minute updates). (a) 2-hour forecast, (b) 3-hour, (c) 4-hour.

(b)

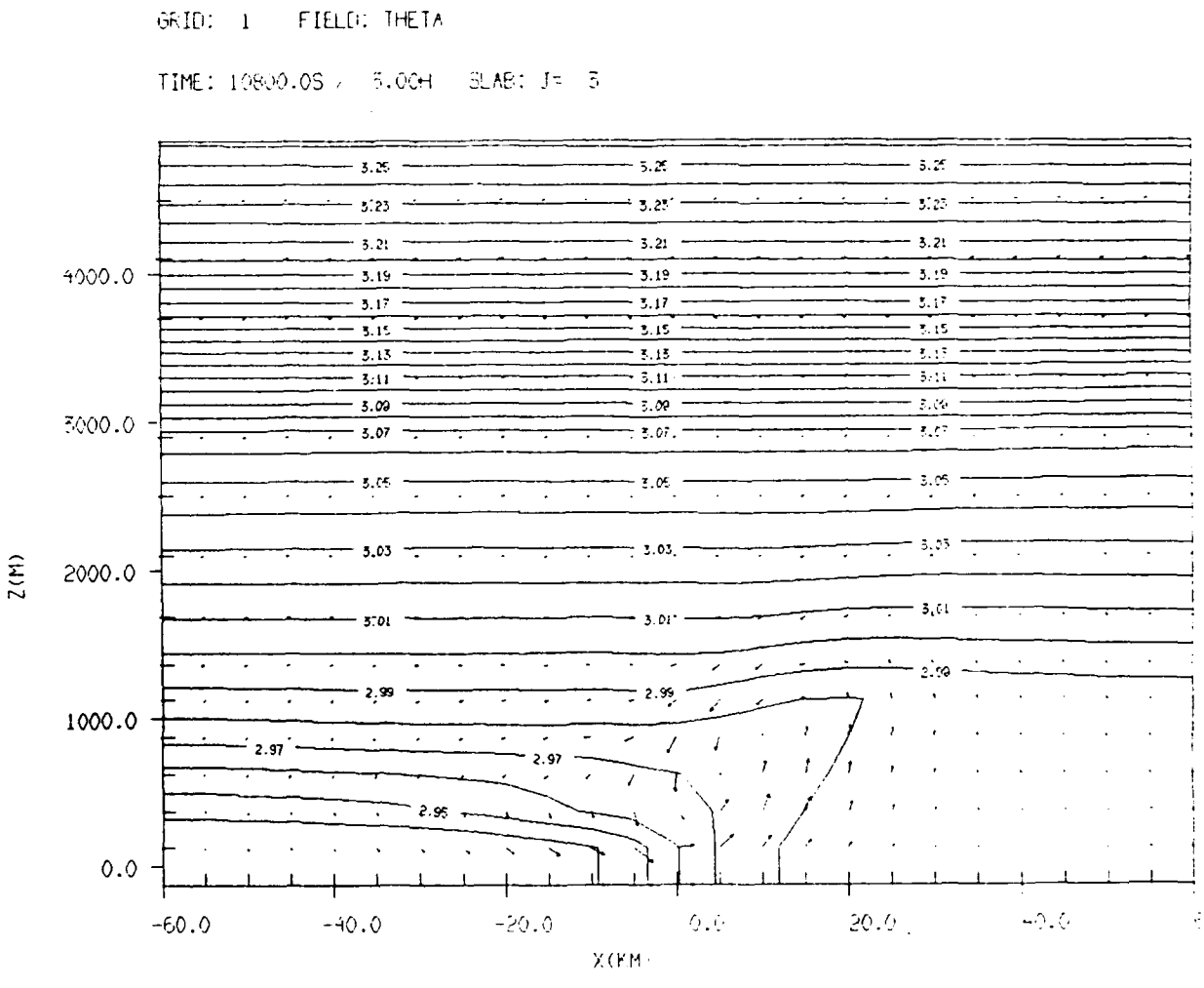

FROM 2.94 TO 3.26 BY .01 LABELS * 100

Figure 10(b)

(c)

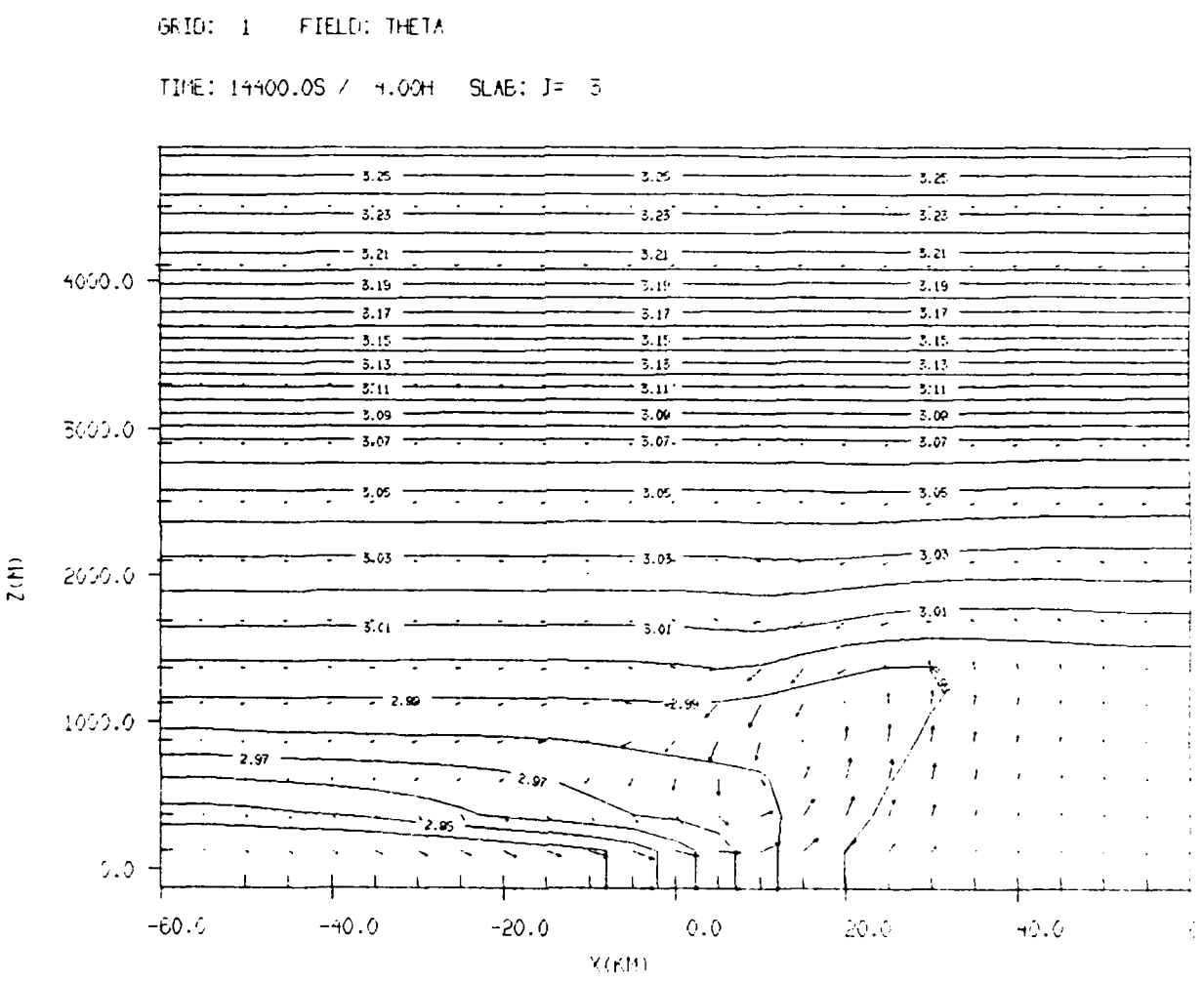
GRID: 1 FIELD: THETA
TIME: 14400.0S / 4.00H SLAB: J= 3
4000.0
3000.0
2000.0
1000.0
0.0
Z(M)
-60.0
-40.0
-20.0
0.0
20.0
40.0
X(KM)
FROM 2.94 TO 3.26 BY .01 LABELS * 100

Figure 10(c)

(a)

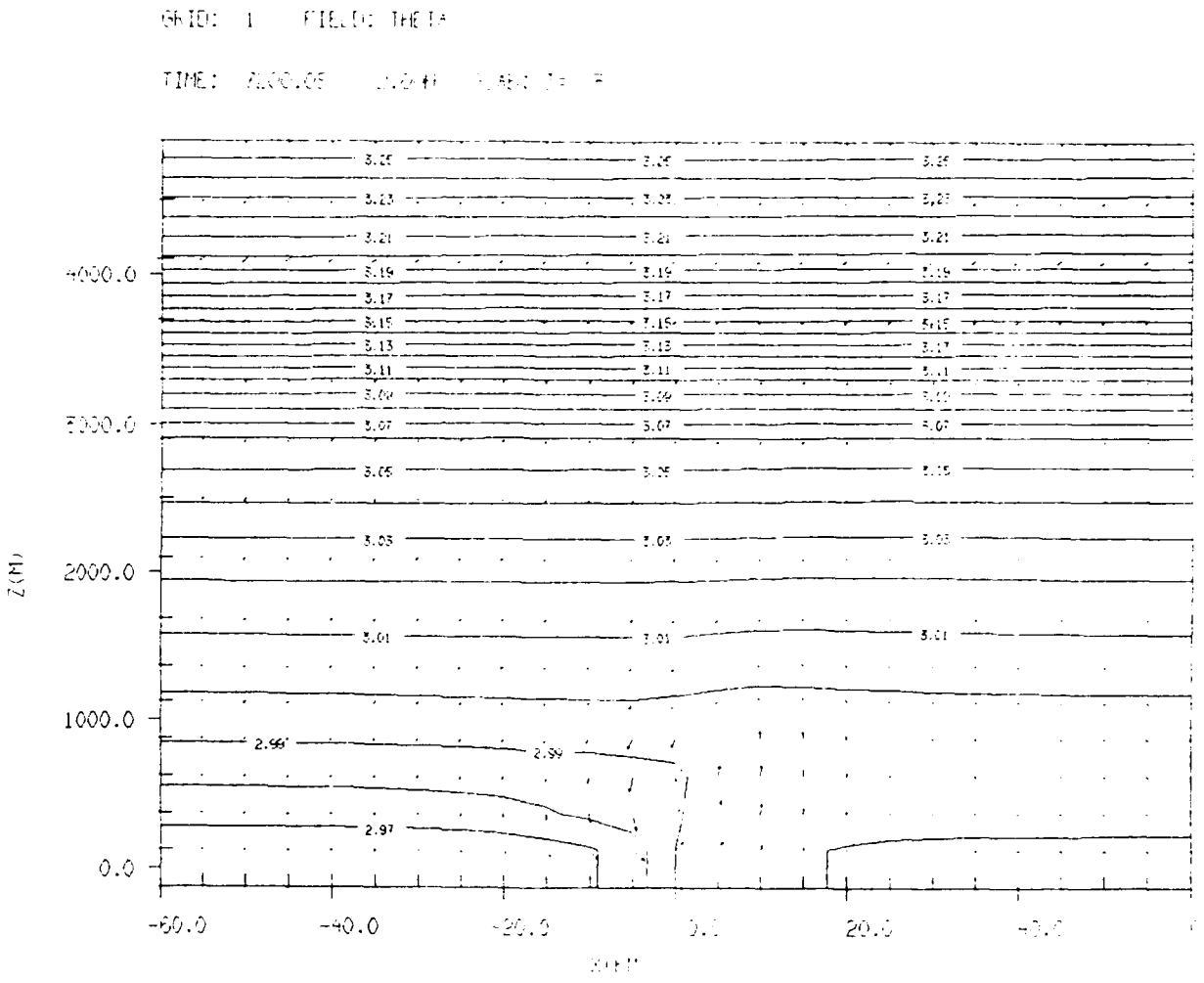

FROM 2.94 TO 3.26 BY .01 LABELS * 100

Figure 11: Output from Experiment 9. Potential temperature and wind forecasts for model initialized with faulty atmospheric conditions, and nudged by nature run's winds and temperatures (using 5.56 *10^{-4} nudging coefficient and 5-minute updates). (a) 2-hour forecast, (b) 3-hour, (c) 4-hour.

(b)

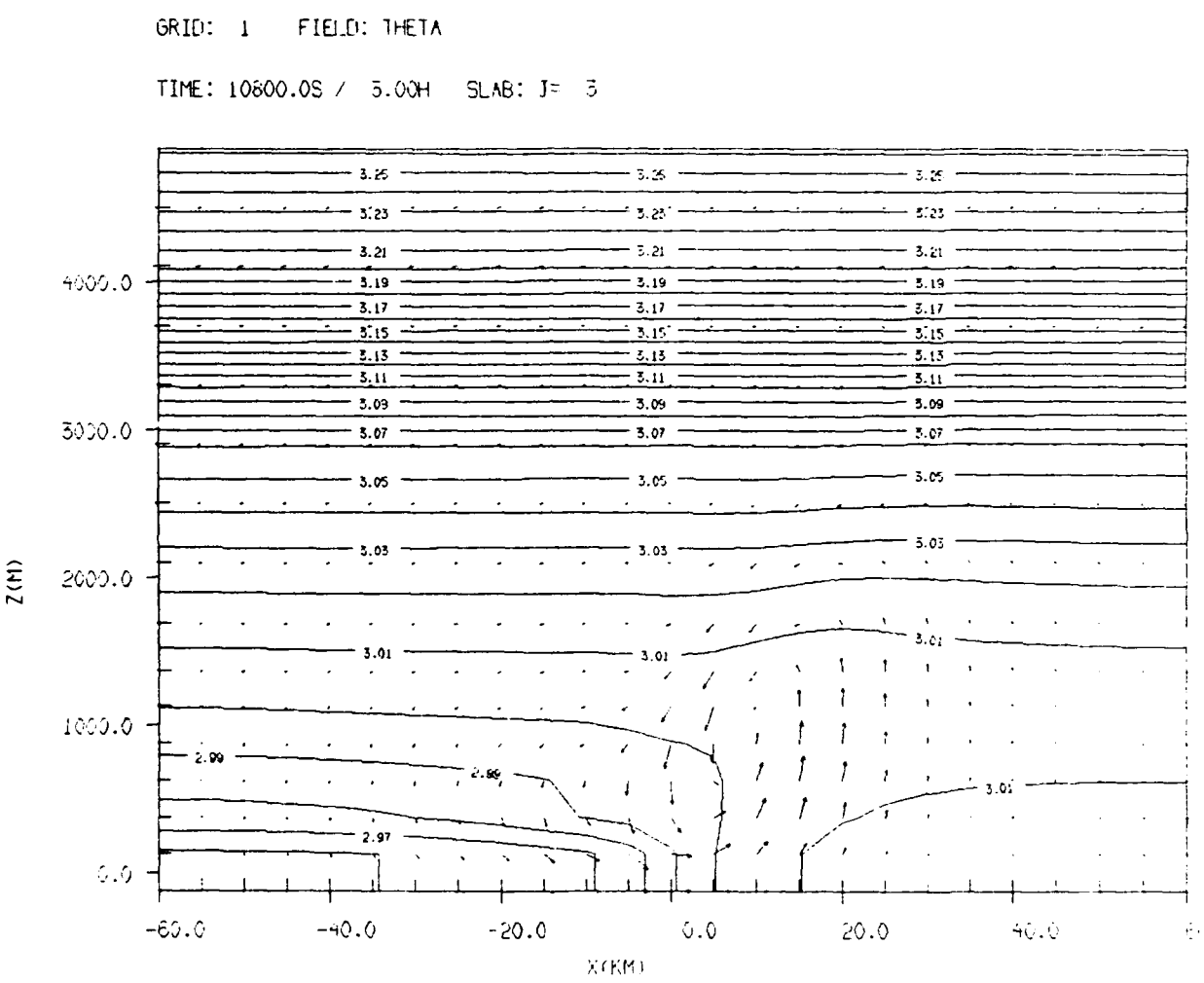
GRID: 1 FIELD: THETA
TIME: 10800.0S / 3.00H SLAB: J= 3
4000.0
3000.0
2000.0
1000.0
0.0
Z(M)
-60.0
-40.0
-20.0
0.0
20.0
40.0
X(KM)
FROM 2.94 TO 3.26 BY .01 LABELS * 100

Figure 11(b)

(c)

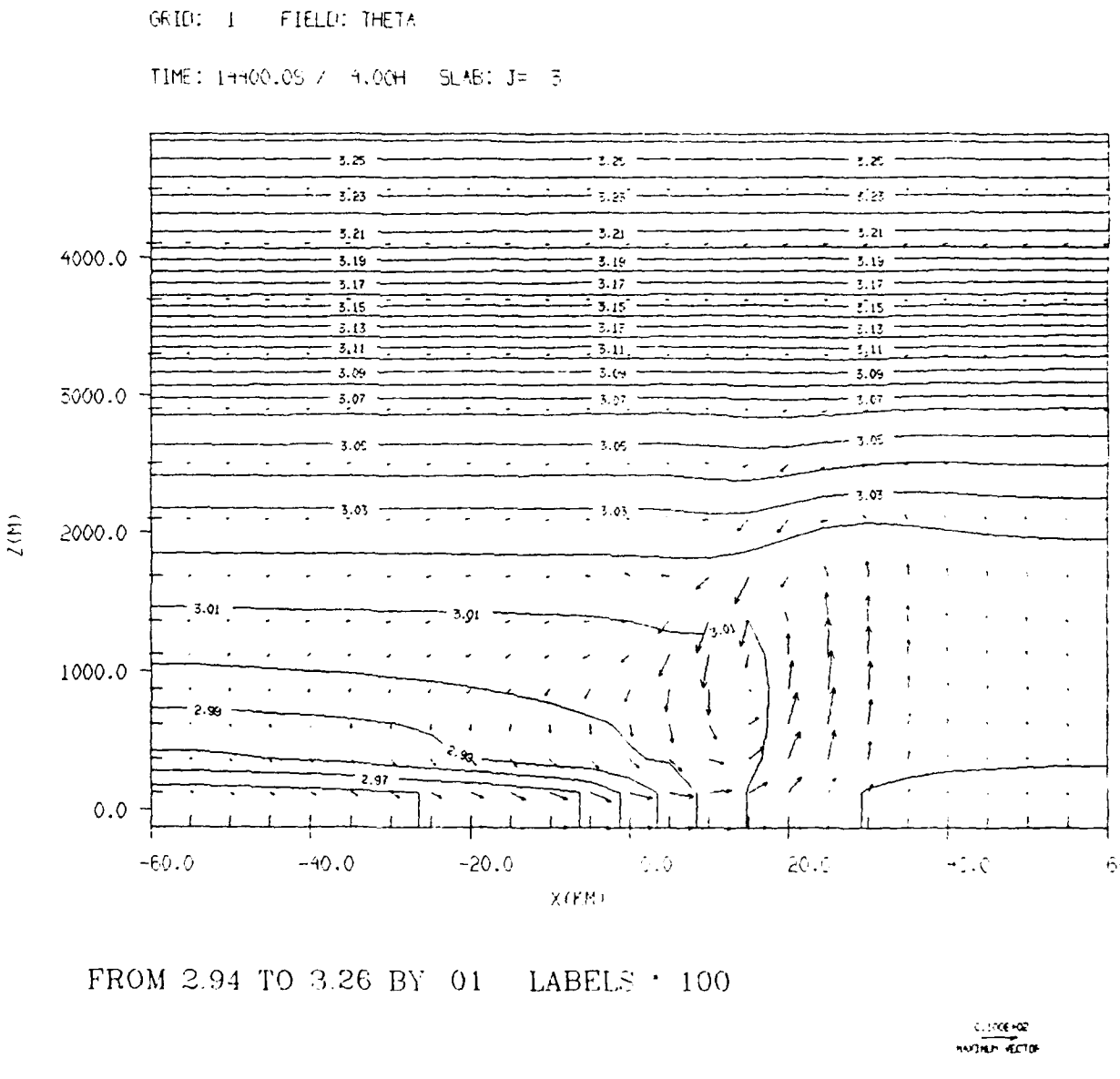
GRID: 1 FIELD: THETA
TIME: 14400.0S / 4.00H SLAB: J= 3
4000.0
3000.0
2000.0
1000.0
0.0
Z(M)
-60.0
-40.0
-20.0
0.0
20.0
X(KM)
3.25
3.23
3.21
3.19
3.17
3.15
3.13
3.11
3.09
3.07
3.05
3.03
3.01
2.99
2.97
FROM 2.94 TO 3.26 BY 01 LABELS * 100

Figure 11(c)

(a)

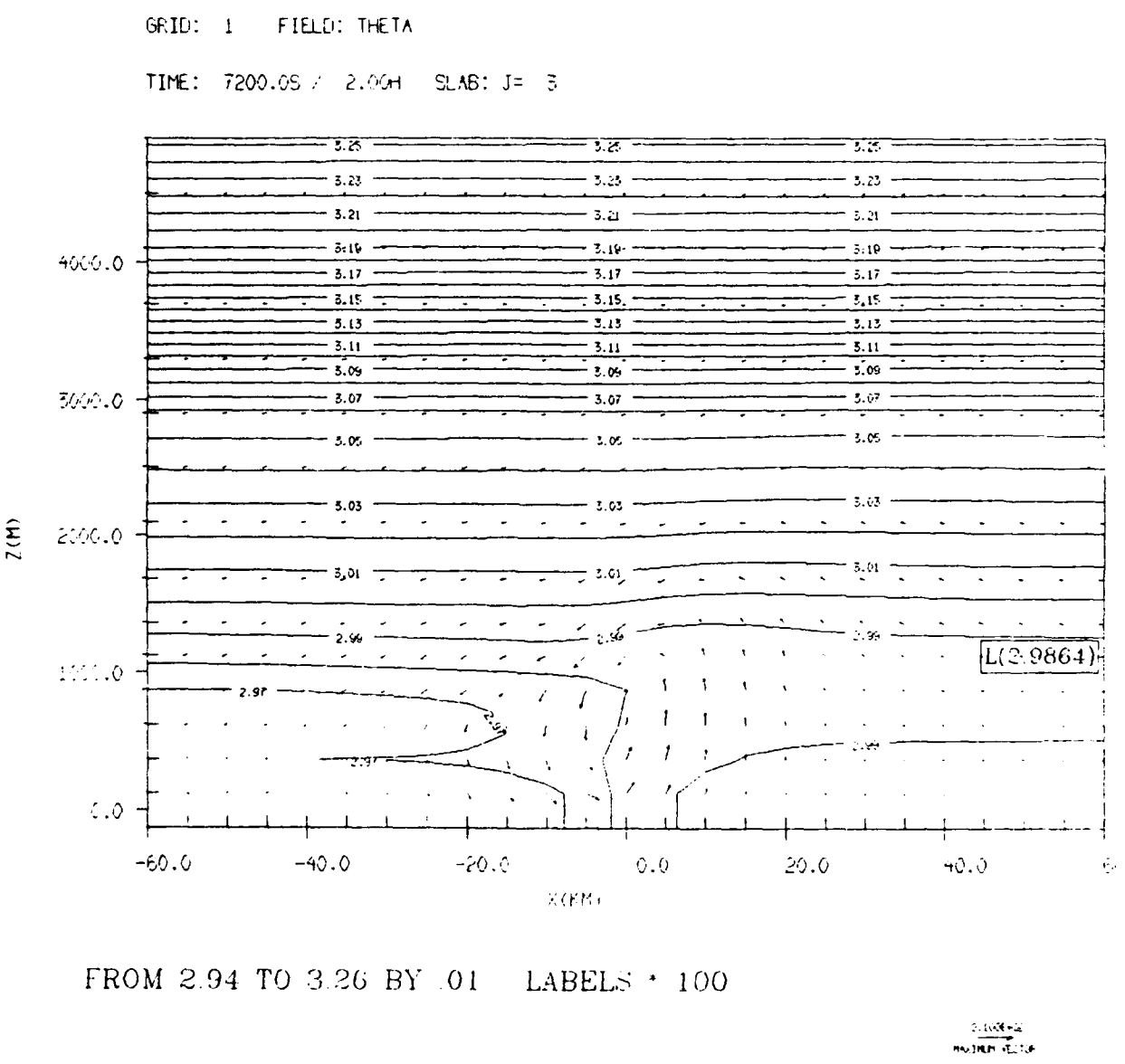

Figure 12: Output from Experiment 10. Potential temperature and wind forecasts for model initialized with faulty atmospheric conditions, and with only vertical levels 2 and 3 nudged by nature run's winds and temperatures (using 5.56 $*10^{-4}$ nudging coefficient and 5-minute updates). (a) 2-hour forecast, (b) 3-hour, (c) 4-hour.

(b)

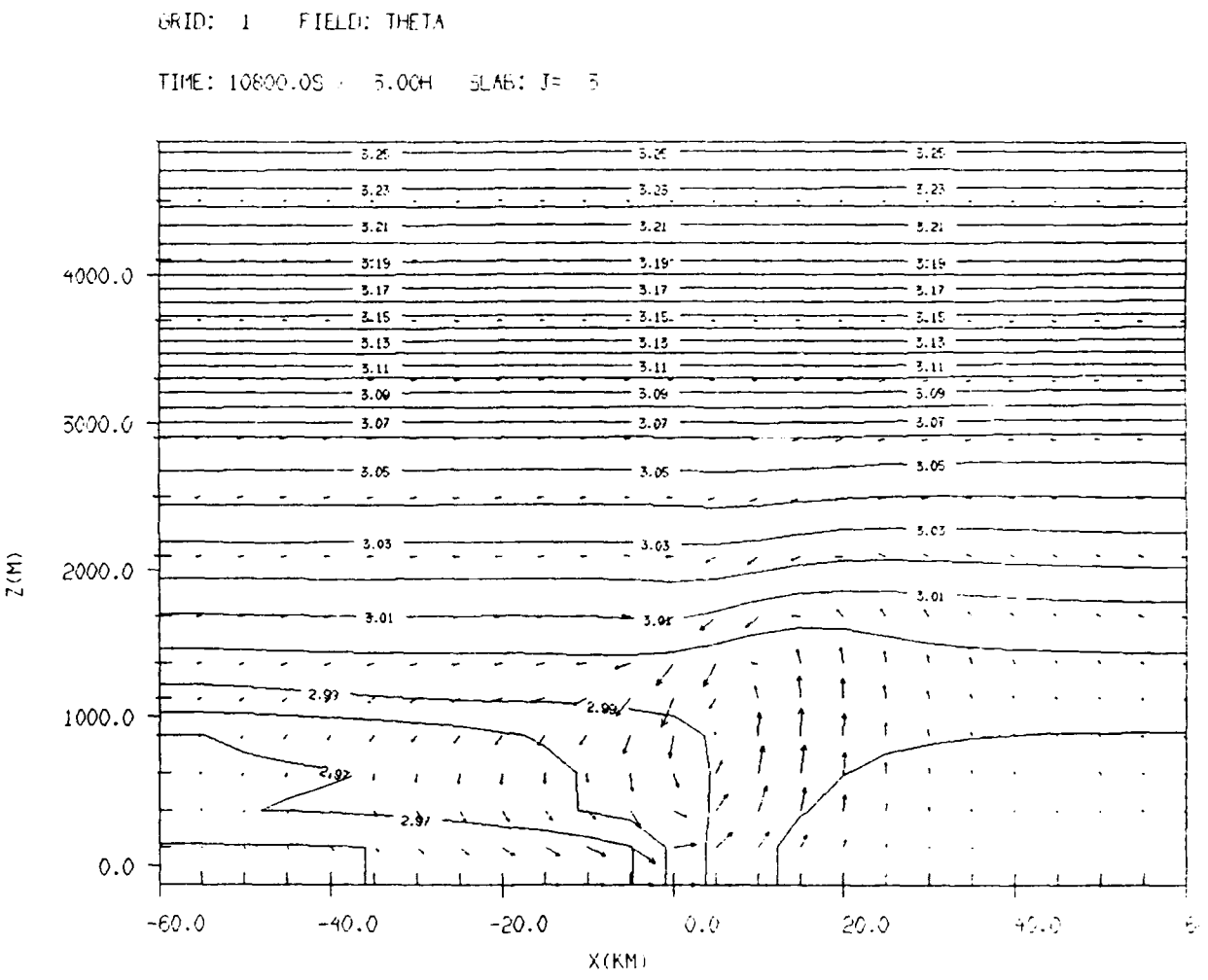
GRID: 1 FIELD: THETA
TIME: 10800.0S = 3.00H SLAB: J= 5
4000.0
3000.0
2000.0
1000.0
0.0
Z(M)
-60.0
-40.0
-20.0
0.0
20.0
X(KM)
FROM 2.94 TO 3.26 BY .01 LABELS * 100

Figure 12(b)

(c)

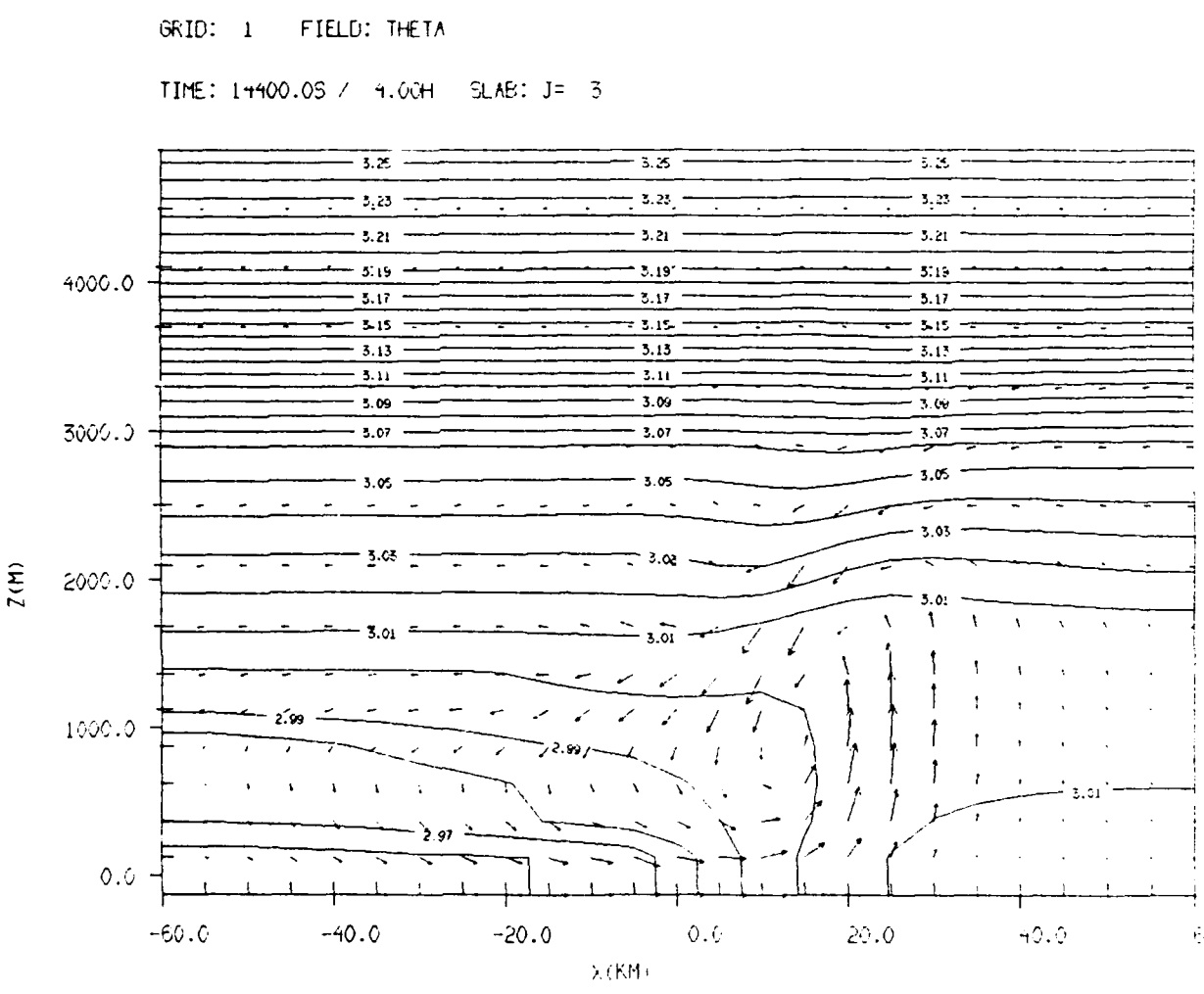

FROM 2.94 TO 3.26 BY .01 LABELS * 100

Figure 12(c)

(a)

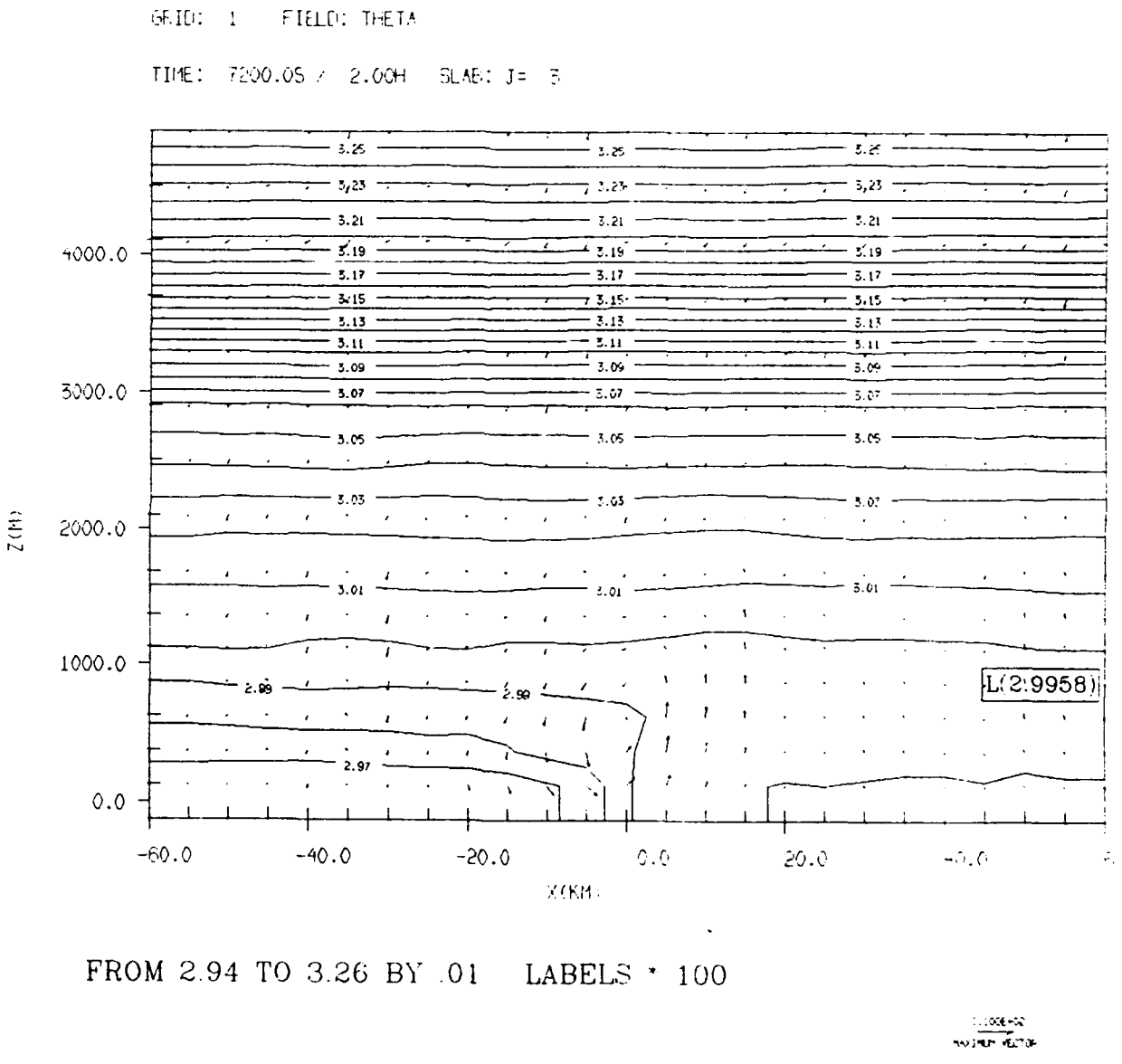

Figure 13: Output from Experiment 11. Potential temperature and wind forecasts for model initialized with faulty atmospheric conditions, and nudged every 5 minutes by degraded nature run winds and temperatures (smoothed field of random +/- 5 ms^{-1} wind and +/- 2 K temperature errors added to nature run). (a) 2-hour forecast, (b) 3-hour, (c) 4-hour.

(b)

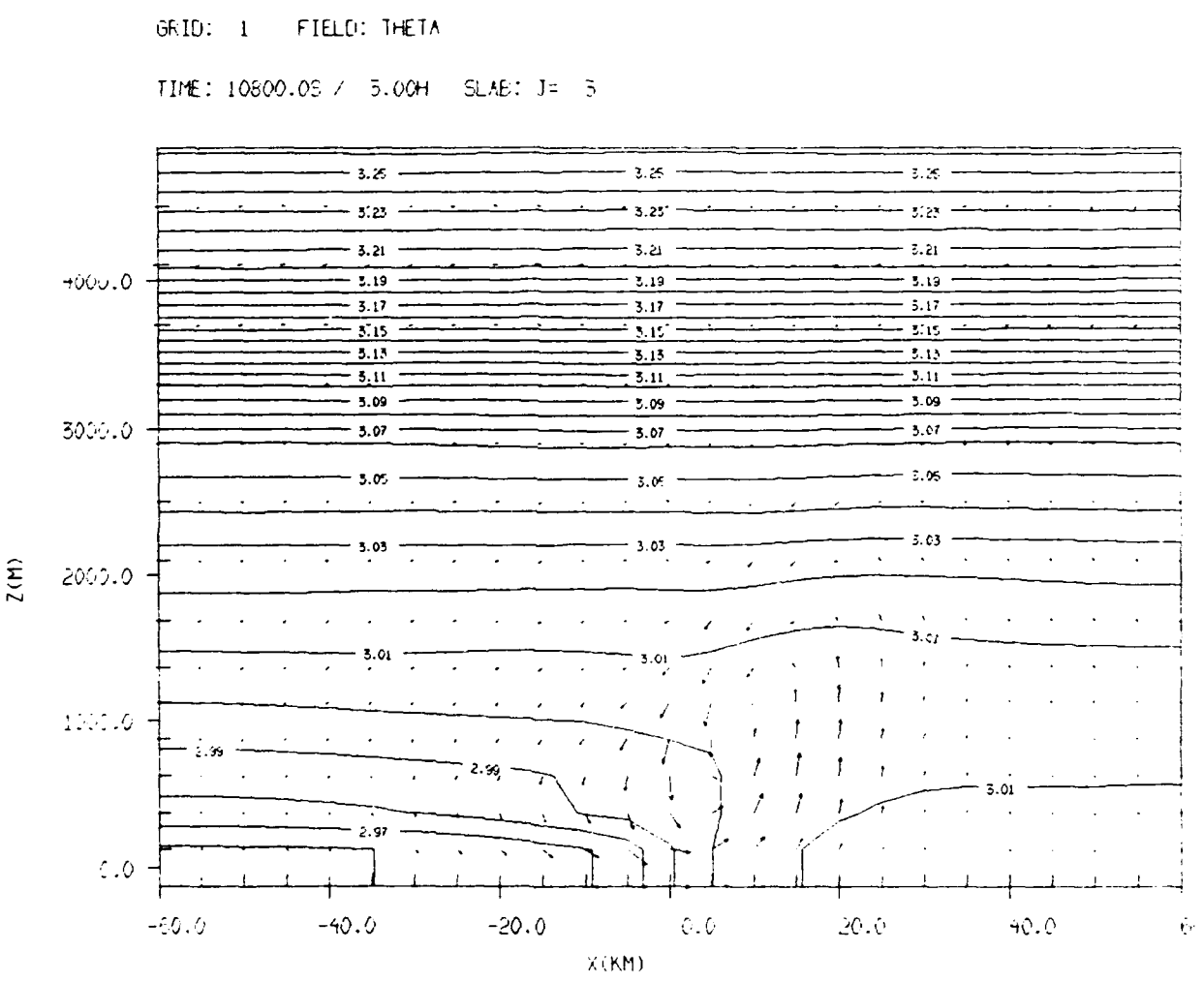
GRID: 1 FIELD: THETA
TIME: 10800.00 / 3.00H SLAB: J= 3
4000.0
3000.0
2000.0
1000.0
0.0
Z(M)
-60.0
-40.0
-20.0
0.0
20.0
40.0
X(KM)
FROM 2.94 TO 3.26 BY .01 LABELS * 100

Figure 13(b)

(c)

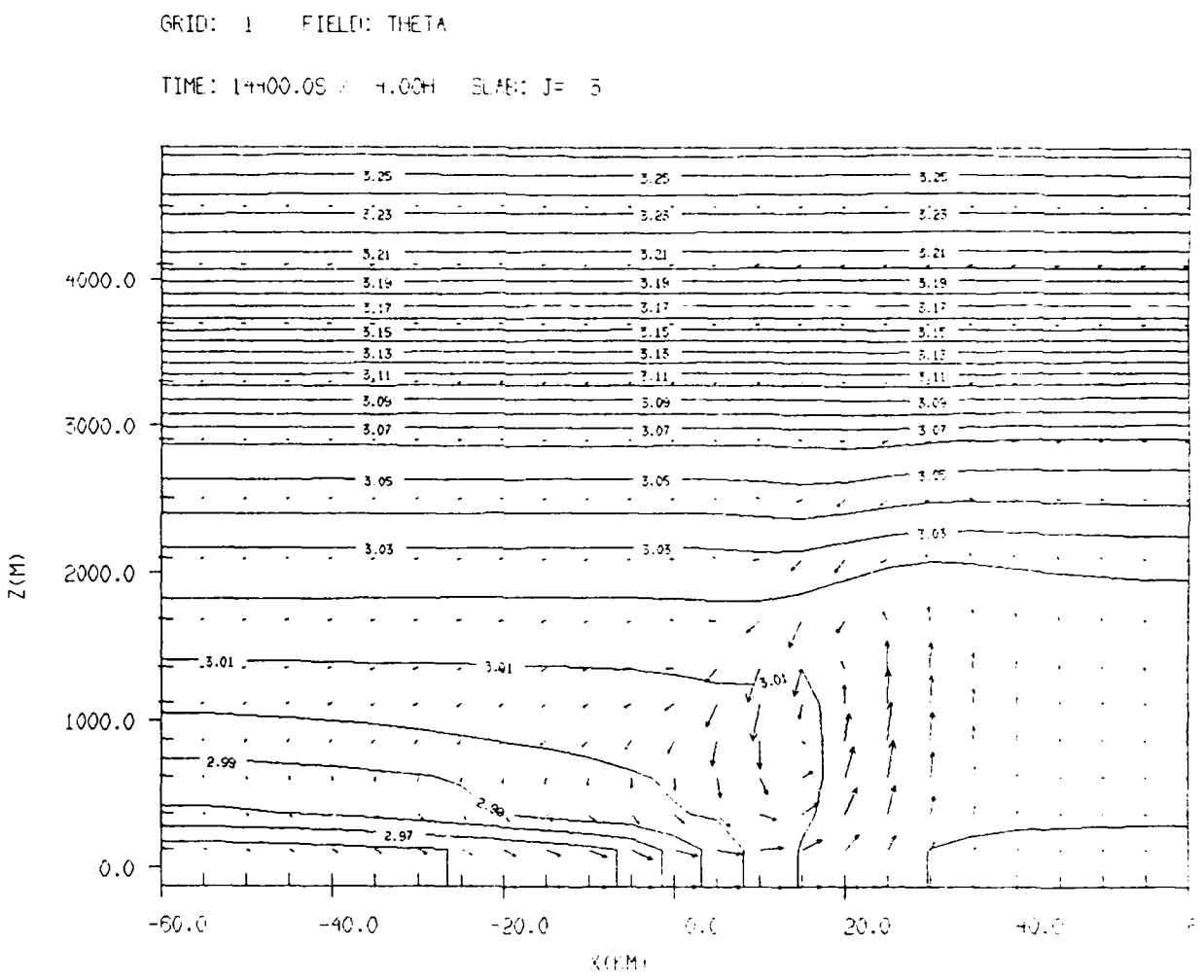

FROM 2.94 TO 3.26 BY .01 LABELS * 100

Figure 13(c)

(a)

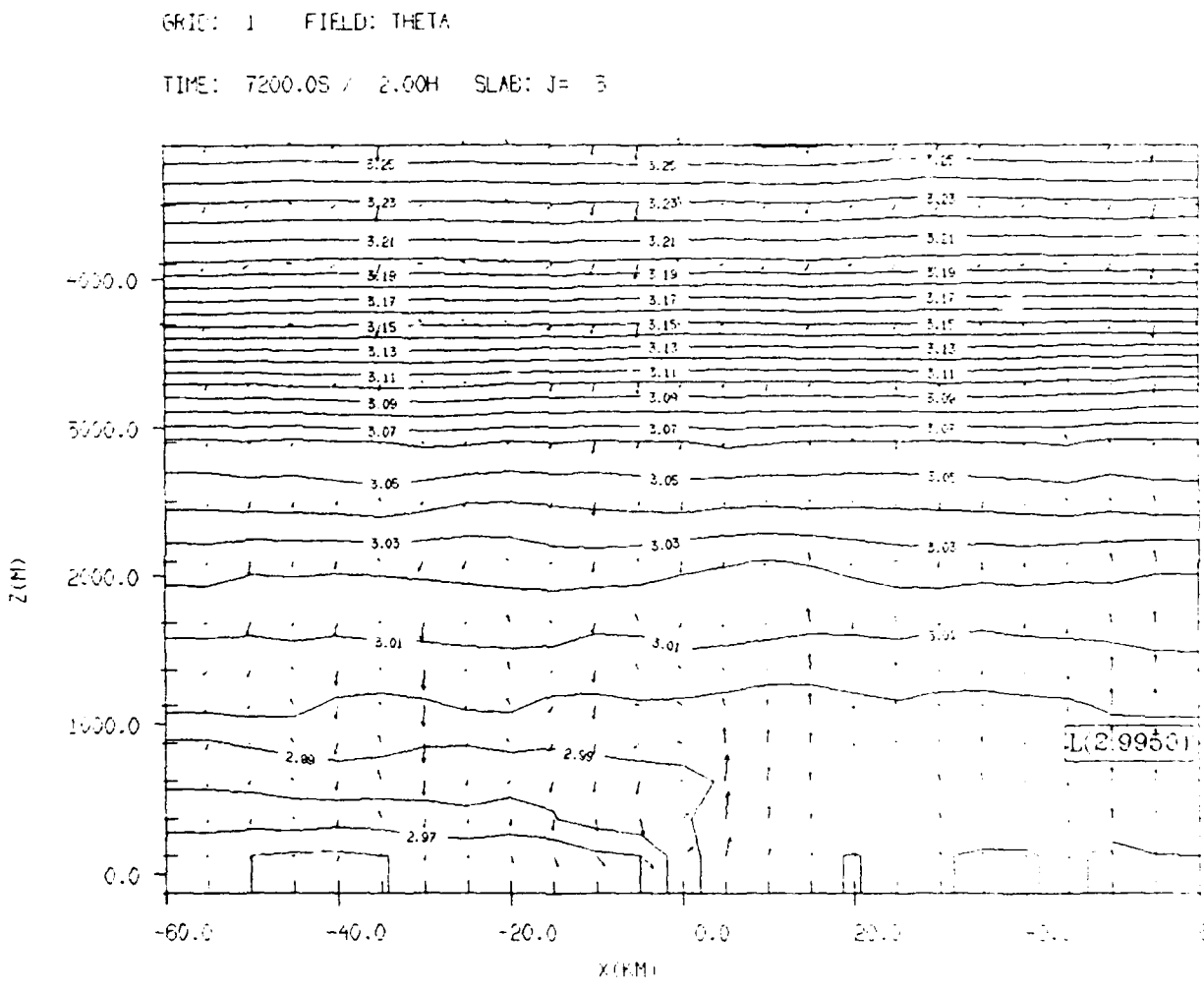

FROM 2.94 TO 3.26 BY .01 LABELS * 100

Figure 14: Output from Experiment 12. Potential temperature and wind forecasts for model initialized with faulty atmospheric conditions, and nudged every 5 minutes by degraded nature run winds and temperatures (smoothed field of random +/- 12 ms^{-1} wind and +/- 5 K temperature errors added to nature run). (a) 2-hour forecast, (b) 3-hour, (c) 4-hour.

(b)

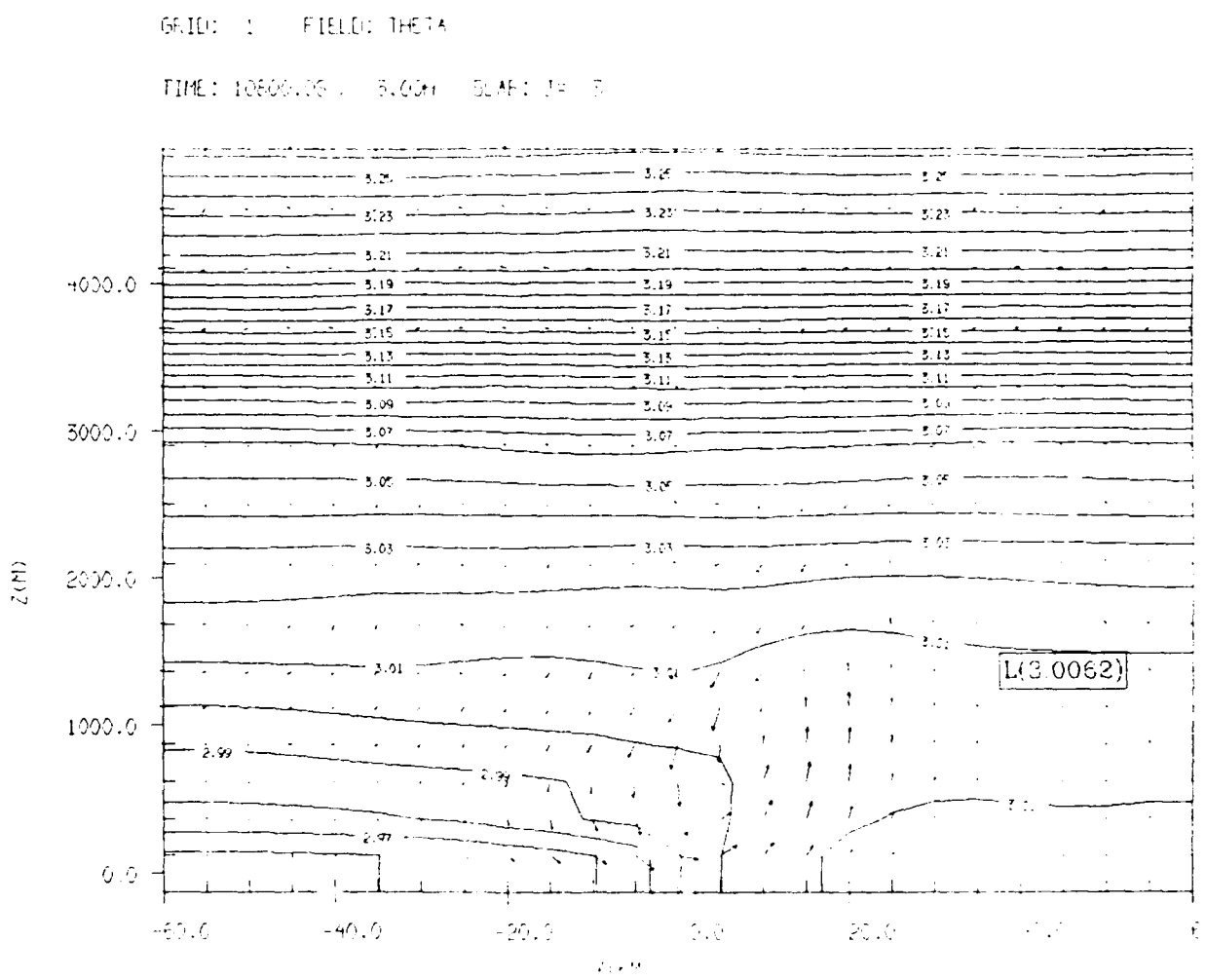

FROM 2.94 TO 3.26 BY .01 LABELS * 100

Figure 14(b)

(c)

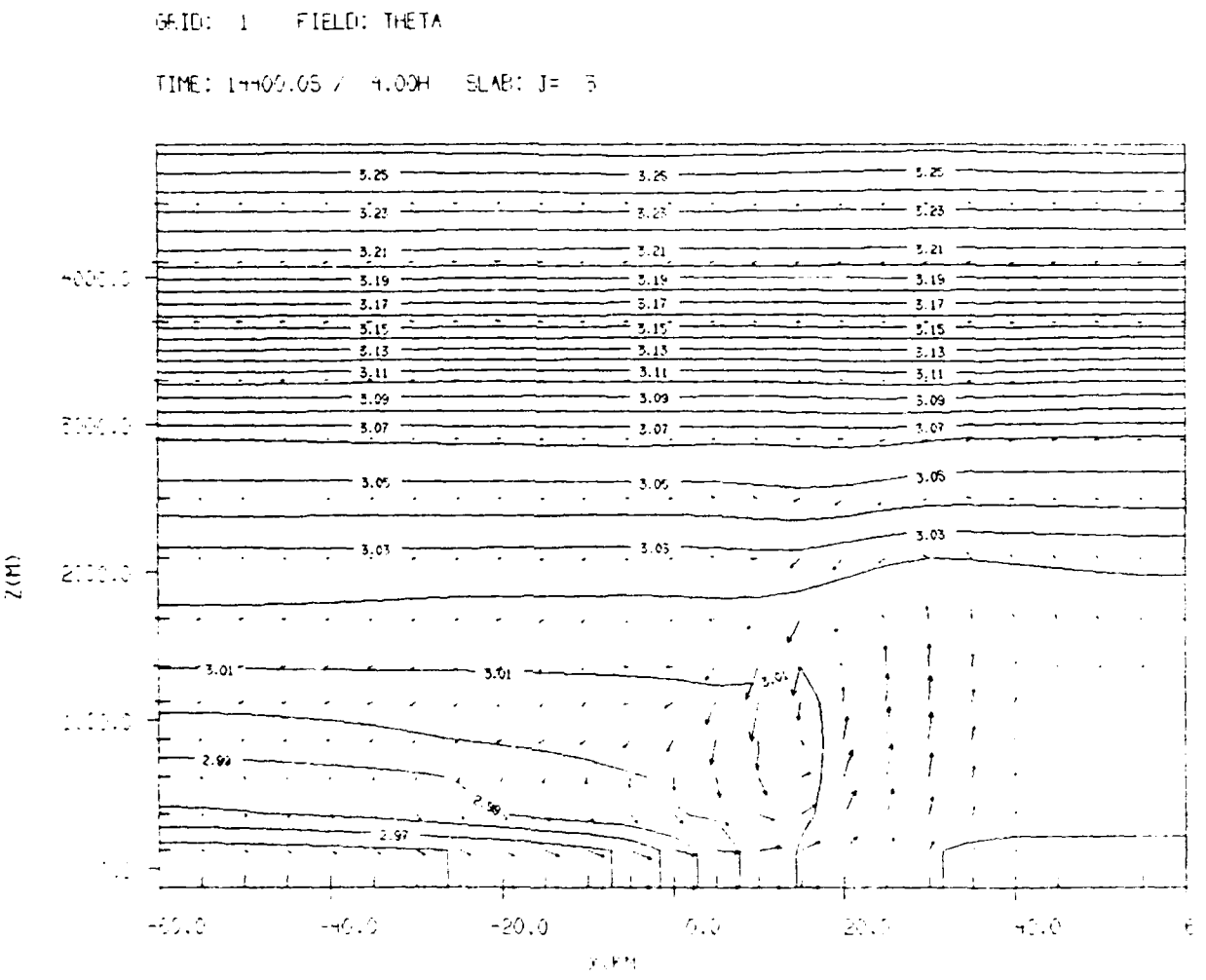

FROM 2.94 TO 3.26 BY .01 LABELS * 100

Figure 14(c)

(a)

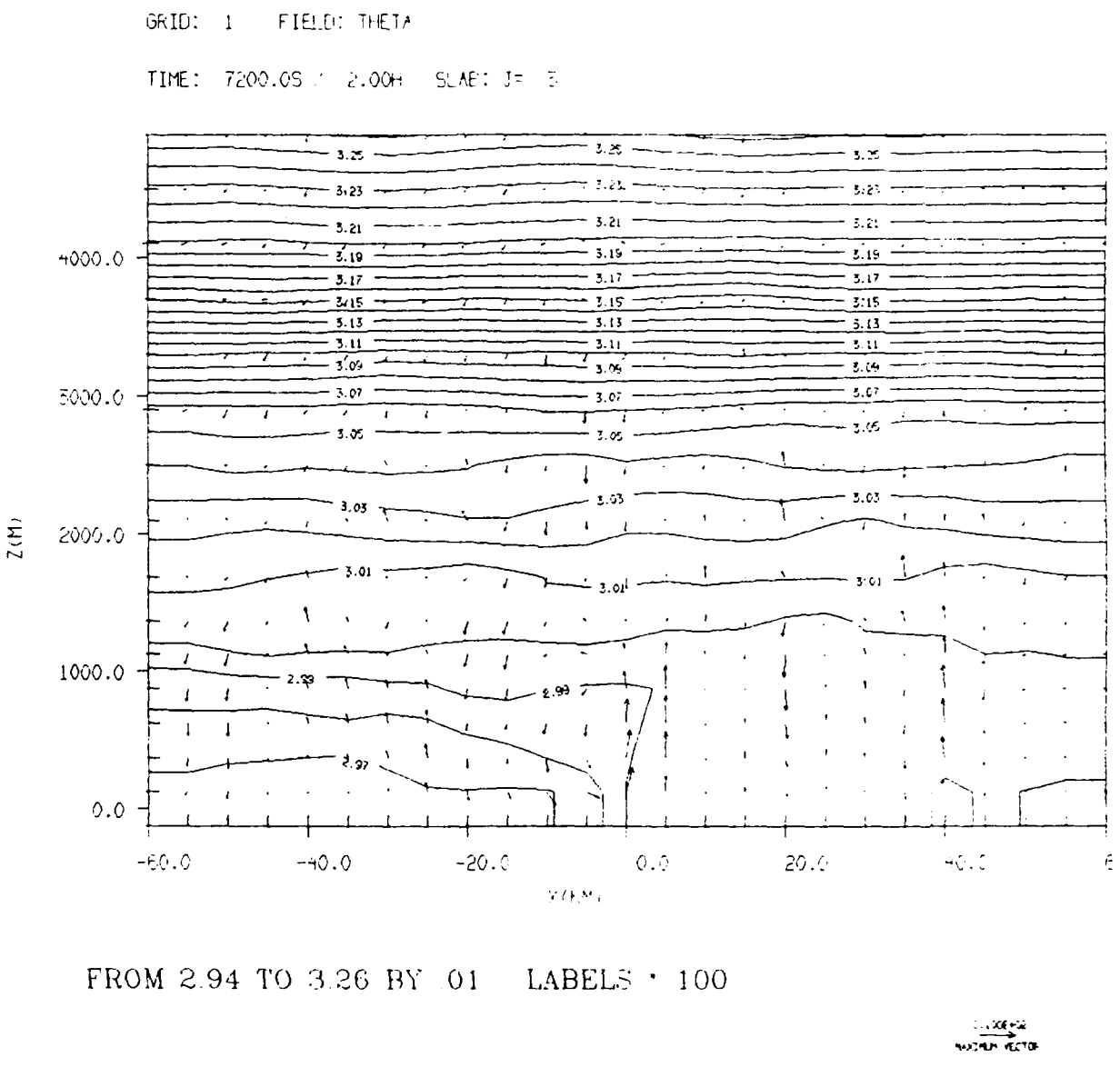

Figure 15: Output from Experiment 13. Potential temperature and wind forecasts for model initialized with faulty atmospheric conditions, and nudged every 20 minutes by degraded nature run winds and temperatures (smoothed field of random +/- 12 ms^{-1} wind and +/- 5 K temperature errors added to nature run). (a) 2-hour forecast, (b) 3-hour, (c) 4-hour.

(b)

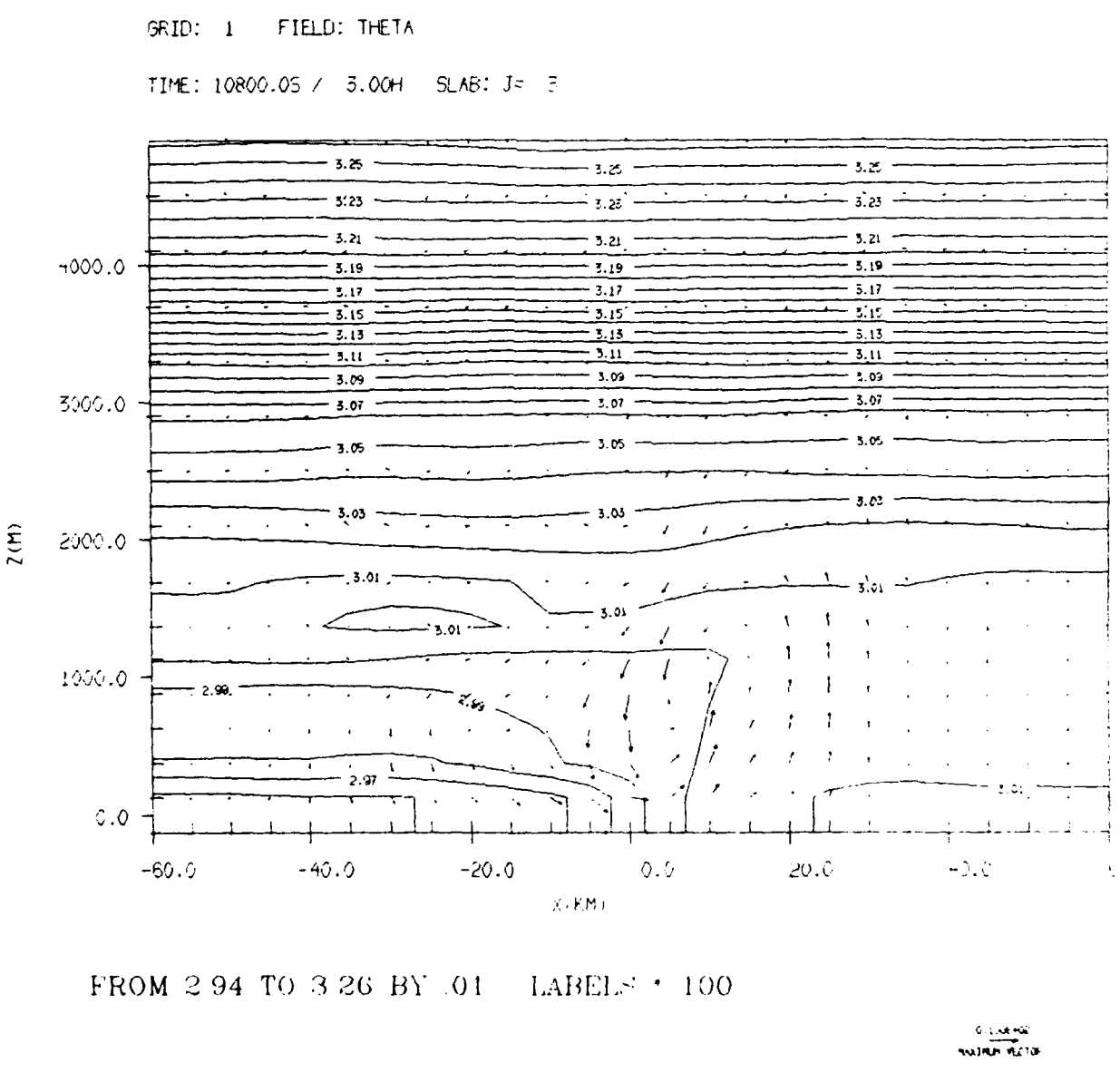
GRID: 1 FIELD: THETA
TIME: 10800.05 / 3.00H SLAB: J= 3
4000.0
3000.0
2000.0
1000.0
0.0
Z(M)
-60.0
-40.0
-20.0
0.0
20.0
3.25
3.23
3.21
3.19
3.17
3.15
3.13
3.11
3.09
3.07
3.05
3.03
3.01
2.99
2.97
FROM 2.94 TO 3.26 BY .01 LABELS * 100

Figure 15(b)

(c)

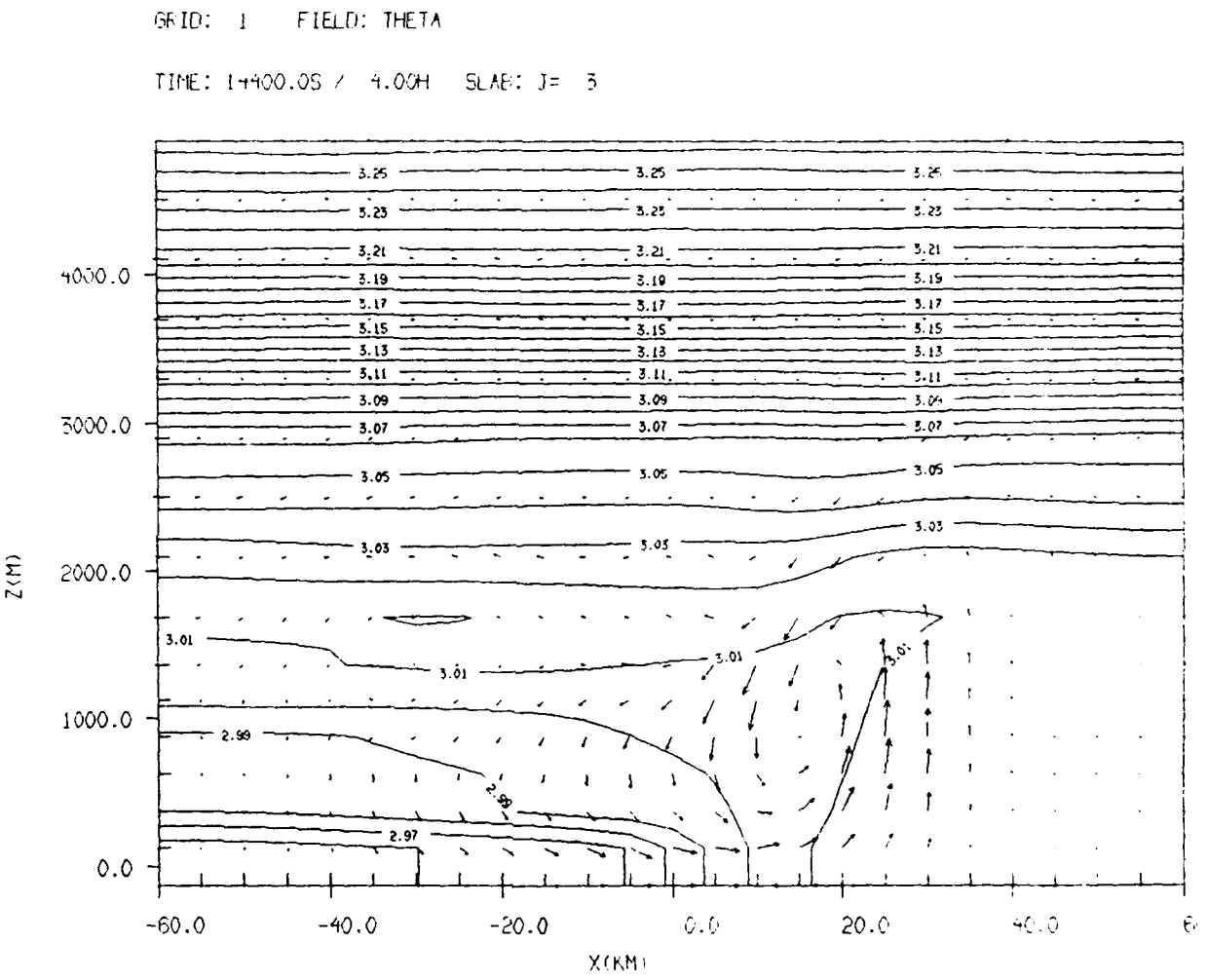
GRID: 1 FIELD: THETA
TIME: 14400.0S / 4.00H SLAB: J= 5
4000.0
3000.0
2000.0
1000.0
0.0
Z(M)
-60.0
-40.0
-20.0
0.0
20.0
40.0
X(KM)
FROM 2.94 TO 3.26 BY .01 LABELS * 100

Figure 15(c)

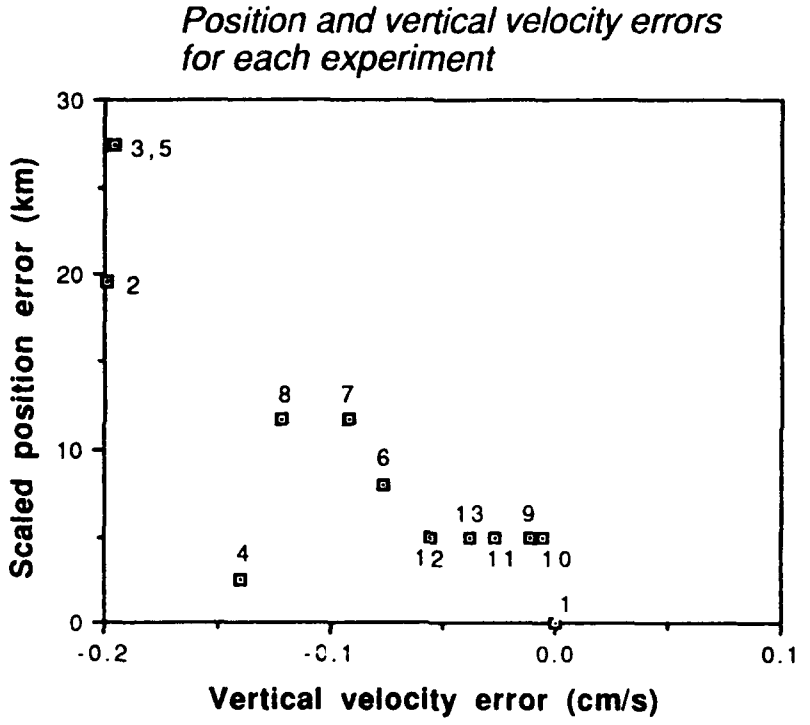

Figure 16: Scatterplot of errors in the position and magnitude of the forecasted maximum vertical velocity for each experiment. Numbers correspond to experiment number.

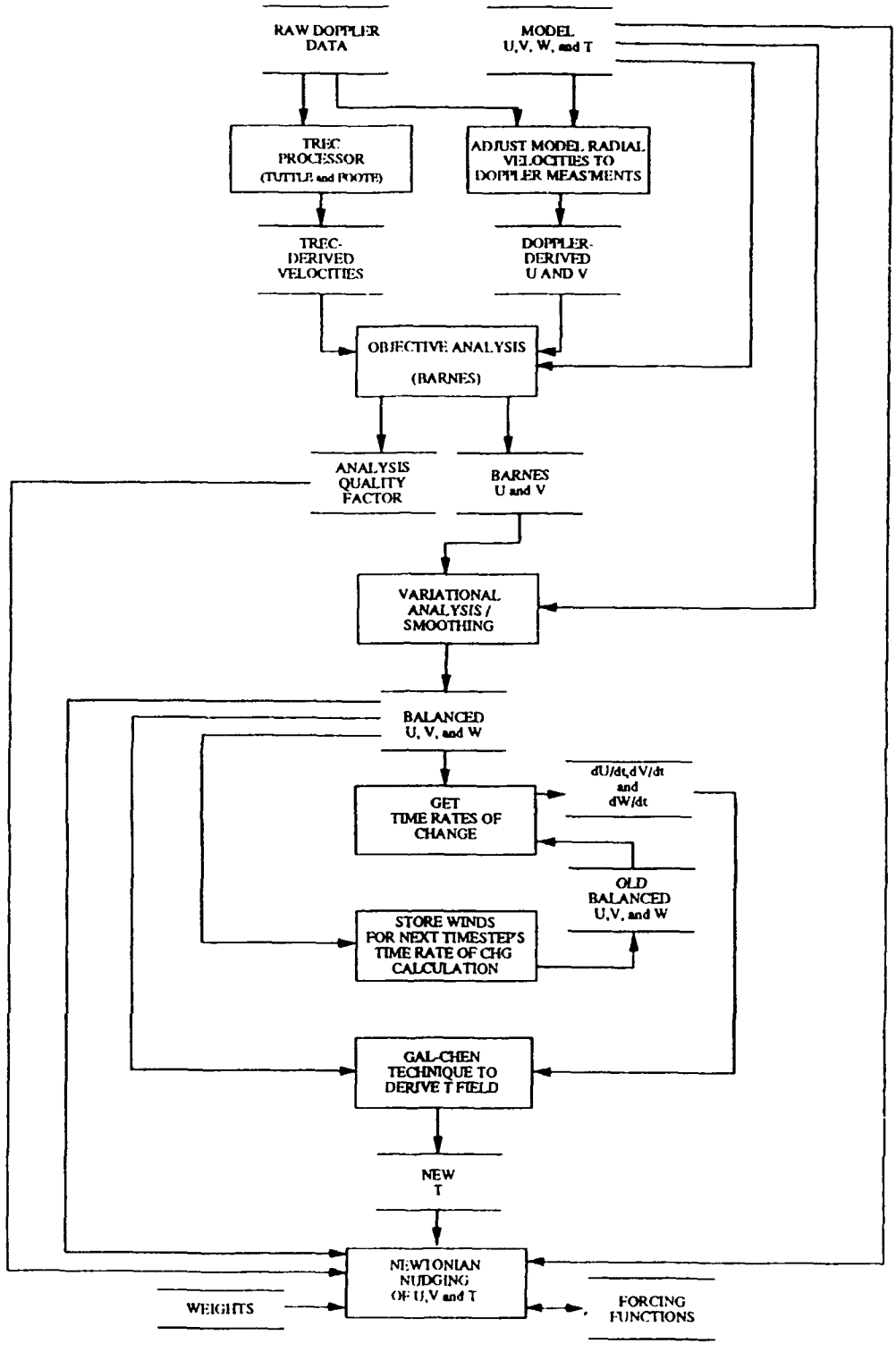

Figure 17: Processing and data flow for the planned Doppler data assimilation system for the PL-3D model.

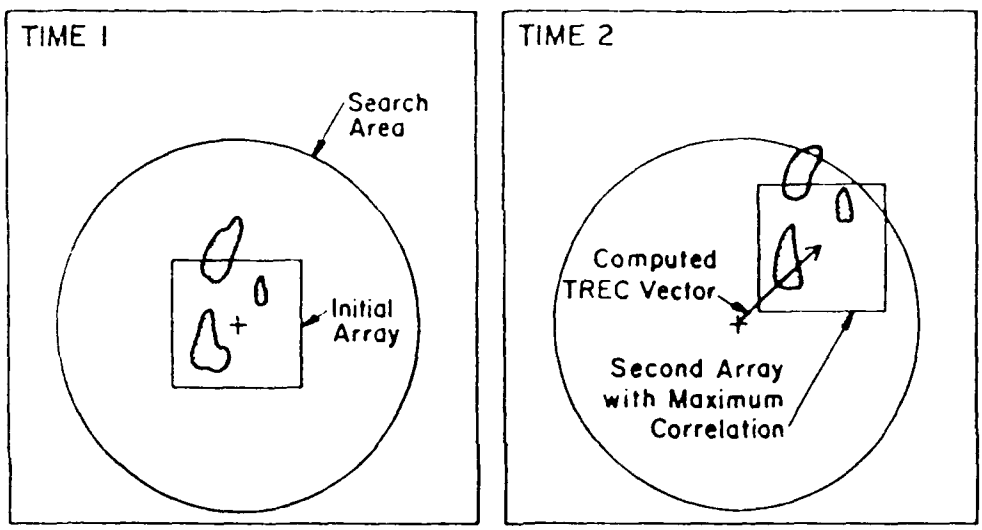

Figure 18: Schematic showing the computation of a TREC vector to determine the motion of reflectivity echoes (shaded) from TIME 1 to TIME 2. The initial array of data at TIME 1 is cross-correlated with all other second arrays of the same size at TIME 2 whose center falls within the search area. The position of the second array with the maximum correlation determines the vector endpoint. (Borrowed from Tuttle and Foote (1990).)

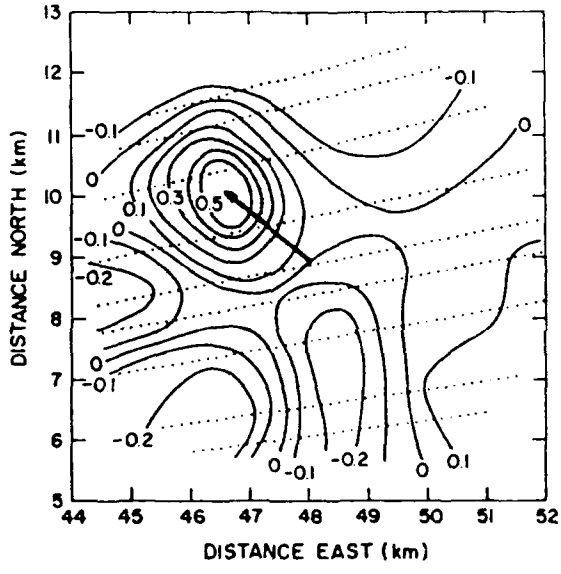

Figure 19: Example of contours of correlation coefficient between first and second arrays computed at each of the points shown. (Borrowed from Tuttle and Foote, 1990.)

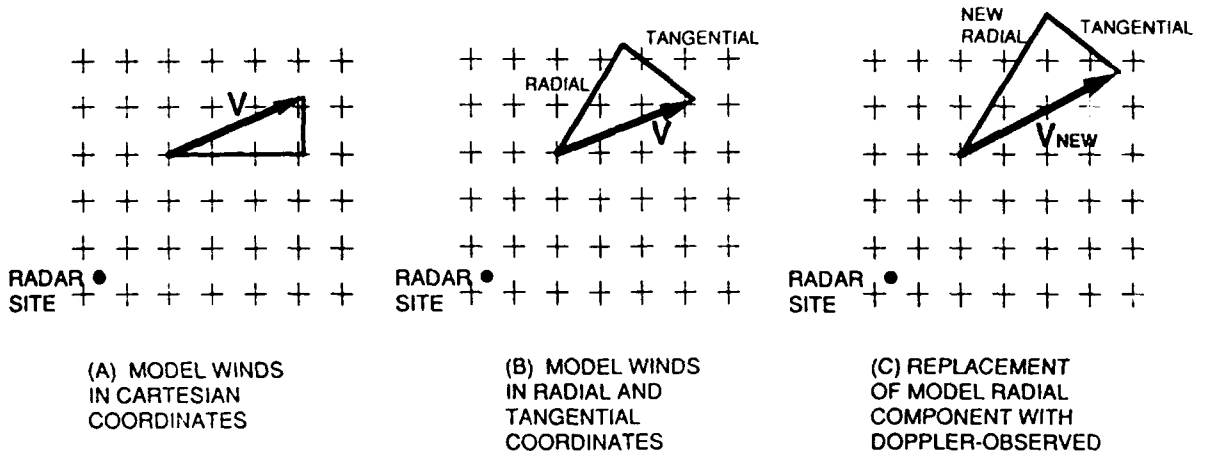

Figure 20: Illustration of the technique for generating a new wind observation using the model forecast wind and the Doppler-observed radial velocity. (a) Model winds expressed in the conventional Cartesian coordinate system. (b) Model winds for the same gridpoint converted to a radial and tangential component, centered around a radar site. (c) Replacement of the model radial component with the new Doppler-observed radial component to generate a new velocity vector.